# Characterization of *Mycobacterium smegmatis* mutant strains deficient in DNA repair and energy metabolism for increased mutagenesis

Nontobeko Maphalala (870470)


A dissertation submitted to the Faculty of Health Sciences, University of the Witwatersrand, Johannesburg, in fulfilment for the degree Master of Science in Medicine. 2021

**DECLARATION**

I, **Nontobeko Maphalala (student number: 870470)** declare that this dissertation is my own work. It is being submitted for the degree of Master of Science in Medicine at the University of the Witwatersrand, Johannesburg. It has not been submitted before for any degree or examination at this or any other University.

31/03/2021

Nontobeko Maphalala Date

**DEDICATION**

From me to me.

Makwande, Kukhanye, Kuvuleke, Kubekuhle!

**ACKNOWLEDGEMENTS**

To God, thank you for locating me to the CBTBR lab and caring me through the whole journey.

To the National Research Fund (NRF) thank you for the funding award for my master's studies.

To Prof Bavesh Kana, thank you for allowing me to use the CBTBR resources in building my career.

To my supervisor, Dr Bhavna Gordhan thank you so much for your supervision, guidance, and encouragement through and through this past 2 years. May God bless you tenfold.

To my CBTBR colleagues, thank you so much for the support, assistance, and good laughs during the good and bad days. May you all make it in your future endeavors. A special thanks to Moagi Shaku, Tebogo Maema, Olivia Jacobs, Bomikazi Nonkula and Dale Liebenberg for your assistance with my experimental work.

To my family and friends, thank you for the constant support.

**ETHICS WAIVER**

UNIVERSITY OF THE WITWATERSRAND, JOHANNESBURG

**HUMAN RESEARCH ETHICS COMMITTEE (MEDICAL)**

**Human Research Ethics Committee (Medical)**

Research Office Secretariat:
Faculty of Health Sciences, Phillip Tobias Health Sciences Building, 3rd Floor, Office 301/2/6, 29 Princess of Wales Terrace, Parktown, 2193
Private Bag 3, Wits 2050
Office email: HREC-Medical.ResearchOffice@wits.ac.za
Website: www.wits.ac.za/research/about-our-research/ethics-and-research-integrity/

Ref: W-CBP-190919-04

19/09/2019

***TO WHOM IT MAY CONCERN:***

| | |
|---|---|
| **Waiver:** | This certifies that the following research does not require clearance from the Human Research Ethics Committee (Medical) |
| **Investigator:** | Ms Nontobeko Maphalala (Student no. 870470) |
| **Supervisor:** | Dr Bhavna Gordhan |
| **Department:** | National Health Laboratory Service |
| **Project title:** | Characterization of *Mycobacterium smegmatis* mutant strains deficient in DNA repair and energy metabolism for increased mutagenesis |
| **Reason:** | *In vitro* laboratory study. Using bacterial strains. No human participants will be involved in the study. |

**Dr CB Penny**

Chairperson: Human Research Ethics Committee (Medical)

Copy – HREC (Medical) Secretariat: Zanele Ndlovu, Mapula Ramaila, Josh Ndlangamandla and Rhulani Mkansi

**TABLE OF CONTENTS**

**List of tables**

**List of figures**

**List of abbreviations**

| | |
|---|---|
| AU | Arbitrary units |
| Amp | Ampicillin |
| AP | Apurinic/apyrimidinic |
| ATP | Adenosine triphospate |
| BCG | Bacille Calmette-Guérin |
| BER | Base excision repair |
| Bps | Base pairs |
| BV510 | Brilliant Violet 510 |
| CR (1-4) | Complement receptors |
| CBTBR | Centre of Excellence for Biomedical TB Research |
| CTAB | CetylTrimethylAmmonium Bromide |
| CFZ | Clofazimine |
| CFU | Colony forming unit |
| CHP | Cumene hydroperoxide |
| CSPD | Disodium 3-phenyl phosphate |
| DCOs | Double crossover |
| $dH_2O$ | Distilled water |
| DNA | Deoxyribonucleic acid |
| DTT | Dithiothreitol |
| dUTP | Deoxyuridine triphosphate |
| *E. coli* | *Escherichia coli* |
| ETC | Electron transport chain |

| | |
|---|---|
| EMB | Ethambutol |
| FITC | Fluorescein Isothiocyanate |
| Fpg | Formamidopyrimidine |
| $H_2O_2$ | Hydrogen peroxide |
| HCl | Hydrogen chloride |
| HIV | Human Deficiency Virus |
| INH | Isoniazid |
| Kan | Kanamycin |
| LA | Luria agar |
| LB | Luria-Bertani broth |
| MAC | *M. tuberculosis complex* |
| MOTT | Mycobacteria other than tuberculosis |
| M. tb | *Mycobacterium tuberculosis* |
| MUT | Mutant |
| MDR-TB | Multidrug Resistant TB |
| $MgSO_4$ | Magnesium sulphate |
| NaCl | Sodium chloride |
| NaOH | Sodium hydroxide |
| NADH | NADH dehydrogenase |
| Nei | Endonuclease VIII |
| NEB | New England Biolabs |
| NER | Nucleotide Excision Repair |
| NIOH | National Institute of |

| | |
|---|---|
| | Occupational Health |
| NTM | Non-tuberculous mycobacteria |
| PBS | Phosphate buffered saline |
| Nth | Endonuclease III |
| PZA | Pyrazinamide |
| $OD_{600nm}$ | Optical density as measured at wavelength 600nm |
| Ori | Origin of replication |
| PCR | Polymerase Chain Reaction |
| QH2 | Ubiquinol |
| qPCR | Quantitative polymerase chain reaction |
| RIF | Rifampicin |
| RNIs | Reactive nitrogen intermediates |
| RNA | Ribonucleic acid |
| ROS | Reactive oxygen species |
| RRDR | Rifampicin Resistance Determining Region |
| RR-TB | Rifampicin resistance |
| SCOs | Single crossover |
| SDS | Sodium dodecyl sulphate |
| Ter | Termination of replication |
| TB | Tuberculosis |
| TBE | Tris borate EDTA |

| | |
|---|---|
| X-gal | 5-bromo-4chloro-3-indolyl-D-thiogalactopyranoside |
| XDR-TB | Extensively Drug Resistant TB |
| USA | United States of America |
| WHO | World Health Organisation |
| WT | Wild type |

**LIST OF SYMBOLS**

| | |
|---|---|
| µl | microliters |
| cm | centimetres |
| ml | millilitres |
| mg | milligrams |
| nm | nanometres |
| ng | nanograms |
| g | grams |
| % | percentage |
| ℃ | degrees Celsius |
| Δ | delta (In this context, it is a symbol used to describe deletion of genes which are then referred to as “mutants”). |
| V | volts |
| µF | microfarad |
| Ω | electrical resistance |
| Xg | centrifugal force |
| Rpm | revolutions per minute |

**Abstract**

Tuberculosis is an ancient menace caused by *Mycobacterium tuberculosis (M. tb*). Nearly, 1.4 million lives are claimed due to this disease annually. Upon infection, *M. tb* is engulfed by alveolar macrophages to form a granuloma as part of the host's immune response to control the infection. The conditions within the granuloma are hostile which can cause DNA damage resulting in spontaneous mutations, drug resistance or leading to cell death. However, mycobacteria have several repair pathways including the base excision repair (BER) pathway which is important for repairing damaged single nucleotides for continued growth and maintenance of genome integrity. DNA glycosylases are the first enzymes in the BER pathway that recognize and excise damaged nucleotides. Previous work has shown that endonuclease III (*nth*) has antimutator properties and a synergistic relationship with the two endonuclease VIII (*nei*) homologs in maintaining mycobacterial genome stability under oxidative stress conditions.

However, DNA repair deficiency may not be the only driver of mutagenesis in mycobacteria. Mycobacteria require oxygen for metabolism and therefore, under oxygen-depleted environments growth of *M. tb* will cease. *M. tb* can also alternate between energy pathways and up-regulate specific genes of the electron transport chain (ETC) under hypoxic conditions thus, enhancing the survival of the bacteria under unfavourable conditions. Therefore, both the BER pathway and the ETC confer *M. tb* with the ability to tolerate high oxidative stress environments generated within the host during pathogenesis. Hence, we hypothesized that deficiency of critical genes in the ETC pathway would exacerbate reactive oxygen species (ROS) levels resulting in increased levels of DNA damage that could be catastrophic in the absence of crucial DNA repair enzymes (from the BER pathway), leading to mutagenesis and eventually to cell death.

In this study, we aimed to generate and characterize combinatorial mutants deficient in genes in both the BER and the ETC pathways in the non-pathogenic *M. smegmatis* strain to gain an understanding of the interplay between these two pathways in the maintenance of mycobacterial genome integrity. Previous findings have reported that mutants deficient in single genes in either of the pathways play a role in genome maintenance under unfavourable conditions. Based on this we hypothesized that combinatorial mutants deficient in genes from both the BER and ETC pathways when exposed to stress conditions, are more likely to show increased mutagenesis.

## CHAPTER 1

## LITERATURE REVIEW

### 1.1 TB background

Tuberculosis (TB) is an ancient menace which has tormented humankind throughout history. It is hypothesised that mycobacteria originated more than 150 million years (Barberis *et al*., 2017). *M. tb* was present in East Africa as early as 3 million years ago (Gutierrez *et al*., 2005).

TB disease is caused by *M. tb* species, which belongs to the *Mycobacteriaceae* family, the *Actinomycetales* order and *Actinobacteria* phylum as shown in Figure 1 (Mohammadipanah and Dehhaghi, 2017). The *Actinobacteria* phylum consists of 6 classes, 6 orders, and 14 suborders (Mohammadipanah and Dehhaghi, 2017). Additionally, species from the Mycobacterium genus are further classified into three major groups namely, *Mycobacterium tuberculosis* complex (MAC), *Mycobacterium leprae* and non-tuberculous mycobacteria (NTM) also known as mycobacteria other than tuberculosis (MOTT) (Sykes and Gunn-Moore, 2013).

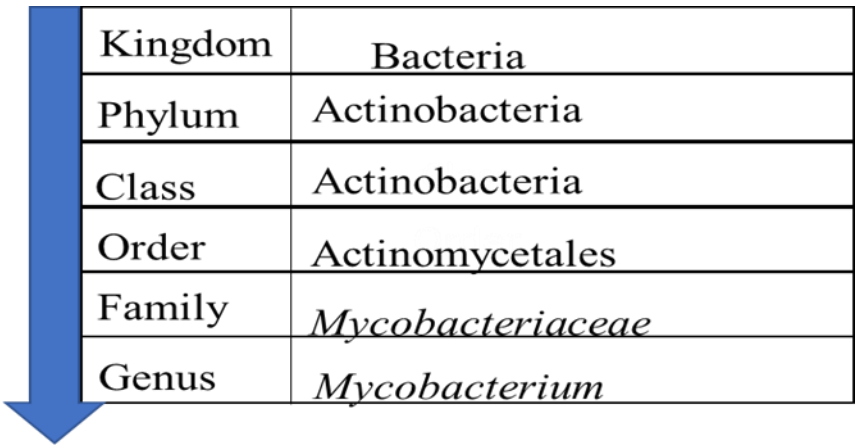


**Figure 1.** Taxonomic classification of *Mycobacteria (*Adapted from *Mohammadipanah and Dehhaghi, 2017).*

All the modern members of the MAC, including not only *M. tb* but its African variants *Mycobacterium africanum, Mycobacterium smegmatis*, *Mycobacterium canetti*i as well as *Mycobacterium bovis*, had a common African ancestor (Gutierrez *et al*., 2005). The bacteria in the MAC are acid fast (Sevilla *et al*., 2015) characterised by a 99% similarity at the nucleotide level and have almost identical 16S rRNA sequences between them (Alemu *et al*., 2016).

### 1.2 TB epidemiology

Tuberculosis is ranked in the top 10 life threatening diseases claiming nearly 1.4 million lives every year (Annabel *et al*., 2019). Globally, an estimated 10 million people were reported in 2019 per 100 000 populations infected with TB (Figure 2) and the decrease in the number of these cases has been a slow-going process over the years (WHO, 2020). Based on global statistics, approximately 56% (men), 32% (women) and 12% (children) accounted for the number of individuals who developed TB (WHO, 2020). About 8.2 % of TB infected people were also living with Human Immunodeficiency Virus (HIV) disease (WHO, 2020).

However, the TB and HIV co-infection incident have merged to deliver a deadly synergy worldwide, notably in the sub-Saharan African region (Annabel *et al*., 2019). Approximately, 1.2 million mortality cases of HIV negative patients that are infected by TB and 208 000 cases in HIV positive patients were documented (WHO, 2020). The emergence of the HIV pandemic has escalated the TB mortality and morbidity rate as the HIV virus compromises the host immune system, providing an opportunity for the latent TB bacteria to cause disease (Annabel *et al*., 2019).

South Africa ranks fourth amongst nations that have the highest TB burden due to the HIV epidemic and living conditions of most people, making them highly susceptible and vulnerable to the TB infection (WHO, 2017). The South African Department of Health in 2019 reported that the TB burden in South Africa was 36 000 for HIV positive patients (Harding, 2020). Moreover, human mortality is escalating due to the emergence of drug resistance to the present TB antibiotics.

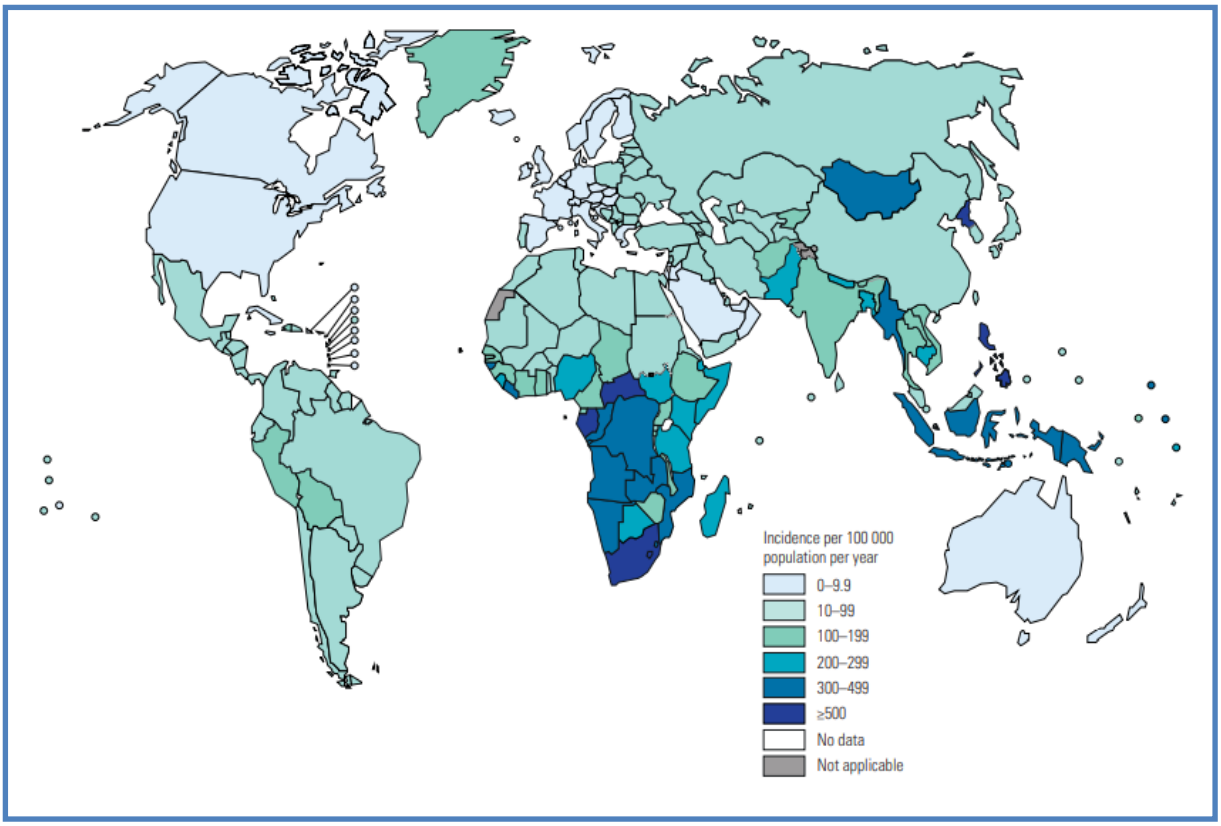


**Figure 2.** The global estimated TB incidence burden rates per 100000 populations in 2019 (WHO, 2020).

### 1.2.1 Drug resistance burden

The second most significant barrier to the eradication of TB is the emergence of rapid multidrug resistant (MDR) and extensively drug resistant (XDR) TB which has caused in a sharp increase in the burden of the disease. Rifampicin resistance (RR-TB) and MDR-TB is TB that is resistant to rifampicin only (RR-TB) and resistant to both rifampicin and isoniazid, the two most powerful first line anti-TB drugs that impels treatment with a second-line regimen (WHO, 2017). XDR-TB is a form of MDR-TB resistant to at least one fluoroquinolone and one of the injectable agents used in MDR-TB treatment regimens (WHO, 2016).

Statistically an estimated 3.3% of new cases and 18% of previously treated cases were RR-TB/ MDR totalling to 465 000 cases worldwide in 2019 resulting in 182 000 deaths in that year (Annabel *et al.*, 2019). Nearly 50% of the MDR-TB cases were distributed in India (27%), China (14%) and the Russian Federation (8%) making these countries to carry the highest burden of drug resistant TB (Figure 3). In that year South Africa had an MDR-TB burden of 14 000 cases. Figure 3 shows the MDR/RR-TB incidence cases for countries with at least 1000 cases.


**Figure 3.** Estimated incidence of MDR/RR-TB in 2019, for countries with at least 1000 incident cases (WHO, 2020).

Due to the public health burden of TB, more knowledge on the different mechanisms employed by the bacteria to cause infection and overcomes the host immune defence strategies is of need. Hence, the transmission, clinical presentations and physiology of bacteria will be discussed.

## 1.3 Transmission, pathogenesis, and clinical presentations

### 1.3.1 Transmission

TB is an airborne disease that primarily affects the alveolar macrophages (Nardell, 2016). TB spreads from an infected person to a susceptible person through droplet nuclei containing the tubercle bacilli (Turner, 2015). The droplet nuclei are transported by means of sneezing, coughing and close contacts talking. The average human cough bursts 1.5 µm of air out of the lungs containing about 3000 droplets of saliva at speeds of up to 80 km/h (Torrelles and Schlesinger, 2017). However, the most effective droplets to transmit the bacterium are 5-10 µm (Flagan, 2011) as droplets greater in size generally fall to the ground with gravity or get potentially deposited in the upper airways during close contact and are therefore, less effective in disease transmission (Torrelles and Schlesinger, 2017).

Transmission occurs more efficiently indoors where airflow is limited, and residents are concentrated in a small space. Common indoor environments for potential transmission include homes, hospitals, prisons, shelters, schools and most modes of transportation (Creswell, 2015). Although some transmission occurs outdoors, the effect is less likely to cause infection primarily due to the dilution of infectious droplet nuclei in the air (Cheremisinoff, 2018). Main factors that play a role in transmission include, the source of infectiousness, cough aerosols, nature and proximity of contact with the bacteria (Acuña-Villaorduña *et al*., 2018). As transmission is difficult to measure, uncontrolled transmission is another factor that is responsible for fuelling the TB epidemic.

### 1.3.2 Pathogenesis

Inhalation of the droplet nuclei containing the tubercle bacteria is followed by the translocation of the bacilli to the lower respiratory tract where it will encounter the alveolar macrophages. The macrophages are the first cells to be affected by the TB bacteria and engulf bacilli upon interaction (Getahun *et al*., 2015). However, if the innate immune system (first line defence) fails to eliminate the bacteria then the disease will progress, and the tubercle bacteria invades the lung tissue. This route can either directly infect the epithelial cells or indirectly by translocation of the infected alveolar macrophage across the epithelium to the lung parenchyma. Entry to the lung parenchyma leads to the host immune system to develop a specific immunity, whereby *M. tb*-specific lymphocytes migrate to the site of infection and accumulates to form granulomas (Nicholas *et al*., 2016). The granuloma consists of infected macrophages encased by a variety of immune cells including foamy cells, epithelioid cells and multinucleated giant cells (Guirado and Schlesinger, 2013). Granulomas serve to regulate the growth of intracellular *M. tb* and to limit the spread of the bacilli to other locations allowing the bacteria to enter a state of latent pulmonary TB infection (Guirado and Schlesinger, 2013). Conversely, when the granuloma has reached its maximum containment capacity, it is likely to burst releasing the bacilli which can than infect other parts of the body to cause active TB disease (Ahmad, 2010).

Notably, *M. tb* has emerged mechanisms to evade the host immune system, which include the prevention of phagosome-lysosome fusion, the hindering of antigen presentation and modulating cell death pathways in macrophages (Weiss and Schaible, 2015). During the engulfment of the bacteria by the macrophage, the bacilli are stored in the phagosome which matures by fusing with the lysosome (Weiss and Schaible, 2015). This fusion will expose the bacterium to hostile conditions including nutrient starvation, acidic pH, RNIs and ROS

resulting in DNA damage (Weiss and Schaible, 2015). Under these conditions failure to repair damaged DNA drives the process of mutagenesis leading to compromised genome integrity. During TB treatment antibiotics results in the emergence of drug resistance due to mutations in the bacterial chromosomal DNA which the bacteria utilize as a survival strategy to cause further disease.

### 1.3.3 Clinical presentations

When active TB occurs, the body's immune system cannot contain the bacilli and proliferation of the bacteria takes place leading to the different signs and symptoms of TB infection. The resultant symptoms tend to develop over a period of 2-3 weeks, months or even years (Tang *et al*., 2016). Coughs lasting for more than 3 weeks, drastic weight loss, low grade fever, night sweats, and fatigue are some of the main examples of the clinical manifestations for active disease (Tang *et al*., 2016).

## 1.4 Treatment and prevention

Effective drugs were developed in the early 1940s to treat and combat the increased mortality rate due to the TB disease (WHO, 2017). There are four first line drugs (Isoniazid (INH), Rifampin (RIF), Pyrazinamide (PZA) and Ethambutol (EMB) given to patients diagnosed with active susceptible TB for a period of 6 months (PZA,EMB,RIF AND INH for the first two months followed by RIF and INH only, for the remaining four months) (WHO, 2017). However, treatment may fail due to patients not taking the medication regularly as prescribed, incorrect diagnosis, wrong dose of the drug, poor penetration of the drug to the site of infection and use of antagonistic combination of drugs which may lead to the path for drug resistance.

With the emergence of the drug resistant TB epidemic, the drug regimen had to be extended to 9-12 months which included the addition of injectable drugs (WHO, 2017) such as, kanamycin (Kan), amikacin, streptomycin, capreomycin and fluoroquinolones such as, levofloxacin, ofloxacin, moxifloxacin, and gemifloxacin (WHO, 2017). However, resistance of MDR-TB strains against the second line drugs leads to XDR-TB (Kendall *et al*., 2017). XDR-TB can be treated with two repurposed drugs, Bedaquiline and Pretomanid which shows unprecedented potential to effectively cure patients with second line drugs resistance (WHO, 2017).

In terms of preventative measures, there is only one licensed TB vaccine; Bacille Calmette-Guérin (BCG) which has been used for 99 years (Luca and Mihaescu, 2013). Development of this vaccine took about 13 years (Luca and Mihaescu, 2013). Although, this vaccine effectively prevent disease for children from the age of 2 years to adolescence, but it is ineffective in

adults. Although research to find a vaccine that surpasses BCG is ongoing for several decades, currently there is no developments in a vaccine for adults. However, several trials have been conducted to develop TB vaccines and from the phase II outcomes the M72/AS01E candidate is showing promise (Van Der Meeren *et al*., 2018).

### 1.5 Host immune response to infection

Although the *M. tb* bacilli primarily replicate within the macrophages it can however, disseminate into the lymph nodes due to both lymphatic and haematogenous diffusion (Torrelles and Schlesinger, 2017). This results in multiple organs of the body being infected, eventually giving rise to extra-pulmonary disease (Getahun *et al.*, 2015). The complement receptors (CR1, CR2 and CR4) on alveolar macrophages then recognise the bacilli triggering the phagocytosis process (Philips and Ernst, 2012). Phagosome formation facilitates engulfing and killing of the bacteria by increasing acidification and release of reactive oxygen and nitrogen species, which then affect the bacterial DNA and other macromolecules (Gengenbacher and Kaufmann, 2012).

DNA is one molecule that is constantly exposed to damage from both external and internal factors. Damage to DNA can be caused by several factors including varying wavelengths of ionizing radiation and ultraviolet rays, highly reactive oxygen radicals and chemicals in the environment. Moreover, there are other several modifications that can cause DNA damage including, crosslink linkages which are lesions that are caused by UV radiation that leads to reactive interactions that causes the DNA to form linkages (Cadet and Davies, 2017). Single or double base pair mismatches are due to DNA bases that interconvert and single or double strand breaks which are caused by the cell's metabolism such as ROS production which can cause DNA damage by blocking the DNA replication process (Cadet and Davies, 2017). Hence, oxidative stress damage due to reactive radical production is the focus of this study it will be discussed in detail.

### 1.6 Oxidative stress and DNA damage

Oxidative stress is the overproduction of ROS and RNIs as part of the cells host defence mechanism to contain the infection. ROS include free and non-free radical molecules such as hydrogen peroxide, hydroxyl radical, superoxide anion, singlet oxygen, and hypochlorous acid while RNIs include nitric oxide, dinitrogen dioxide, dinitrogen trioxide, peroxynitrous acid and nitrosoperoxycarbonate (Sharma *et al*., 2012). Presence of these various types of stresses results in uncontrolled production of ROS causing progression of oxidative damage to nucleic acids and proteins, enzyme inhibition, apoptosis and eventually cell death (Mittler, 2002).

Thus, efficient anti-oxidative systems that scavenges or detoxify excess ROS and RNIs and repair pathways that repair DNA damage are crucial for cell survival (Foudah *et al*., 2014). Antioxidants are compounds that can counteract unstable molecules like free radicals that cause damage to DNA and other macromolecules of the cell. The antioxidative system for bacterial organisms include superoxide dismutase, glutathione peroxidase and catalase (Nimse and Pal, 2015). Since free radicals lack a full complement of electrons, normally the antioxidants then neutralise these free radicals by giving off some of their electrons. The antioxidants also serve to remove the free radicals (ROS and RNIs) produced during cellular metabolism to prevent cell damage due to oxidative stress (Nimse and Pal, 2015).

Oxidative damage due to ROS can compromise the genomes integrity and consequently cause damage to different macromolecules such as lipids, proteins, and DNA. Oxidative damage in DNA can cause strand breakage, deoxyribose oxidation, DNA-protein crosslinks and mostly single nucleotide base modifications (Imlay and Linn, 1988). ROS affects all four nucleotides in different ways, it converts thymine to thymine glycol which can block DNA replication (Valerie and Povirk, 2003) and can cause spontaneous oxidative deamination of cytosine resulting in uracil. Guanine is converted into 7, 8-dihydro-8-oxoguanine (8-oxoG) by oxidation and adenine is oxidised the same way as the guanine base resulting in 8-oxo-7, 8-dihydroadenine as the product. (Mizrahi and Andersen, 1998, Wallace, 2002).

Oxidative damage is an inevitable consequence of cellular metabolism which results in detrimental base lesions. The effects of DNA damage can lead to different types of mutations including transversions and transitions. For instance, deamination of cytosine to uracil produces G:C→T:A transition mutations (Gedik and Collins, 2005), while 8-oxoG pairs with adenine and cause G:C→T:A transversion mutations (Candeias and Steenken, 2000). In mycobacteria, the oxo-8-gaunine is the most common mutagenic lesion during DNA damage as guanine can rotate on its glycosidic bond pairing with undamaged alkylated base in its sync conformation (Gedik and Collins, 2005). Further, guanine can pair with deaminated alkylated bases in its anti-conformation (Gedik and Collins, 2005). Therefore, oxo-8-guanine damaged bases if not repaired during DNA synthesis can result in mutations in the cell.

Mycobacteria have a high (67%) G+C content, therefore, guanine is more prone to mutations. Moreover, due to its low redox potential between midpoint -1.17 mV on the nickel hydrogen electrode (Candeias and Steenken, 2000), excess oxidized guanine products are produced when exposed to ROS (Yanagawa *et al*., 1992). Lack of repair of damaged bases before replication

can result in the mutation being permanently incorporated into the genome, causing pre-mutagenic lesions leading to further cytotoxic lesions in subsequent replications and eventually cell death.

### 1.7 DNA repair pathways

Maintenance of the cell's genome is essential for the survival of the organism. Since bacterial organisms are continually exposed to different external or internal source of damages that constantly alter the integrity of the cell and if not monitored large amounts of cell damage will occur. However, cells have evolved multiple mechanisms to repair damage and safeguards the genomic integrity of the cell. These include the mismatch repair system (MMR), SOS response and mutagenesis, nucleotide excision repair (NER) and base excision repair pathway (BER) which is the focus in this study.

#### 1.7.1 Mismatch repair (MMR) system

The MMR system repairs mismatched base pairs due to errors that occur during DNA replication, forming a hetero-duplex between homologous DNA strands (Mizrahi and Andersen, 1998). In *E. coli* the MutHLS pathway is responsible for rectifying the mismatches during DNA replication (Marti *et al*., 2002). The MutS protein repair damage by binding to the mismatch and then activates the MutL and MutH endonucleases by ATP hydrolysis. Following this, the MutH incises the methylated *dam* sites and allows DNA helicases to unwind the strands. Polymerase III then facilitates re-synthesis of the DNA strands and DNA ligase seals the nicks (Marti *et al*., 2002).

However, bioinformatics analysis of the genome sequence has revealed that the mycobacterial genome of *M. tb*, *M. smegmatis*, *M. leprae* and *M. bovis* lack the MMR since genes encoding the MutS and MutL MMR proteins could not be identified (Mizrahi and Andersen, 1998, Springer *et al*., 2004). Springer and colleagues showed this, where frameshifts mutation rates were high in *M. smegmatis* parental strain in comparison to normal mutation rates by MutS deficient strains (Springer *et al*., 2004).

#### 1.7.2 SOS response and mutagenesis

The SOS response mechanism is due to DNA damage caused by cell cycle arrest, thereafter DNA repair and mutagenesis is induced to rectify the damage. This is facilitated by the LexA and RecA proteins where LexA is a repressor that binds to the uninduced state of the SOS box (Dos Vultos *et al*., 2009). When DNA damage occurs due to DNA replication blockage, single stranded regions suffice. RecA then controls the expression of genes that promote survival after

DNA damage by binding to single stranded regions of the DNA to form a nucleoprotein filament which stimulates the autocatalytic cleavage of LexA (Dos Vultos *et al*., 2009). This results in the repression of LexA and an increase in SOS gene expression. In *M. tb* all the essential regulatory elements for a functional SOS system are available except for the *polB* and *umuD* genes which are associated with the SOS response and mutagenesis system in *E. coli* (Davis *et al.*, 2002).

### 1.7.3 Nucleotide excision repair (NER) pathway

The NER is a repair pathway that acts on the removal of lesions that distort the DNA double helix that interferes with base pairing resulting in the blockage of DNA transcription and duplication (Costa *et al*., 2003). This damage is commonly associated with bulky lesions like pyrimidine dimers all induced by chemical agents and UV light radiation. To repair the damage, the Uvr protein system recognises the damage with UvrB playing a central role in the repair pathway (Kurthkoti *et al*., 2008). Helicases and endonucleases will open the double helix and cleave the damaged strand (Kurthkoti *et al*., 2008). Thereafter, removal of the DNA segment containing the lesion follows. Thereafter, gap polymerisation using an intact strand as a template to repair the damage follows.

In *M. smegmatis*, the NER pathway has been shown to play an essential role. A UvrB deficient mutant displayed sensitivity when exposed to acidic conditions as generated by sodium nitrate and hydrogen peroxide (Kurthkoti *et al*., 2008). Similarly, a *M. tb* mutant deficient in UvrB displayed sensitivity to UV radiation and hypoxic conditions (Darwin and Nathan, 2005). These findings showed that in mycobacteria the UvrB protein of the NER pathway is essential and plays an important role in DNA repair in mycobacteria.

### 1.7.4 Base excision repair (BER) pathway

The BER pathway is a multi-functional DNA repair system that deals with the repair of base modification like alkylation, oxidation and deamination (Kurthkoti *et al*., 2020). This system requires various enzymes working in synchrony to excise and replace the damaged nucleotide with the correct appropriate base.

BER pathway is facilitated by DNA glycosylases which are the first enzymes in the pathway that recognize and excise the damaged DNA base (Kurthkoti and Varshney, 2011). The DNA glycosylase cleaves the N-glycosidic bond between the sugar and base in the sugar-phosphate backbone to release the damaged base (Fromme *et al*., 2004). This cleavage results in an apurinic/apyrimidinic (AP) site and the resulting gap is filled by DNA polymerases that insert

the correct base with DNA ligase finally sealing the phosphate-sugar backbone of the DNA (Dianov and Lindahl, 1994). The various steps of the BER pathway are shown in Figure 4.

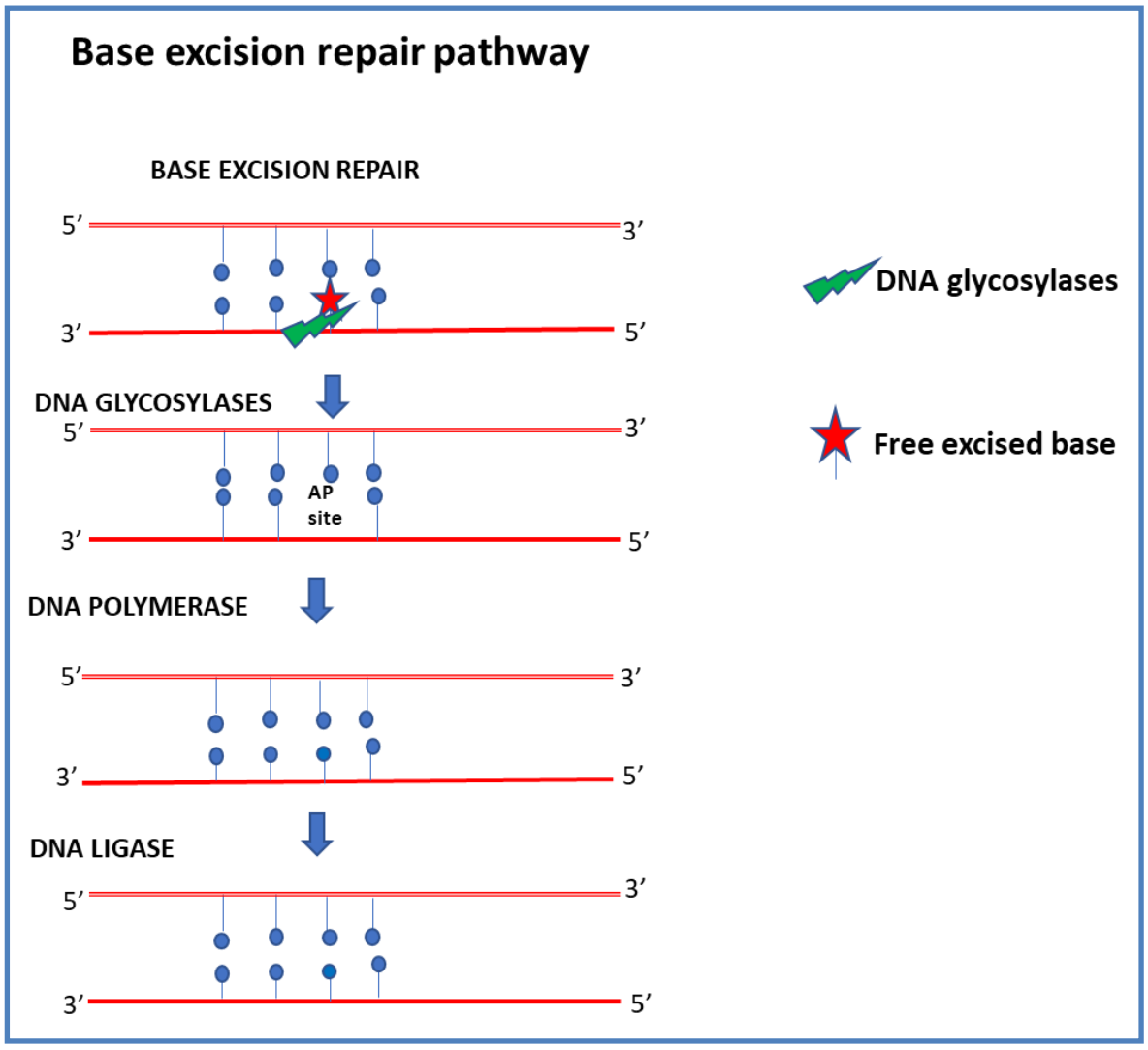


**Figure. 4** An illustration of the base excision repair pathway, facilitated by different DNA enzymes (glycosylase, polymerase, and ligase). This figure is modified from (Kurthkoti and Varshney, 2011).

### 1.8 DNA glycosylases

DNA glycosylases fall under two families based on their structure and sequence homology (Olsen *et al*., 2009). These are divided into the formamidopyrimidine family of endonucleases which constitutes enzymes Fpg/MutM/Fapy that recognize and excise oxidized purines (Wiederholt *et al*., 2005) whilst endonucleasesVIII (Nei) repair oxidatively damaged pyrimidines (Wallace, 2002). The endonuclease III *(*Nth) superfamily, is similar to Nei in that this glycosylase also has the ability to remove oxidized pyrimidine (Cunningham and Weiss, 1985). Moreover, mycobacteria have genetic redundancy in the BER system as bioinformatic analysis have identified two homologues for MutM and Nei DNA glycosylases as well as four

MutT homologues, that deal with damaged DNA bases in the nucleotide pool (Kurthkoti and Varshney, 2012, Mizrahi and Andersen, 1998). The role of each of these enzymes in repairing damaged DNA is discussed in detail below.

The endonucleases VIII (Nei) and endonuclease III *(*Nth) superfamilies repair oxidatively damaged pyrimidines (Moolla *et al*., 2014). The Nth enzyme is widely distributed among prokaryotes, eukaryotes and archaea while Nei is found mostly in proteobacteria, actinobacteria and metazoans (Wallace *et al*., 2003). In mycobacteria there is a single Nth homologue whilst there is a duplication of both the MutM and Nei homologues in both *M. smegmatis* and *M. tb* suggesting that this duplication may be deliberate for the survival of mycobacteria under unfavourable conditions (Sidorenko *et al*., 2008). Moreover, studies have showed an overlapping function between the Nth and Nei DNA glycosylases (Wallace *et al*., 2003, Guo *et al*., 2010, Moolla *et al*., 2014). The Nth and Nei DNA glycosylase can recognise and excise different oxidised bases such as urea, 5, 6-dihydrouracil, 5-hydroxyuracil, 5-hydroxycytosine and methyl hydantoin and both are capable of excising thymine glycol. MutM (Fpg1) recognises and excise 8-oxoG and Fapy lesions (Guo *et al*., 2010). Nei has also been shown to have uracil DNA glycosylase activity, hence during catalysis, the N-terminal proline moiety of Nei attacks the C1' atom of the damaged nucleoside, leading to loss of the base and formation of a Schiff base intermediate (Kropachev *et al*., 2006).

The MutM (Fpg) DNA glycosylase acts on modified purines and catalyses the excision of 8-oxoG to rectify the damage. In addition to the DNA glycosylases, the four *MutT* homologues involved in scavenging the nucleotide pool for oxidised dGTPs ensures that the new base that will be inserted by the DNA polymerase is undamaged (Aguiar *et al*., 2013). Studies show that *MutT* expressing cells have more resistance to oxidative stress when treated with hydrogen peroxide ($H_2O_2$), as well as increased growth both in vivo and in vitro tests (Aguiar *et al*., 2013). In addition, another DNA glycosylase MutY, is present in mycobacteria and is able to identify 8-oxoG mis pairs such as adenine bases with 8-oxoG (Manuel *et al*., 1996). MutY removes the mis-paired adenine base thereby providing a second chance for the Fpg/Nei DNA glycosylases to repair the damaged 8-oxoG lesion. Deficiency of MutY in *M. smegmatis* affected transversion mutations with an escalation in mutation rates and sensitivity to oxidative stress suggesting that MutY plays a role in maintaining mycobacterial genome integrity (Hassim *et al*., 2015). The redundancy of enzymes in the BER suggests that mycobacteria are well equipped to deal with oxidative damage for survival under oxidative stress conditions.

### 1.9 Energy metabolism

In addition to DNA repair mycobacteria also require efficient respiration pathways for energy metabolism and growth. Due to the metabolic flexibility of mycobacteria, adaptation to stressful conditions during pathogenesis allows for survival of the organism. When the electron transport chain (ETC) is energized and maintained throughout the pathway, it allows the bacteria to maintain the metabolic activity and keeps the cell viable. Therefore, energy in the form of adenosine triphosphate (ATP) is required and this activity is driven by the ETC pathway which is elucidated further below.

The ETC maintains the electrochemical gradient of protons in the intermembrane space and electrons in the periplasmic space of the cell for efficient respiration. A disturbance in the electron transport results in the cytochrome terminal oxidases unable to accept electrons nor donate protons for the formation of cellular energy in the form of ATP (Lodish *et al*., 2000). Therefore, electrons will accumulate and form ROS that will propel mutagenesis (Liu *et al*., 2002) whilst un-pumped protons into the inter-membrane space to generate energy will result in cell death.

In prokaryotes, the ETC is made up of several enzymes and enzyme complexes that are found in the cytoplasmic membrane. There are four distinct complexes in the ETC; complex I-IV that regulates the oxidative phosphorylation pathway to generate a proton motive force for ATP synthesis (Figure 5). Complex I and II are two electron donors to the menaquinone pool. Complex I constitute the NADH dehydrogenase which oxidises NADH to $NAD^+$ and electron transfer is initiated to the menaquinone pool while protons are pumped in (Figure 5). In complex II succinate is oxidised to fumarate by the succinate dehydrogenase enzyme and electrons are transferred to the menaquinone pool (Figure 5). Complex III is a cytochrome *c* reductase which oxidises ubiquinol (QH2), reduces cytochrome *c* and pumps protons into the intermembrane space (Figure 5). Complex IV is a cytochrome *c* oxidase, which oxidises cytochrome *c* and reduces molecular oxygen to water, coupled with pumping of protons (Figure 5). Finally, complex V (ATP synthase) catalyses formation of energy in the form of ATP using the adenosine diphosphate (ADP) and inorganic phosphate ($P_i$) (Figure 5).

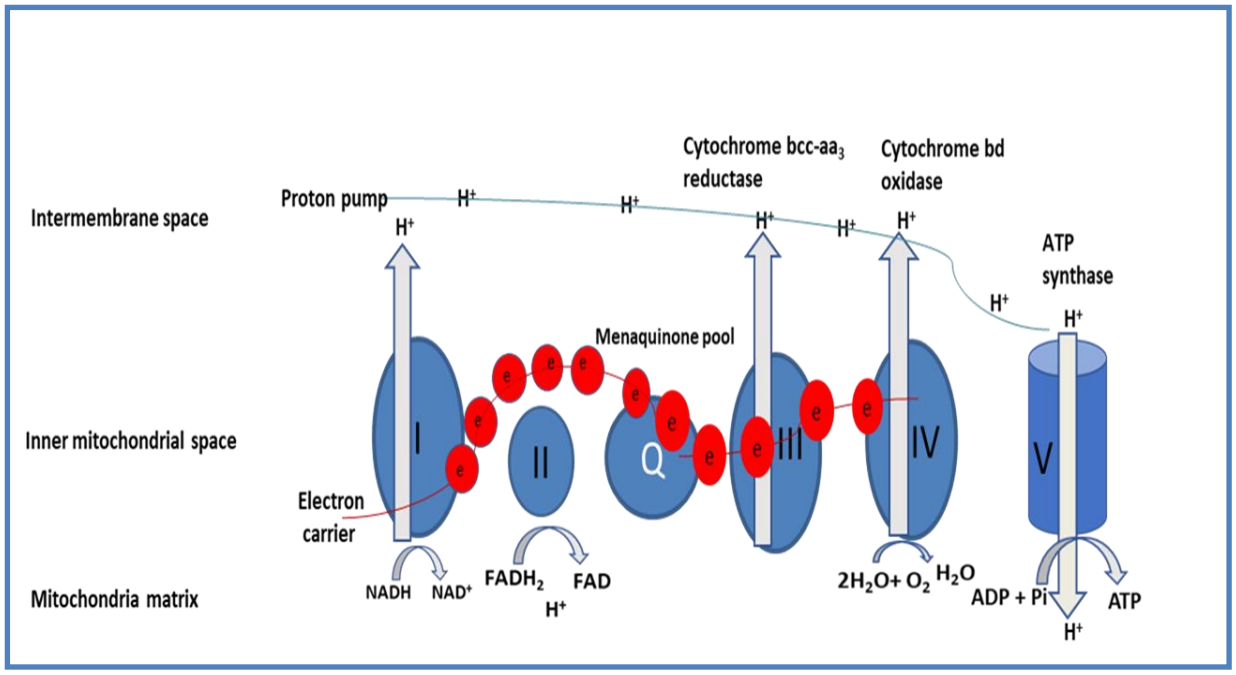


**Figure 5**. Stepwise flow of the ETC pathway of prokaryotic bacteria. The electrons flow from mitochondrial matrix to the inner mitochondrial space (NADH or FADH to the menaquinone pool). Thereafter they move through the cytochrome channels in the inner mitochondrial space. The ATP synthase in the plasma membrane is an energy generating complex. Complex I-IV is shown with an additional ATP synthase complex for energy synthases (V). This figure was modified from (Lodish *et al*., 2000).

### 1.9.1 Mycobacterial ETC

Mycobacteria employ a branched respiratory chain in which electrons are shunted from NADH dehydrogenases and succinate dehydrogenases complexes into the menaquinone pool, from where they are transferred to either of the two terminal oxidases; the cytochrome bcc/$aa_3$ super complex or cytochrome bd (Matsoso *et al*., 2005). The cytochrome bd oxidase plays a crucial role during adaptation to an oxygen depleted environment (Matsoso *et al*., 2005).

The cytochrome bcc/aa3 complex consists of a menaquinol–cytochrome c oxidoreductase named $bc_1$ complex which is encoded by the qrcCAB operon whilst the $aa_3$ type cytochrome c oxidase family is encoded by ctaBCDE (Boshoff and Barry, 2005). Cytochrome bcc/$aa_3$ complex serves as an energy efficient complex as well as a target of the imidopyridine class of drugs (Bloom *et al*., 2012, Pethe *et al*., 2013) but yet no drug candidates have been targeted to cytochrome bd yet. It is also considered as a less energy efficient complex since, it does not show additional proton pumping activity resulting in lower protons/electrons ratio and less efficient ATP compared to cytochrome bcc/$aa_3$ (Miller and Gennis, 1985). This complex has been shown to be essential for mycobacterial growth as generation of *M. smegmatis* mutants

lacking the cytochrome $bc_1/aa_3$ showed a growth defect that resulted in the cytochrome bd to be upregulated to compensate partially for the defect (Kana *et al*., 2001). However, cytochrome bd has been shown to play a crucial role during host infection under stressful conditions which is of high interest lately (Kana *et al*., 2001).

Cytochrome bd is an integral membrane protein complex that constitutes of two subunits, *cydA* and *cydB* (Borisov *et al* 2011). The *cydA* subunit consist of the active quinol binding site and three heme groups (Safarian *et al,* 2016). *M. tb* shares the two subunits and contain genes that encodes *cydDC* which is a putative ABC transporter that has been reported to be essential for biogenesis of cytochrome bd in *E. coli* (Sherperd 2015). However, in *M. smegmatis* the *cydDC* genes are in a separate operon within the same gene cluster as *cydAB* (Aung *et al* 2014).

In *E. coli,* cytochrome bd displays a higher affinity for oxygen, which may facilitate bacterial survival under hypoxic conditions (Poole and cook, 2000). A study by Mascolo and Bald reported findings that confirm that *M. tb* cytochrome bd has a high oxygen affinity and may be an essential factor for metabolic flexibility during host infection, enabling the pathogen to survive the various rapidly changing unfavourable conditions (Mascolo and Bald, 2019). Cytochrome bd is also essential under anaerobic conditions as a culture of *M. smegmatis* grown under oxygen depleted conditions in rich medium showed no significant reduction in the viability of the organism (Kana and Berney *et al* 2014). In addition deletion of the mycobacterial cytochrome bd genes revealed impaired growth in vitro under microaerophilic conditions (Kana *et al*., 2001) and impaired survival under oxidative stress conditions as generated by hydrogen peroxide showed (Lu *et al* 2015).

**1.10 Previous findings that led to this study.**

Much research has been done at the CBTBR to evaluate the role of the different DNA glycosylases in mycobacteria over the past few years. The bioinformatics analysis conducted by Goosens confirmed the previous findings showed that there were two copies each of *Fpg* and *Nei*-encoding genes in both *M. tb* and *M smegmatis* (Goosens, 2009, Mizrahi and Andersen, 1998, Kurthkoti *et al*., 2008). To further understand the function and/or redundancy of these genes in DNA repair, single and combinatorial mutants deficient in these genes were generated and assessed under standard culture conditions and oxidative stress conditions as generated by hydrogen peroxide ($H_2O_2$) in *M. smegmatis*, a non-pathogenic close relative of *M. tb.* These mutants displayed no difference in viability and survival under the conditions

tested suggeting that other DNA glycoyslases or DNA repair enzymes in the BER pathway were compensating for the loss of the Fpg/Nei homologues.

Next the role of the Nth DNA glycosylase was investigated individually and in combination with the Nei DNA glycosylases as these two enzymes although structurally dissimilar are functionally similar in maintaining genome stability (Moolla *et al*., 2014). Moolla and colleagues showed that *nth* displays antimutator properties as deletion of *nth* resulted in increased spontaneous mutation rates against rifampicin and decreased survival under oxidative stress conditions as generated by $H_2O_2$ (Moolla *et al*., 2014). However, under standard aerobic conditions all mutant strains displayed similar growth kinetics to the wild type strain indicating that the Fpg/Nei family and the Nth superfamily of DNA glycosylases are not essential for growth (Moolla *et al*., 2014). In addition, the *nth* single deletion mutant when tested under UV induced conditions showed an increased mutation frequency that was not observed for any of the other single DNA glycosylase deletion mutants suggesting that the *nth* gene had antimutator properties (Moolla *et al*., 2014). As the Nth DNA glycosylase shares functional similarity with the Nei homologues a deletion mutant lacking both the *nei* homologues together with the *nth* gene displayed reduced survival and increased mutagenesis compared to the individual gene deletion mutants, suggesting a synergistic interplay between the *nth* and *nei* genes in the maintenance of genome integrity in *M. smegmatis* under oxidative stress conditions (Moolla *et al*., 2014). To further interrogate the individual role of the two Nei homologues, double deletion mutants lacking the *neiI* or the *neiII* DNA glycosylase in conjunction with *nth* were generated (Rantsi, 2017 unpublished). Phenotypic analysis of the deletion mutants indicated that the NeiI homologue seems to have a greater role in DNA repair for the maintenance of cell integrity compared to NeiII (Rantsi, 2017, unpublished). In this study these DNA repair deficient mutants were further manipulated to include deletion of genes in the ETC to better understand the impact of oxidative stress on the survival of mycobacterial cells.

With respect to the respiratory chain pathway in mycobacteria, several studies have shown that the terminal cytochrome of the ETC may be a potential drug target for development of novel drugs for TB (Lodish *et al*., 2000, Kana *et al*., 2001). Particularly the cytochrome bd as inhibition of the complex resulted in impaired functioning of *M. smegmatis*. Mutant strains of *M. smegmatis* lacking the cytochrome bd quinol oxidase displayed no growth defects compared to the parental strain under standard culture conditions but showed a reduction of bacterial growth under anaerobic conditions (Kana *et al*., 2001). Exposure of the cytochrome bc1/aa3

deficient strain to $H_2O_2$ had little effect on survival whilst the Δ*cydA* deficient in cytochrome bd quinol pathway displayed 99% decreased cell viability within an hour of $H_2O_2$ exposure (Lu et al., 2015b). In oxygen-limiting conditions, cytochrome bd quinol oxidase is up-regulated and this increase could play a role in preventing the collapse of the electron flow during infection thus, ensuring the provision of energy for the cell (Berney and Cook, 2010).

As mycobacterial respiration and energy metabolism provide potential opportunity as drug targets for TB chemotherapy, the ETC has gained much research interest in these past few years. As described above, understanding DNA repair mechanisms and their role in drug resistance is of paramount importance if we are to overcome the persistent current burden and effects of drug resistant TB. Thus, the various mutants lacking genes in the BER pathway and the ETC available at the CBTBR provided a unique opportunity to generate novel deletion mutants defective in both these pathways to explore the role and or interplay between the various genes in maintaining mycobacterial genome integrity and survival under stressful conditions.

## AIMS AND OBJECTIVES OF THE STUDY

This study aimed to generate and phenotypically characterize combinatorial mutant strains of *M. smegmatis* deficient for genes in both the BER and ETC pathways to understand the synergy between these two pathways in maintaining mycobacterial genome integrity under oxidative stress conditions.

### Objectives

Mutants deficient in DNA repair and energy metabolic pathways genes were previously generated at the CBTBR (Chapter 2, Table 1). Hence to achieve the aim of the study the following was conducted:

- Generation of combinatorial deletion mutants lacking genes encoding cytochrome bd oxidase terminal of the ETC (*cydA*) and the DNA glycosylases *nth* and *neiI* using the two-step allelic exchange methodology (Gordhan and Parish, 2001).
- Confirmation of the genotype of the combinatorial deletion mutants by PCR and Southern blot method.
- Assessment of the viability of the mutants under oxidative stress conditions generated by hydrogen peroxide and menadione.
- Assessment of oxidative stress signal within the cell generated by Cumene hydroperoxide, Dithiothreitol and menadione with Flow cytometry.

- Comparison of the spontaneous mutation rates of the various mutants and the respective parental strains using the fluctuation assay.
- Phenotypic characterization of the mutants under biofilm culture conditions to assess growth under hypoxic conditions.

## CHAPTER 2

## METHODS AND MATERIALS

### 2.1 Bacterial strains

The parental and mutant *M. smegmatis* strains (Table 1) were grown in Middlebrook 7H10 solid media supplemented with 0.5% glycerol and 1% glucose salts or Middlebrook 7H9 liquid media supplemented with 0.2% glycerol, 1% glucose salts and 0.05% Tween 80 with shaking at 37℃ (Labcon incubator). For selection, the media was supplemented with Kan at 25 µg/ml, 75% sucrose and 2% X-gal when necessary. All culturing of the strains was carried out in a Bio-safety level 2 laboratory. All cultured strains were stored as freezer stocks in 66% glycerol in the -80℃ freezer. The composition of the components mentioned above are discussed in detail in Appendix A.

**Table 1. *M. smegmatis* and *E. coli* strains used in this study.**

| Strain | Features | Source |
|---|---|---|
| $mc^2$ | High-frequency transformation mutant | Snapper *et al*., 1990 |
| Δ*nth* | Derivative of $mc^2$155 carrying a 570bp deletion in the *nth* gene | Moolla *et al*., 2014 |
| Δ*nei* | Derivative of $mc^2$155 carrying a 486bp deletion in the *neiI* | Goosens MSc dissertation unpublished, 2009 |
| Δ*nth*Δ*neiI* | Derivative of $mc^2$155 carrying a 570bp deletion in the *nth* gene and a 486bp deletion in the *neiI* gene | T. Rantsi MSc dissertation unpublished, 2017 |
| Δ*nth*Δ*neiII* | Derivative of $mc^2$155 carrying a 570bp deletion in the *nth* gene and a 486bp deletion in *neiII* gene | T. Rantsi MSc dissertation unpublished, 2017 |
| Δ*cydA* | Derivative of $mc^2$155 carrying a marked deletion in *cydA*; $Km^r$ | (Kana *et al*., 2001) |
| Δ*nth*Δ*cydA* | A derivative of Δ*nth* carrying a marked deletion in *cydA*; $Km^r$ | This study |
| Δ*nth*Δ*neiI*Δ*cydA* | A derivative of Δ*nth*Δ*nei* carrying a marked deletion in *cydA*; $Km^r$ | John, Honours dissertation unpublished, 2018 |
| *PcydA* | An E.coli derivative carrying a marked deletion in *cydA*; $Km^r$ | (Kana *et al*., 2001) |

| | | |
|---|---|---|
| $mc^2$-GFP<br>*Δnth-GFP*<br>*ΔneiI-GFP*<br>*ΔnthΔneiI-GFP*<br>*ΔcydA-GFP*<br>*ΔnthΔcydA-GFP*<br>*ΔnthΔneiIΔcydA-GFP* | Derivatives of the $mc^2$ 155 carrying the plasmid expressing mycoredoxin-1 coupled with a redox-sensitive GFP tag (GFP-reporter). | This study |

$Km^r$ =kanamycin resistant, GFP=green fluorescent protein

### 2.2 Chemicals and reagents

All cloning vectors (Table 2) and primers (Table 3) used in this study were supplied by Inqaba Biotech Company. Enzymes were provided by Roche, New England Biolabs or Fermentas.

**Table 2. Cloning vectors used in the study for mutant generation.**

| Vector | Characteristics | Size | Culture media | Reference |
|---|---|---|---|---|
| pCYDAaphKO | pBk1 carrying *cydA*:*aph*, *hsp60-sacB,* and *hsp60-lacZ*; used for targeted knockout of *M. smegmatis cydA*; $Km^r$ | 13 055 bps | LA/LB with amp and X-gal | Kana *et al*., 2001 |
| pTweety | Mycobacterial integrating vector; $Km^r$, oriE, int | 5308 bps | 7H10 with X-gal and kan | Pham *et al*., 2007 |

$Km^r$=kanamycin resistant; int = integrating site, OriE = origin of replication, Kan =kanamycin

**Table 3. PCR primers used for conformation of strains.**

| Gene | Primer sequence (5' to 3') | Annealing temperature | Amplicon sizes (bp) |
|---|---|---|---|
| NthCF | GGCATATGAGTGCGGGTGCCGCCCGG | 65℃ | WT=833 MUT=270 |
| NthCR | GCGCCTGCAGTCACCAAACCGCCAGCGC | | |
| NeiF | GGCCCCGGGATGAGGGGCACACCCTG | 63℃ | WT=801 MUT=270 |
| NeiR | GGCGGATCCTCAGGACTGAGGTGGG | | |
| CydUSscrF | CTTCTCCTCGTAGCTGCGC | 57℃ | WT=157 MUT=1400 |
| CydDSscrR | CGTCCTTCTCGGTCCTCAC | | |

WT= wild type strain; MUT=mutant

### 2.3 Generation of mutants by homologous recombination

The two-step homologous recombination method was used to generate the Δ*nth*Δ*cydA* deletion mutant described by (Gordhan and Parish, 2001). A suicide vector (p*cydAaphKO*) containing a non-functional copy of *cydA* disrupted by the *aph* gene encoding for kanamycin (kan) with selectable marker genes (*lacZ,* and *sacB*) (Kana *et al*., 2001) was introduced into the *Δnth* DNA glycosylase deficient strain. A single crossover (SCO) event between the chromosome and one of the regions of homology on the vector results in the integration of the vector into the chromosome. Post electroporation clones that have undergone a SCO event were identified on 7H10 media supplemented with Kan antibiotic and X-gal for blue/white selection. The *lacZ* gene breaks down X-gal to 5-bromo-4-chloro-indoxyl resulting in blue colonies. The SCO containing both the wild type and truncated *cydA* genes together with the selectable marker genes (*aph*, *lacZ,* and *sacB*) than underwent a second crossover selection process. Counter selection of the SCO clones to identify double cross over (DCO) clones containing the mutated *cydA* allele were identified on sucrose supplemented 7H10 media. The *sacB* gene encodes for levansucrase which breaks downs sucrose to levan which is toxic to cells and results in death. Hence, only colonies that have lost the *sacB* and the *lacZ* genes during the second cross over event will be white and resistant to sucrose. These colonies were then screened by PCR and Southern blot analysis to identify the positive deletion mutant strains. An illustration of the homologous recombination technique is shown in Figure 6.

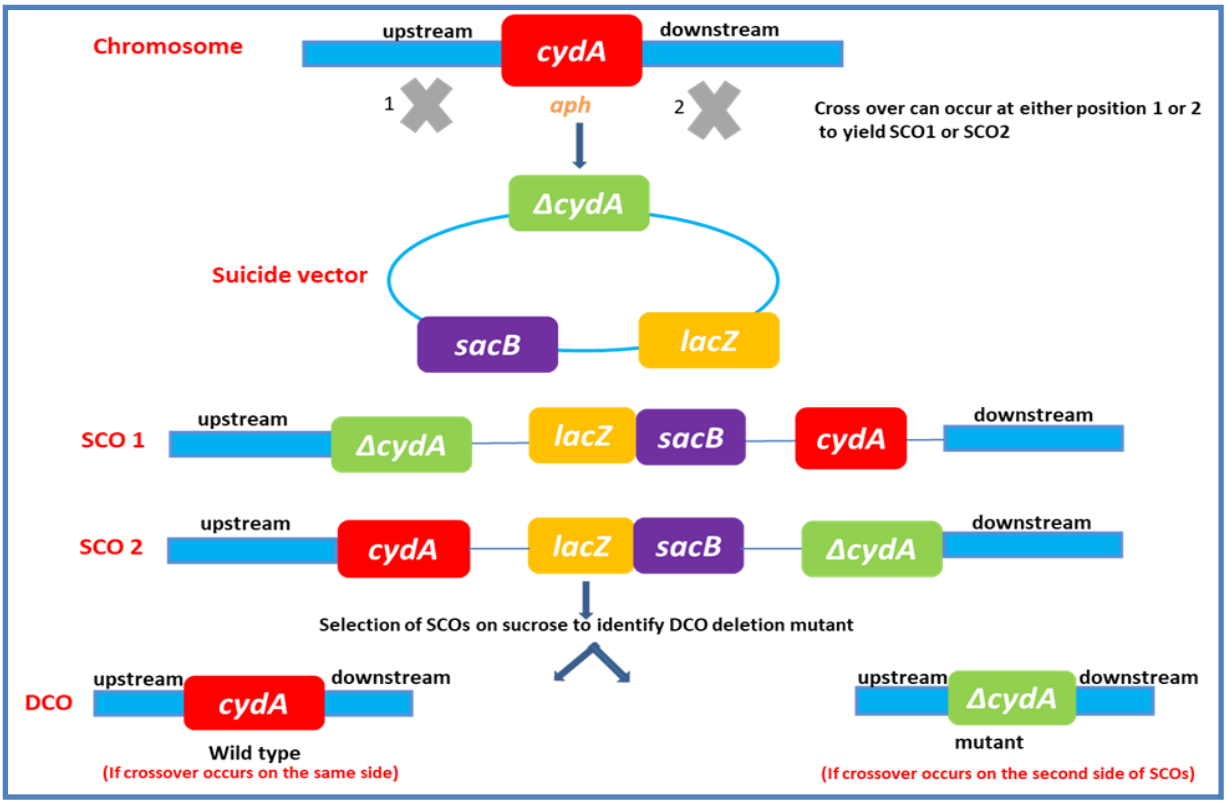


**Figure 6. Illustration of the *cydA* gene deletion by homologous recombination** in the *Δnth* DNA repair deficient mutants to generate the *ΔnthΔcydA* mutant strain. A suicide vector containing the mutated *cydA* gene can crossover into the chromosome at either site 1 or 2 resulting in single cross over (SCO1 or SCO2) mutants both the wild type and truncated *cydA* genes together with the selectable marker genes (*aph*, *lacZ*, and *sacB*). Counterselection of the SCO on sucrose supplemented media allowed for the second cross over event to occur resulting in either the wild type genotype if the crossover took place on the same side or the mutant strain if the crossover occurred on the second side.

### 2.3.1 Preparations of competent *M.smegmatis* cells

A 100 ml culture for all strains from freezer stocks was grown to mid-log phase of $OD_{600nm}$ = 0.5-0.8 overnight. Cells were harvested by centrifugation at 2360 xg and 4℃ for 10 minutes. The bacterial cell pellet was re-suspended in 10 ml of 10 % glycerol (ice cold) and harvested as mentioned. The washing steps were repeated three times to make the cell wall weaker. Thereafter, the cell suspension was resuspended in 1 ml of cold 10% glycerol and dispensed into 300 µl aliquots in micro centrifuge tubes and stored on ice until use.

### 2.3.2 Electroporation into compentent *M.smegmatis* cells

The BIO-RAD GENE PULSER XCell system was used to perform electroporation using parameters; 2500V, 25 µF, 1000Ω and 0.2 cm. Four different concentrations (5 µg, 10 µg, 20 µg, and 30 µg) of plasmid DNA (*pcydAaphKO*) was added to separate aliquots of the electro-competent cells and mixed gently by inverting up and down, then transferred to 0.2 cm

electroporation cuvettes. The control samples: positive (*pTweety*, 1 µg) and negative (cells only) were also mixed with the cells and transferred into an electroporation cuvette. The cells were pulsed and 800 µl of 2×TY was added to the samples and incubated overnight to allow for phenotypic expression of the selectable marker genes (*lacZ* and *sacB*). Thereafter, the cells were spread on 7H10 plates supplemented with 2% X-gal and Kan and incubated for 7 days at 37℃ .

### 2.4 DNA Extraction from *M. smegmatis.*

#### 2.4.1 Small scale genomic DNA extraction (colony boil).

A single colony (10 mm diameter) of *M. smegmatis* was re-suspended in 50 µl of distilled water, mixed into a suspension and boiled at 95℃ for 2-3 minutes in the heating block. The mixture in the 1.5 ml micro centrifuge tubes was cooled on ice for a minute and then centrifuged at 12470 xg for 5 minutes to separate the cellular debris. Chloroform (50 µl) was added to the suspension and mixed by tapping to lyse the cells. The suspension was centrifuged at 12470 xg for 5 minutes and the top aqueous layer containing the DNA was transferred into a sterile 1.5 ml micro centrifuge tube without disturbing the cellular debris. The DNA was used for PCR as described in section 2.8.1.

### 2.4.2 Large scale genomic DNA extractions

The cetyltrimethylammonium bromide (CTAB) method was used to isolate chromosomal DNA from solid culture. Loopfuls of cells from a full solid culture plate was resuspended in 500 µl of TE buffer. Cells (500 µl) were heat killed at 75℃ for 20 minutes then cooled on ice for 5 minutes followed by the addition of 50 µl lysozyme (10 mg/ml) to the suspension and incubation at 37℃ for an hour to break down the cell wall. Thereafter, 6 µl of proteinase K (10 mg/ml) and 70 µl 10% SDS were added to the suspension, mixed by gently tapping the tube and incubated for 2 hours at 65℃ for protein digestion. Following this, 100 µl of 5 M NaCl and 80 µl of warm CTAB/NaCl solutions were added to the suspension and incubated at 65℃ for 10 minutes to aid in the separation of proteins bound to the DNA. An equal volume (750 µl) of chloroform-isoamyl alcohol (24:1) was added, mixed then centrifuged at 12470 xg for 10 minutes. The top aqueous layer was aliquoted into a fresh 1.5 ml micro centrifuge tube containing 450 µl of isopropanol and the DNA was precipitated by centrifugation at 12470 xg for 20 minutes. The pellet was washed with 1 ml of 70% ethanol (ice cold) by centrifugation at 12470 xg for 5 minutes. The pellet was dried at 60 ℃ in the speed vac (Thermo Fischer Scientific™) for 10 minutes and then resuspended in 50-100 µl of TE buffer.

### 2.4.3 Mini-prep plasmid DNA extraction

An *E. coli* culture grown in 2 ml LB media to stationary phase, was centrifuged at 12 470 xg for 5 minutes, the supernatant discarded, and the pellet was resuspended in 100 µl of solution I. The cells were incubated at room temperature for 10 minutes before adding 200 µl of solution II. The contents of the tube were mixed by inverting the tubes 6-8 times and incubated in ice for 5 minutes. Next 150 µl of precooled solution III was added, mixed and the tube incubated on ice for 5 minutes. The suspension was then centrifuged for 5 minutes and using a 200 µl pipette, the supernatant was transferred into a fresh Eppendorf tube to which 100 µl of RnaseA was added and incubated at 42 ℃ for 10 minutes. The DNA was precipitated with the addition of 450 µl of isopropanol and centrifugation at 12470 xg for 20 minutes. The supernatant was discarded making sure the pellet is not dislodged. The pellet was washed with 70% cold ethanol (1 ml) and centrifuged at 12 470 xg for minutes. The supernatant was poured off and the pellet was vacuum dried for 10 minutes at 60℃. The pellet was resuspended in 50 µl distilled water and quantified using the nanodrop (section 2.5). The DNA was stored at -20 ℃ until use for downstream experiments.

### 2.5 Nucleic acid quantification

The DNA was quantified using the Nanodrop ND-1000 spectrophotometer (Nanodrop Technologies). The system quantifies DNA by measuring absorbance of the sample at a wavelength of 260 nm.

### 2.6 Restriction digestion of plasmid and genomic DNA

Restriction enzymes are enzymes that cleave DNA at specific sites. All restriction enzymes used were purchased from New England Biolabs (NEB) or Roche Applied. Clone manager software was used to select the enzymes to cut the genomic DNA of the parental and mutant strains. A master mix for the genomic DNA digest (10-20 µl reaction) was prepared with the components; 1 µl buffer, 1 µl enzyme, 3 µl nuclease free water and 5 µl of DNA. The DNA was digested by incubation at the recommended temperature for the chosen enzyme. For plasmid screening, about 0.5-1 µg of plasmid DNA (*pcydAaphKO*) was digested in a reaction volume of 10-20 µl (master mix as stated in above reaction) and incubated at 37℃ for an hour whilst genomic DNA for Southern blot analysis was digested overnight (not more than 16 hours). The digested DNA was analysed and viewed on an agarose gel (Section 2.7).

### 2.7 Visualisation of DNA by agarose gel electrophoresis

Gel electrophoresis was used to separate DNA fragments according to size. A 1% agarose gel was prepared using 1x TAE buffer to which ethidium bromide (0.5 µg/ml) was added. Ethidium bromide intercalates between the DNA and fluoresces under UV light therefore, allowing visualization of the DNA. The DNA samples were mixed with loading dye to allow for the samples to sink into the wells of the gel and for tracking the DNA sample during electrophoresis. An appropriate Roche Applied Science molecular weight marker was selected to determine the size of the DNA fragments. The electrophoresis process was performed in 1x TAE buffer at a voltage of 80 and gel visualization was done under UV light, using the SYNGENE G-box system (BIORAD).

The percentage of gels used differs based on the pore sizes which are directly related to the migration of the different DNA fragments. For instance, for small fragments 2% gels were used for good separation whilst large fragments were separated on 0.8% gels. Gels were poured on a level surface and ran at a low voltage for even separation of the fragment. High voltage generates heat causing the gel to swell and enlarge the pore size which, causes the bands to diffuse.

## 2.8 DNA manipulations

### 2.8.1 DNA amplification to confirm mutant strains by Polymerase Chain Reaction

Polymerase Chain Reaction (PCR) is a screening procedure that amplifies a specific region of a DNA target. The PCR reactions were made to a volume of 25 µl with the components: 2.5 µl of 10x buffer, 5 µl 5x GC Rich solution, 4 µl of dNTPs (stock concentration 2.5 mM), 2.5 µl (10 mM) forward and reverse primers each, 0.2 µl of Roche Faststart Taq polymerase, 3.3 µl of nuclease-free water and 5 µl of template DNA (at a concentration between 20-100 ng). Control reactions (non-template control) were included in all PCR reactions to rule out DNA contamination or non-specific amplification.

The thermo cycler system (Bio-Rad laboratories) was used to carry out the reaction. Cycling conditions used were as follows; one cycle of initial denaturation at 94 ℃ for 4 minutes in order for the DNA polymerase to be heat activated, 30 cycles of denaturation at 94℃ for 30 seconds to break down the hydrogen bonds of double stranded DNA into single strands, 30 cycles of annealing for the primers at primer specific temperature to bind to the single stranded DNA, 30 cycles of initial elongation at 72℃ for 30 seconds to synthesize new complementary DNA and a final single elongation step at 72 ℃ for 5 minutes to ensure all the single stranded DNA have been fully elongated. Notably, the annealing temperature was specific for each primer set used (Table 3). This PCR reaction method was used for the confirmation of existing and newly generated deletion mutant strains.

## 2.9 Southern blot analysis to confirm deletion of a gene in the mutant strains

Southern blot is a method that allows for the identification of a specific DNA sequence within a chromosome. The digested DNA fragments are separated by size and charge using gel electrophoresis and identified using a radioactively labelled hybridising probe. The various steps involved in this process are discussed below and shown in Figure 7. In this study the genotype of mutants at the deletion site was confirmed by the Southern blot method.

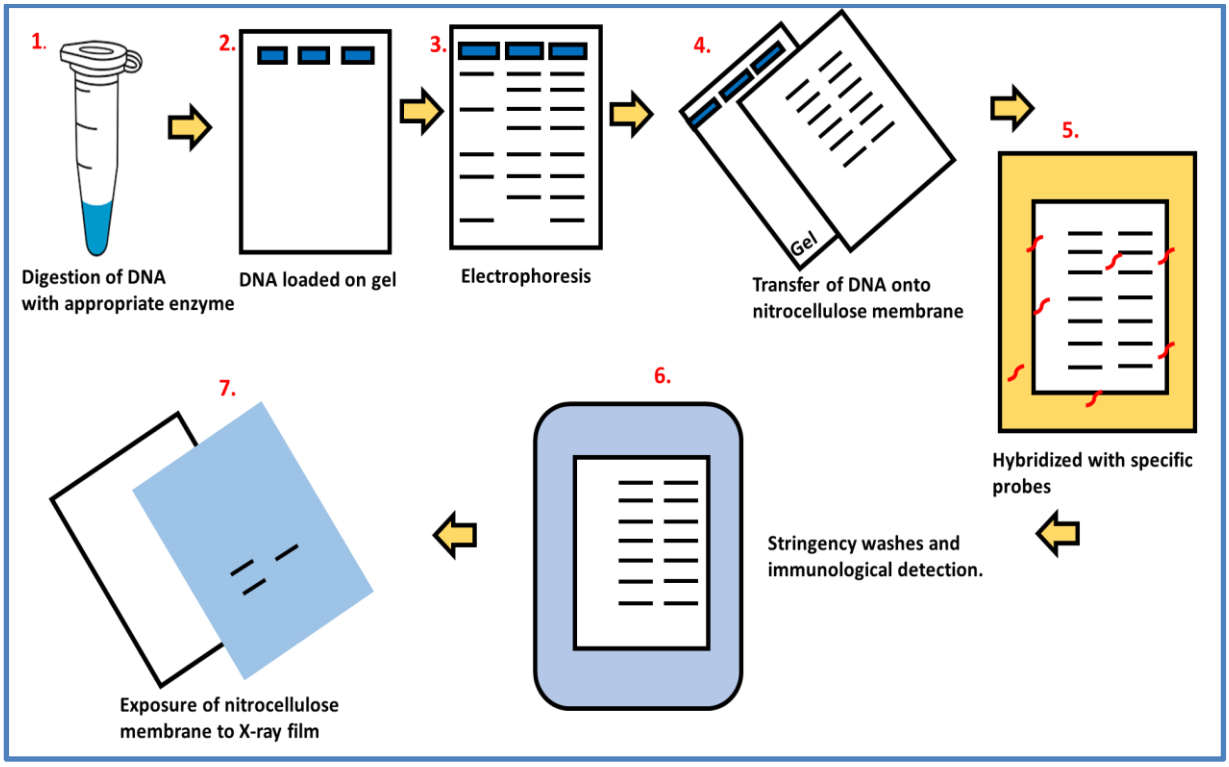


**Figure 7. Schematic illustration of the Southern blot analysis method.** *M. smegmatis* parental and mutant strains genotypes were confirmed with Southern blot analysis. (1) The DNA was digested with the appropriate enzyme overnight and thereafter the DNA was run on a 0.9% agarose gel for 2 hours (2). **(**3-4) Following the gel was transferred onto the nitrocellulose membrane with electrophoresis. (5) Hybridisation with the specific probe was performed overnight at 42 ℃ . Stringency washes and immunological detection of the membrane was done (6) then finally the exposure of the nitrocellulose membrane to the X-ray film for 30 minutes was carried out.

### 2.9.1 Electro-blotting

Briefly, approximately 5 µg of genomic DNA from the parental strain, SCO and DCO mutants was digested with either KpnI, PstI at 37 ℃ overnight (Figure 7 (1)) as detailed in section 2.6. The DNA was then separated on a 0.9% agarose gel together with marker IV for approximately 2 hours (Figure 7 (2) and 7(3)). An image of the gel was taken using a ruler under UV light, using the SYNGENE G-box system (BIORAD). Thereafter, the separated DNA was prepared for transfer to a nitrocellulose membrane (Figure 7 (4)).

The gel was soaked in denaturation solution (0.2M HCl) for 15 minutes with shaking every 5 minutes. When the loading dye on the gel turned yellow because of the lower pH, denaturation solution was decanted, the gel was rinsed with ds$H_2O$ twice. The DNA was denaturated by the addition of depurination solution (0.5M NaOH/ 1.5 M NaCl) to the gel and left for 30 minutes with shaking every 5 minutes. Once the incubation period was over depurination solution was

decanted, and the gel was equilibrated in 1 × TBE buffer. Thereafter, the gel was transferred to the nitrocellulose membrane (6.5 9.5 cm - Amersham Biosciences) in a sealed cassette as follows. Two sponges soaked in TBE buffer were placed on the base of the cassette followed by two soaked filter papers (Whitman), then the gel (well side facing up) on top of which the nitrocellulose membrane with a cut on the right corner was placed. Finally, two more soaked filter papers and two sponges were placed on top of the nitrocellulose membrane and the cassette sealed. The cassette was placed in an OmniPAGEElectro-blotting Unit (Cleaver Scientific Ltd CS-300V) and the DNA transferred from, the gel onto the nitrocellulose membrane for 2 hours at 0.5V, 0.6A. The DNA was cross-linked at 2000 mJ/cm$^2$ in a strata linker onto the nitrocellulose membrane (Amersham Biosciences) using a UVC 500 Crosslinker (Amersham Biosciences) (Figure 7 (4)).

### 2.9.2 Probe labelling

An appropriate probe was designed to bind specifically to the relevant homologous regions of the genomic DNA to allow identification of the DCO mutant from the SCO and the parental strains. PCR DIG Probe Synthesis kit (Roche) was used as per manufacturer's instructions to generate the labelled dUTP probe. The PCR reaction was prepared with the same components as mentioned in section 2.8.1 except with the addition of labelled dNTPs (DIG-dUTP;2.5 µl) to the components. The annealing temperature used was 57ºC for the Cyd primers and 65 °C for Nth primers. An unlabelled control was included, and the fragments were analysed on a 1% agarose gel. The labelled DIG-dUTP is expected to run slower than the unlabelled amplicon as it has a higher molecular weight.

### 2.9.3 Hybridisation

Nitrocellulose membranes with the bound DNA were pre-hybridised using the Hybaid HB-OV-BM roller bottle (Thermo Scientific) for 30 minutes in 12 ml DIG Easy Hyb solution from the DNA High Prime DNA labelling and Detection Starter kit II (Roche biochemicals). The labelled probes were denatured at 95℃ for 10 minutes then 22 µl was added to the pre-hybridisation solution. Hybridisation was carried out overnight at 42°C in Hybaid HB-OV-BM roller bottles (Figure 7(5)). After the hybridization period the Hyb buffer and probe were transferred into a Falcon tube and stored at -20℃ . Thereafter, membranes were subjected to stringency washes (to remove unbound probe and to decrease the background on the blots. First the membrane was washed twice in solution I (2× SSC, 0.1 % SDS) at 68°C for 5 min followed by two washes with solution II (0.5 × SSC, 0.1 % SDS) at 68 ℃ (Figure 7 (6)).

### 2.9.4 Immunological detection

For immunological detection of the signal, the membrane was placed in blocking solution for 30 minutes followed by incubation in antibody solution for 30 minutes. The membrane was washed twice and briefly equilibrated for 5 minutes in detection buffer. The membrane was then placed in a hybridization bag with 1ml of substrate (CSPD) and incubated at 37 ℃ for 10 minutes. The membrane was exposed to X-ray film (CL-Xposure$_{Tm}$ Film, Thermo Scientific) for an hour (Figure 7 (7)) and developed by placing it in developer fluid for 40-60 seconds with shaking, then rinsed with water. The developed film was then immersed in fixer fluid for 40-60 seconds with shaking, rinsed with water and dried by hanging it up on a string (Figure 7 (7)).

## 2.10 Phenotypic characterization of deletion mutants

### 2.10.1 Growth Kinetics under normal culture conditions.

Briefly, a pre-culture of the parental *M. smegmatis* and mutant strains (Δ*nth*, Δ*neiI*, Δ*nth*Δ*neiI*, Δ*cydA*, Δ*nth*Δ*cydA*, and Δ*nth*Δ*neiI*Δ*cydA*) was started from a 1 ml freezer stock in 5 ml 7H9 media and incubated at 37 °C overnight with shaking at 100 rpm. The overnight pre-culture was diluted to an $OD_{600nm}$ = 0.01 in 50 ml 7H9 media and incubated at 37°C with shaking at 100 rpm. The growth rate was determined by monitoring the $OD_{600nm}$ at 3-hour intervals for 24 hours. Colony forming units (CFU) counts were also computed to confirm the number of bacteria by making 10-fold serial dilutions at each time point and select dilutions were spread on 7H10 agar plates. The plates were incubated at 37°C for 3-4 days, following which colonies were counted and CFU/ml was determined. The $OD_{600nm}$ data for the growth rate was represented as scatter plots and bar charts for the CFU counts.

### 2.10.2 Survival of various deletion mutants under oxidative stress conditions

The ability of bacterial strains to survive under oxidative stress conditions as generated by hydrogen peroxide was tested. The parental *M. smegmatis* and mutant strains (Δ*nth*, Δ*neiI*, Δ*nth*Δ*neiI*, Δ*cydA*, Δ*nth*Δ*cydA*, and Δ*nth*Δ*neiI*Δ*cydA*) were grown in 30 ml 7H9 supplemented with Kan where necessary to an $OD_{600nm}$ of 0.35. Hydrogen peroxide (2.5 mM) was added to each culture, the flasks were covered in foil to prevent degradation of $H_2O_2$ and incubated at 37℃ with shaking. For each strain, an untreated culture was included as the control. Viability of the cells for the treated and untreated cultures was monitored at 2 hourly intervals over 6 hours. These cultures were serially diluted and 100 µl aliquots of the appropriate dilutions were

plated on 7H10 plates and incubated at 37 ℃ for 3-4 days before scoring colonies for growth. The details of the experimental process are shown in Figure 8.

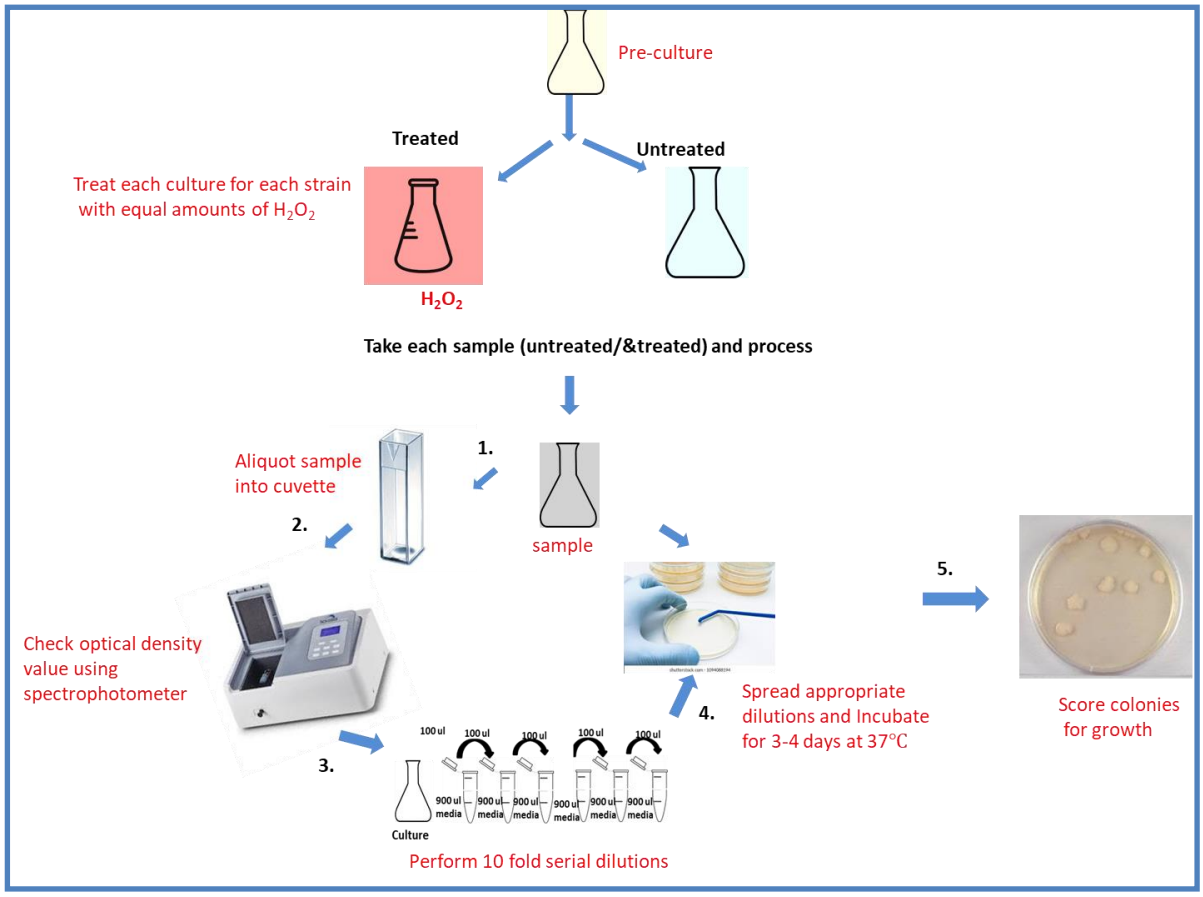


**Figure 8. Illustration of the hydrogen peroxide assay.** The wild type ($mc^2$) and mutant strains (Δ*nth*, Δ*nei1*, Δ*nth*Δ*nei1*, Δ*cydA*, Δ*nth*Δ*cydA* and Δ*nei1*Δ*nth*Δ*cydA*) were exposed to oxidative stress ($H_2O_2$) to assess the ability of the strains to survive under these unfavourable conditions. **(1)**. The culture of each strain was aliquoted into a cuvette which was inserted into the spectrophotometer to check the $OD600_{nm}$ **(2)**. Thereafter, serial dilutions were prepared **(3)** and the appropriate dilutions were spread on the plates then incubated for 3-4 days at 37 ℃ **(4)**. Finally, the plates are scored for growth **(5)**.

### 2.10.2.1 Redox state assessment of the GFP-marked mutant strains using CHP, DTT and menadione.

The redox heterogeneity of cells was assessed for oxidative stress response to cumene hydroperoxide (CHP) oxidant, dithiothreitol (DTT) reductant and menadione. The CHP and DTT treatments serve as controls to represent 100% oxidation and 100% reduction respectively of the cells. A plasmid expressing mycoredoxin-1 coupled with a redox-sensitive GFP tag (Bhaskar, 2014) was introduced into the *M. smegmatis* parental strain and the various mutant strains (Table 1). These strains *(*$mc^2$*-GFP, Δnth-GFP, Δnei1-GFP, ΔnthΔnei1-GFP, ΔcydA-GFP, ΔnthΔcydA-GFP and ΔnthΔnei1ΔcydA-GFP)* were grown to exponential phase ($OD_{600nm}$

= 0.5-0.8). The cells were treated separately with CHP (10mM), DTT (40mM) and menadione (1mg/ml) in a total volume of 1500 µl for 5 minutes. After treatment, the cells were harvested and resuspended in phosphate buffered saline (PBS). About 20 000 cells were analysed for each strain using the Beckman Coulter Gallios flow cytometer (Beckman Coulter, USA). Excitation of the cells was measured by the biosensor between 405 and 488 nm. The redox potential of the cells was measured at an emission of 510 nm. Data was analysed using the FCSalyzer software.

### 2.10.3 Biofilms

#### 2.10.3.1 Biofilm culturing

Bacteria have the ability to attach to solid surfaces and form biofilms that constitutes a matrix of polysaccharides, proteins and nucleic acids (Flemming and Wingender, 2010). This matrix aids in protecting bacteria against exposure to desiccation, biocides, and antibiotics, (Flemming and Wingender, 2010). During formation of the biofilm microorganisms on the surface consume oxygen creating an oxygen-depleted (hypoxic) environment.

*M. smegmatis* parental strain and the mutant strains were grown in 10 ml 7H9 media overnight at 37℃ until stationary phase ($OD_{600nm}$ = 2). The cells were harvested and re-suspended in Sauton's media (0.4% asparagine, 0.05% $MgSO_4$, 0.2% citric acid, 0.05% ammonium ferric citrate and 60% glycerol) and washed twice in the same media, after which the pellet was resuspended in 1 ml of Sauton's media. The cells were diluted to an $OD_{600nm}$ = 1 and the appropriate volume was aliquoted into a 24 well plate. The plates were sealed with biohazard tape and incubated at 37℃ for 7 days for biofilm formation (Figure 9).

#### 2.10.3.2 Microscopy to visualize biofilm formation.

The Zeiss Stemi 2000 stereomicroscope, together with the Zen software was used to capture images of colonies growing on solid media and in biofilms for the parental and mutant strains to identify any morphological variations due to deletion of the various BER and ETC enzymes (Figure 9 (1)). Two magnification points were used to view the biofilms at 1x and 1.25x at a scale of 100 pixels.

#### 2.10.3.3 Biomass quantification of biofilms

Biomass quantification of biofilms is a method that assesses the biofilm maturity by quantifying the formed biofilm. Staining with crystal violet dye was carried out to quantify the biofilm biomass. Once the biofilms are formed, 1 ml of crystal violet (10 ml 95% ethyl alcohol, 0.4 g ammonium citrate monohydrate and 40 ml deionized water) was aliquoted to each well

and allowed to stain at room temperature for 10 minutes. The cells beneath the biofilm were removed with a pipette without disrupting the biofilms. One ml of absolute ethanol was added to each well and cellular material from the sides of the well were dislodged from the edges, mixed, and incubated for 15 minutes at room temperature. Each sample was diluted to 1:100 and the $OD_{600nm}$ was measured (Figure 9 (2)). The data were represented as a function of the biomass for each strain. The experiment was done in triplicate for statistical significance.

#### 2.10.3.4 Cell adherence capacity of biofilms

Cell adherence is a method that assesses how cells attach to the biofilm surfaces. The contents of the biofilm plates were decanted by turning the plates over into a container. Crystal violet was added to each well to stain any remaining cells on the sides of the well and the plates incubated at room temperature for 10 minutes after which the crystal violet was removed. Plates were dried (upside down) for 10 minutes and 1 ml of 100% ethanol was added to each well and incubated for 15 minutes. While incubating, the mixture in each well was mixed with a pipette tip to disperse the cellular material. Each sample was diluted 1:100 and the $OD_{600nm}$ was measured (Figure 9 (3)). The data were represented as a function of cell adherence for each strain and the experiment was done in triplicate for statistical significance.

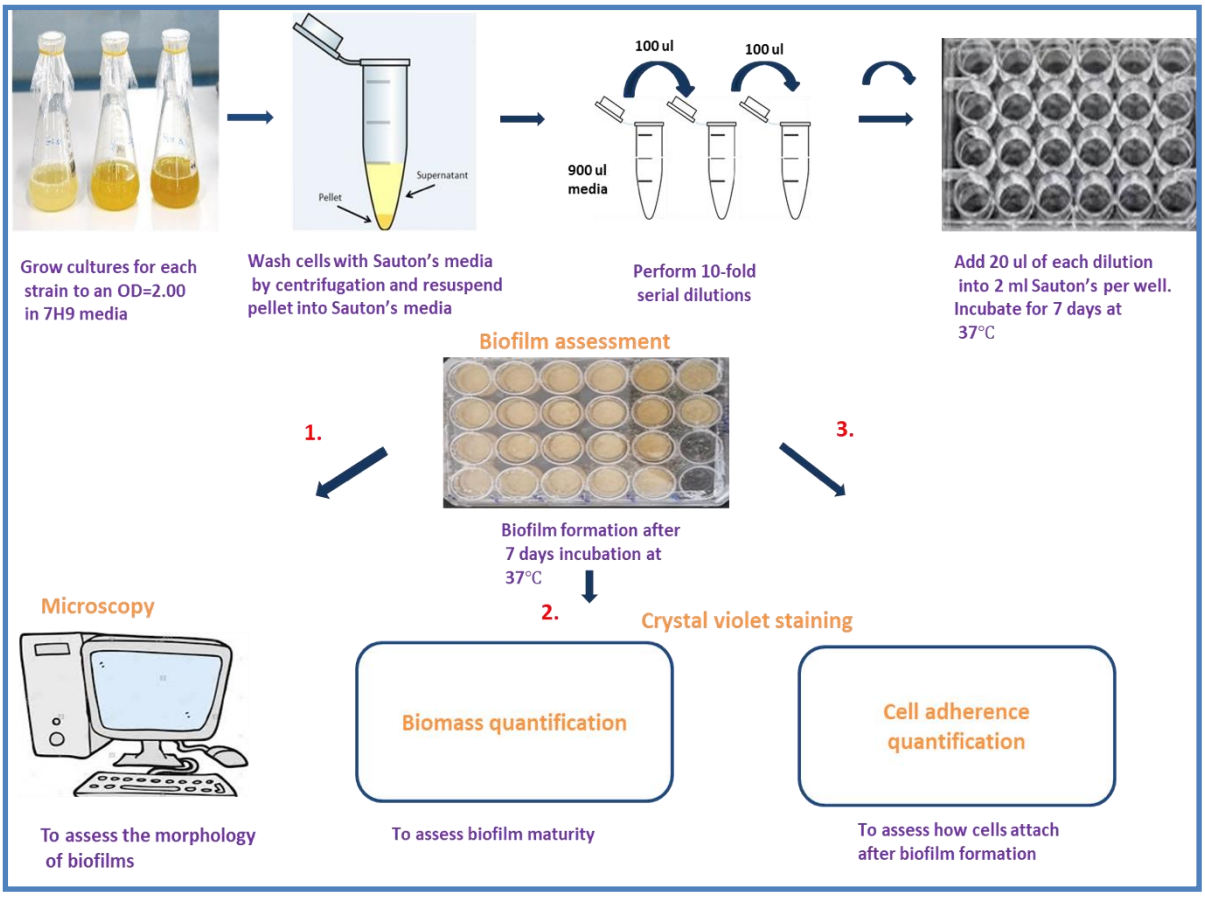


**Figure 9. Schematic representation of the biofilm formation and assessment of strains.** The wild type ($mc^2$) and mutant strains (*Δnth, Δnei1, ΔnthΔnei1, ΔcydA, ΔnthΔcydA* and *ΔnthΔnei1ΔcydA*) were grown into biofilms for 7 days. The biofilms once formed were viewed under the microscopy for morphology changes (9 (1)). Thereafter the biofilms were quantified using crystal violet staining (Figure 9 (2). This was to assess the maturity of the biofilm and its cell adhesion ability (Figure 9 (3)).

### 2.10.4 Minimum inhibitory concentration (MIC) Assay

The broth micro dilution minimum inhibitory concentration assay was used to determine the lowest concentration of the menadione required to inhibit the growth of replicating wild type and mutant strains deficient in genes from the DNA repair and ETC pathway. Menadione is a stable ketone compound that plays a vital role as a precursor in the synthesis of vitamin K (Loor *et al*., 2010). Through redox cycling, the compound can generate ROS which may lead to DNA damage and cell death.

Each strain was cultured overnight at 37 ºC in 10 ml of 7H9 media supplemented with Kan where required to log phase ($OD_{600nm}$ = 0.5). The next day the cells were diluted 1:10 to $OD_{600nm}$ = 0.05. Stocks for menadione were prepared at 1mg/ml.

Using a multichannel pipette 50 µl of 7H9 was added to each well in a 96 well microtiter round bottom plate, in rows 2 to 12. In the first row of wells, 100 µl of media and an equivalent concentration of DMSO used to make up the required menadione concentrations was diluted in media and added to the first and second wells of the first row, respectively. While 100 µl of menadione (1mg/ml) was added to the remaining 6 wells, therefore each strain was evaluated in triplicate on one plate. After menadione was aliquoted in the first row, a 2-fold serial dilution was performed by pipetting out 50 µl of liquid from row 1 using a multichannel pipette and adding it to row 2. The liquid in row 2 was mixed and 50 µl from row 2 was taken out and added into row 3. This step was repeated until row 12 and at the end of the dilution series, 50 µl from row 12 was discarded, to bring the volume in each well to 50 µl. Thereafter, 50 µl of 1:500 diluted cells for each strain were added to all the wells. The details of the plate set up is shown in Figure 10 (1). The plates were packed into zip lock bags and incubated at 37°C in an incubator overnight.

### 2.10.4.1 Alamar blue survival assay

Alamar blue (Thermo Fisher$^{TM}$) was used to determine the viability of cells. After incubation of the plate overnight at 37ºC, approximately 10 µl (1:10) Alamar blue was added to each well in row 1-12 and incubated at 37ºC for 3-4 hours (Figure 10 (2)). The MIC of menadione required for survival of the cells was measured using a spectra max Gemini EM plate reader (Molecular devices) at wavelength 570 nm (Figure 10 (3)).

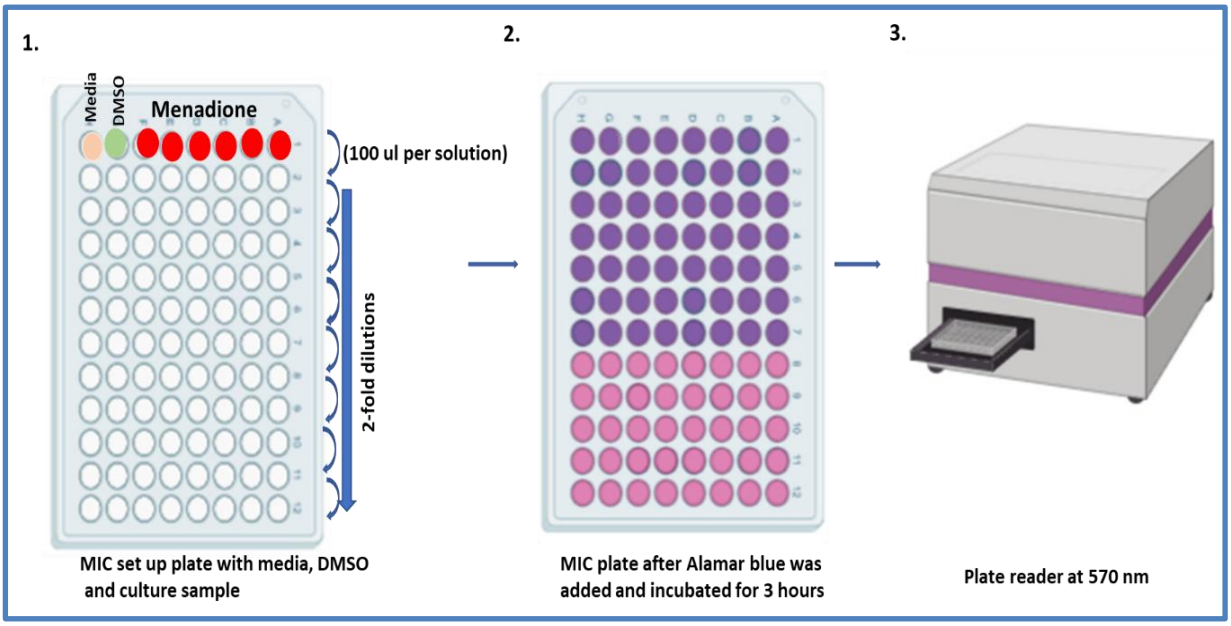


**Figure 10**. **Schematic representation of minimum inhibitory (MIC) assay.** The wild type ($mc^2$) and mutant strains (*Δnth, Δnei1, ΔnthΔnei1, ΔcydA, ΔnthΔcydA* and *ΔnthΔnei1ΔcydA*) were grown

overnight at 37ºC to $OD_{600nm}$ = 0.5. Thereafter, the cultures were treated with menadione at 1mg/ml in an MIC plate **(1).** The plate was incubated at 37ºC overnight then treated with Alamar blue dye for 3 hours **(2)** before assessing for the minimal concentration required for growth inhibition at wavelength 570 nm using a plate reader **(3)**.

### 2.10.5 Assessing mutation rates by fluctuation assay.

The fluctuation assay is based on the use of parallel cultures to determine the distribution of the number of mutations in a given culture (Luria and Delbrück, 1943). Briefly, a culture of each strain $mc^2$, Δ*nth*, Δ*neiI*, Δ*nth*Δ*neiI*, Δ*cydA*, Δ*nth*Δ*cydA* and Δ*nth*Δ*neiI*Δ*cydA* was grown in 7H9 media until late log phase ($OD_{600nm}$ =1) at 37℃ with shaking. The culture was diluted from $10^0$-$10^{-8}$ CFU/ml and the appropriate dilutions ($10^{-5}$-$10^{-8}$ CFU/ml) were spread on 7H10 media plates in duplicate to determine initial cell count ($N_0$). One ml of this culture was spread in duplicate on 7H10 media plates supplemented with 200 µg/ml rifampicin to check for the presence of pre-existing mutations (Figure 11 (A)). The culture was diluted from ($10^8$-$10^2$) by adding 100 µl culture into 9900 µl (9, 9 ml) of 7H9 in a 50 ml flask which was equivalent to $10^6$ CFU/ml. This culture was then vortexed for 10s and 100 µl removed and added to 9900 µl ($10^4$) of 7H9 media in another 50 ml flask and vortexed for 10s. Then 1 ml from the $10^4$ dilution was aliquoted into 99 ml of 7H9 in a 250 ml flask ($10^2$) containing a sterile stirrer bar. The culture was vortexed for 10s and placed on a stirring pad to make sure that the cells do not clump at the bottom of the flask. Using 25 ml serological pipette 2 ml aliquots from the $10^2$ culture were dispensed into 30 parallel 15 ml Falcon tubes. The 30 parallel cultures were grown at 37℃ with shaking for 7 days to stationary phase (Figure 11(B)). After 7 days 5 random tubes were selected, and diluted ($10^0$-$10^{-8}$) and appropriate dilutions ($10^{-5}$-$10^{-8}$) were spread in duplicate on 7H10 media plates to determine total cell count ($N_t$) (Figure 11(C)). The contents of the remaining 25 tubes were poured onto 7H10 media plates supplemented with 200 µg/ml rifampicin to determine the mutation rate for each strain (Figure 11(B)). The initial cell count was compared with the total cell count by determining the colony forming units (CFU/ml) to calculate the number of mutational events per culture. Mutation rate was calculated using the formula: $\mu = \ln 2 \times m / N_t$ (Luria and Delbrück, 1943), where m= number of mutational events per culture and $N_t$ = total number of cells in the culture using a previously created excel spreadsheet (E. Machowski, CBTBR).

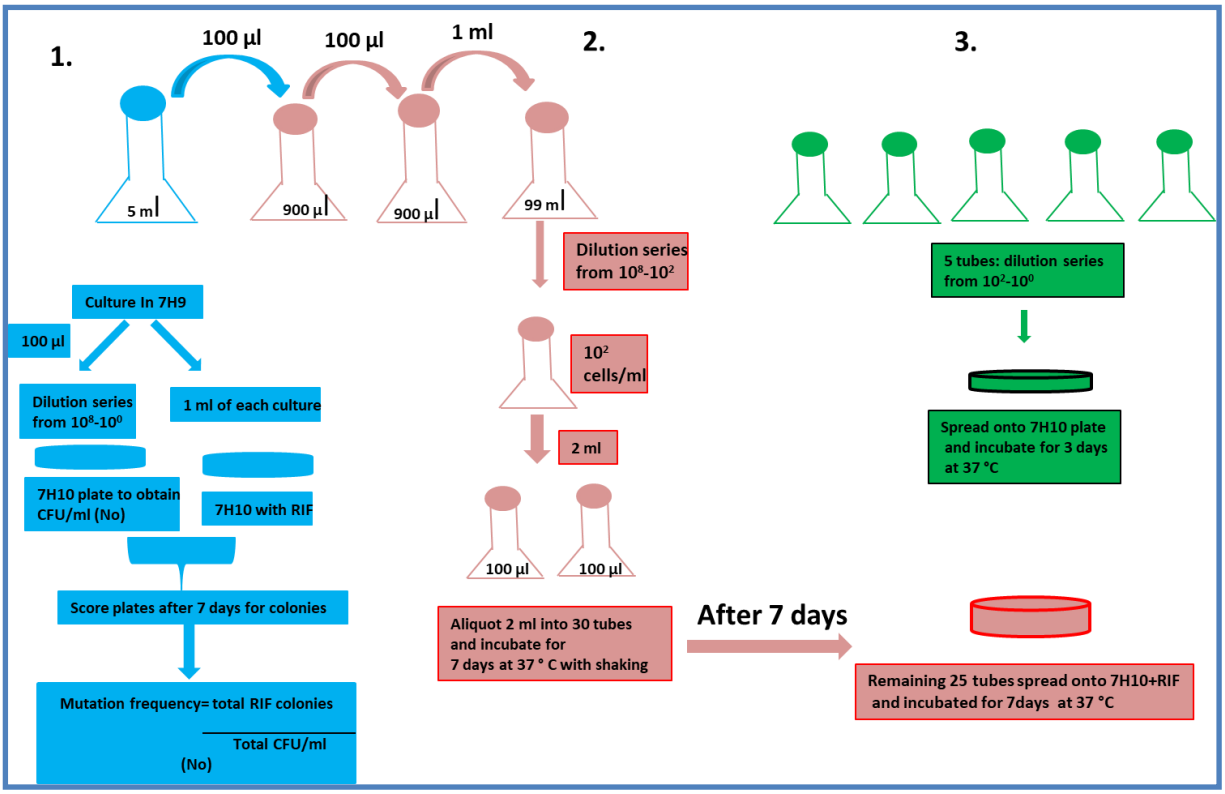


**Figure 11. Schematic representation of the fluctuation assay. (1)** A starter culture of 10 ml was grown overnight and 100 µl of appropriate dilutions were spread on 7H10 plates to get the initial bacterial count (No) and 1 ml of the neat culture was spread in duplicate on a RIF supplemented 7H10 plate to assess for pre-existing mutants. **(2)** The starter culture was diluted to $10^2$ and 2 ml of the culture was aliquoted to 30 parallel tubes and incubated for 7 days at 37℃ with shaking. **(3)** Of the 30 tubes, five were selected randomly and diluted down ($10^0$-$10^{-8}$) thereafter appropriate dilutions were spread on 7H10 plates which were incubated for 3 days at 37℃ and CFU/ml were calculated to obtain the total population size ($N_t$). **(3)** Lastly, the remaining 25 tubes were spread on 7H10 plates supplemented with RIF and incubated for 7 days at 37 °C before scoring for RIF-resistant colonies. The Luria- Delbruck method was used to calculate the mutation rates of the parental and mutant strains (Rosche and Foster, 2000).

### 2.10.5.1 Jones median estimator method

Alternatively, to the Luria- Delbruck's method two additional methods were used to calculate mutation rates observed amongst bacterial populations. The Jones estimator method although new method in the field, it is still reliable when the mutation rates to be calculated are low to moderate (Jones *et al.*, 1994). The *r* represents the number of mutants observed while m is the number of mutations per culture (Rosche and Foster, 2000). The formula for calculating the mutation rates is as follows:

$$m=\frac{r-\ln(2)}{\ln(r)-\ln(\ln(2))}$$

### 2.10.5.2 Koch Quartiles method

In this method the mean number of mutations $m_1$, $m_2$ and $m_3$ are calculated per observed number of colonies on the rifampicin plates (Koch and Wang, 1982). This will calculate the number of observed mutations (r) at the $25^{th}$ ($Q_1$), $50^{th}$ ($Q_2$) and $75^{th}$ ($Q_3$) position of the distribution of mutations per strain (Rosche and Foster, 2000, Sarkar *et al*., 1992). To get the m values the respective Q values are inserted into the equation. Based on the number of observed mutations; if the m is the same for all 3 experiments then m can be defined, however if the m values are different, then this may indicate variation in the assumptions of the Luria-Delbruck method (Rosche and Foster, 2000) which is that the initial number of cells is negligible compared to the final number of cells (Rosche and Foster, 2000). The formula for calculating the mutation rates includes:

$m_1=1.7335+0.4474Q_1 - 0.002755(Q_1)^2$

$m_2=1.1580+0.2730Q_2 - 0.000761(Q_2)^2$

$m_3=0.6658+0.1497Q_3 - 0.0001387(Q_3)^2$

### 2.10.6 Data analysis

GraphPad prism8 software was used to construct tables, figures, and graphs in this study. The statistical significance to rule out the differences between the data groups was assessed by the unpaired student's t- test using GraphPad.

## Chapter 3

## RESULTS

### 3.1 Genotypic confirmation of previously generated strains using PCR screening.

The first aim of this study was to confirm the genotype of previously generated *M. smegmatis* mutant strains at the CBTBR (Table 1) by PCR screening. Three primer sets specific for the *nth, nei1* and *cydA* genes were used for the genotypic confirmation (Table 3). Negative and positive controls were included during the reaction to rule out any traces of contamination.

#### 3.1.1 Confirmation with the *neiI* primers

The *nei1* primers in the wild type strain is expected to amplify the full-length amplicon of 801 bp whilst the mutant allele due to the deletion of the gene results in a smaller 250 bp fragment. In Figure 12C, Lane 2 of the agarose gel represents the expected 801 bp fragment amplified from the wild type strain while lanes 4, 5 and 7 represent the amplicon from the mutant strains lacking *nei1* gene which all showed the expected 250 bp band size. In the case of the Δ*nth*, Δ*cydA* and Δ*nth*Δ*cydA* mutant strains (lane 3, 6 and 8), the wild type fragment is expected as these mutants have the *nei1* gene intact.

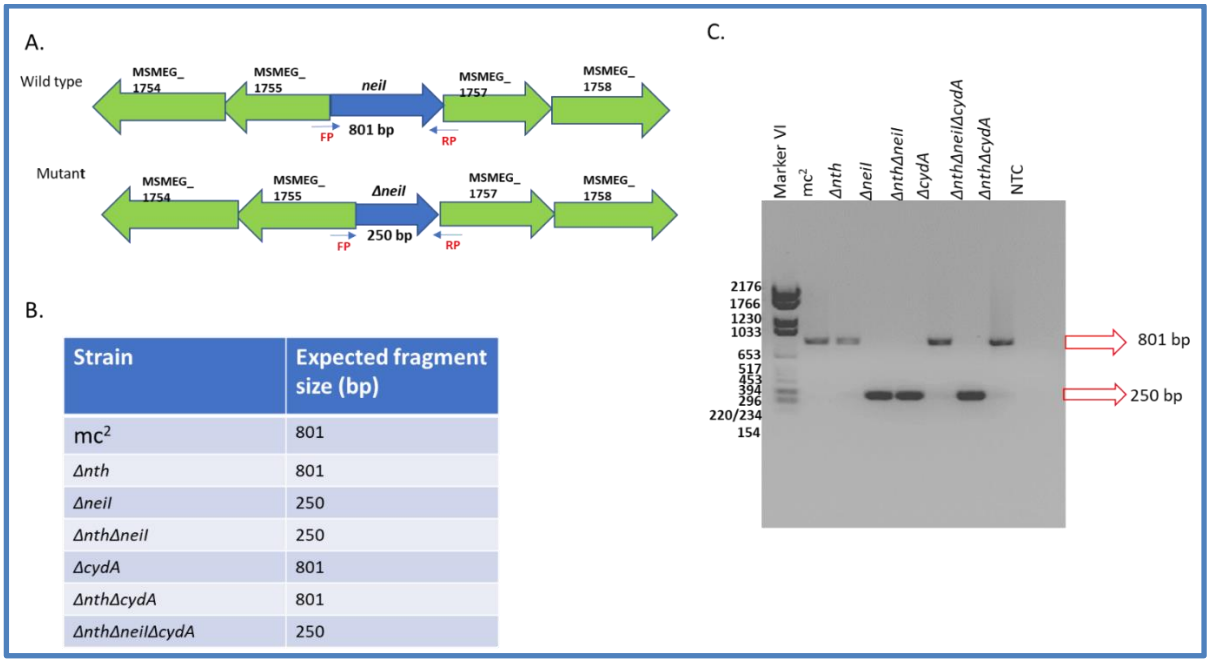


| Strain | Expected fragment size (bp) |
|---|---|
| mc² | 801 |
| Δnth | 801 |
| ΔneiI | 250 |
| ΔnthΔneiI | 250 |
| ΔcydA | 801 |
| ΔnthΔcydA | 801 |
| ΔnthΔneiIΔcydA | 250 |

**Figure 12. PCR screening for *nei1* mutants with *neiI* specific primers A** Genomic map showing the wild type and mutant band sizes generated using clone manager software. **B** A table showing the strains and the expected fragment sizes. **C**. 1% agarose gel electrophoresis showing the expected band sizes for each strain. The expected fragment sizes for the wild type *nei1* allele were 801 bp and 250 bp for the mutant allele. The FP and RP notation stand for forward and reverse primer.

### 3.1.2. PCR confirmation using *cydA* primers.

The *cydA* primers were used to amplify the full length and mutant *cydA* gene in *M. smegmatis* using PCR. In the wild type strain a 157 bp amplicon is expected whilst for the mutant allele 1400 bp is expected. In this case the mutant allele is larger than the parental allele since the disruption of the *cydA* gene was an insertion of the *aph* gene coding for kanamycin resistance (Figure 13A) (Kana *et al.*, 2001). The mutants deficient in the DNA repair genes only amplified the intact parental 157 bp fragment. While the mutants deficient in the energy metabolism genes amplified the mutant allele fragment of 1400 bp (Figure 13C).

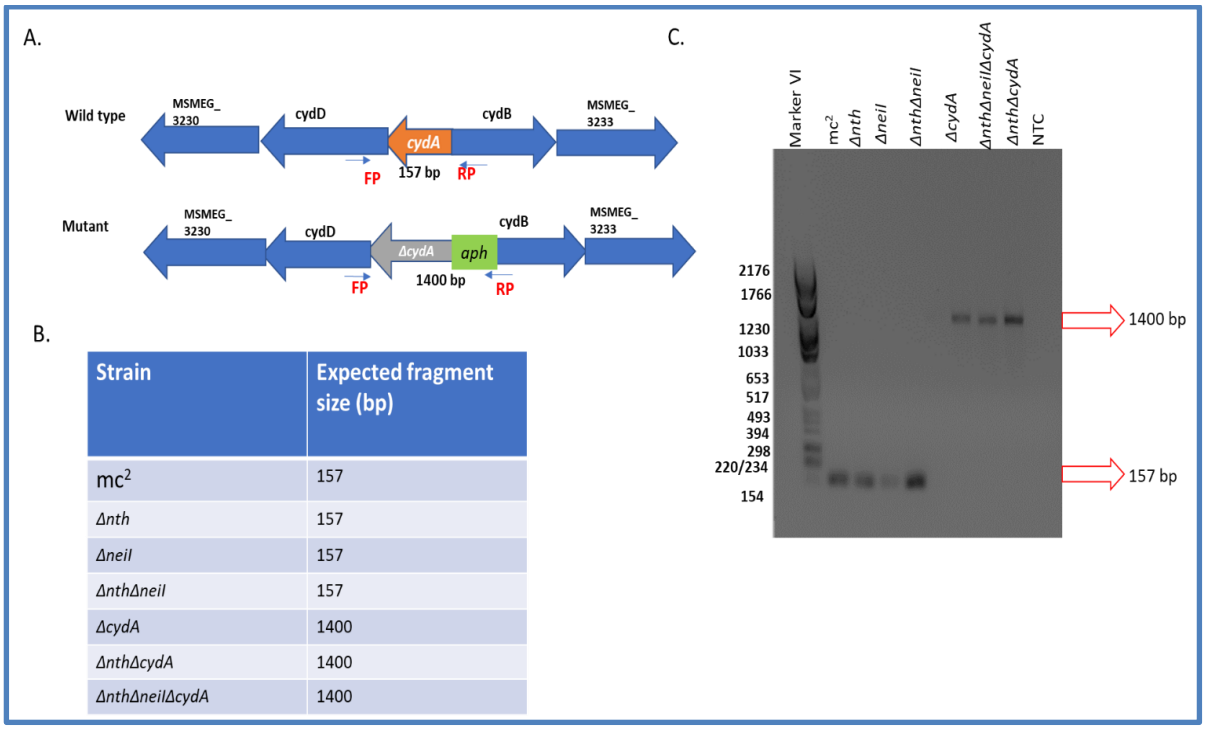


| Strain | Expected fragment size (bp) |
|---|---|
| mc² | 157 |
| *Δnth* | 157 |
| *Δneil* | 157 |
| *ΔnthΔneil* | 157 |
| *ΔcydA* | 1400 |
| *ΔnthΔcydA* | 1400 |
| *ΔnthΔneilΔcydA* | 1400 |

**Figure 13. PCR screening using the *cydA* primers for mutant strain confirmation**. (**A)** Genomic map showing the wild type and mutant band sizes generated using clone manager software. (**B)** A table showing strains and the expected fragment sizes. **C**. 1% agarose gel electrophoresis showing the expected band sizes for each strain. The expected fragment sizes for the wild type *cydA* allele were 157 bp and 1 400 bp for the mutant allele. FP represents forward primer and RP represents reverse primer.

### 3.1.3 Confirmation with the *nth* primers

The *nth* primers were used to amplify the full length and the deleted *nth* gene in *M. smegmatis* using PCR. In the wild type strain an amplicon length of 833 bp is expected whilst a 270 bp fragment is expected for all the mutant strains with the *nth* deletion. PCR confirmed the presence of the expected band size (833 bp) in the wild type strain and the 270 bp fragment in the mutant strains containing the *nth* deletion in lane 3, 5 and 7 (Figure 14C). In lane 6, the

Δ*cydA* mutant also displayed the wild type allele fragment of 833 bp as expected (Figure 14C). However, the *ΔnthΔcydA* strain (lane 8) amplified the wild type amplicon (833 bp) for *nth* gene indicating that the *nth* gene was still intact (Figure 14). Therefore, the *ΔnthΔcydA* mutant strain was re-generated by deleting the *cydA* gene in the *Δnth* background.

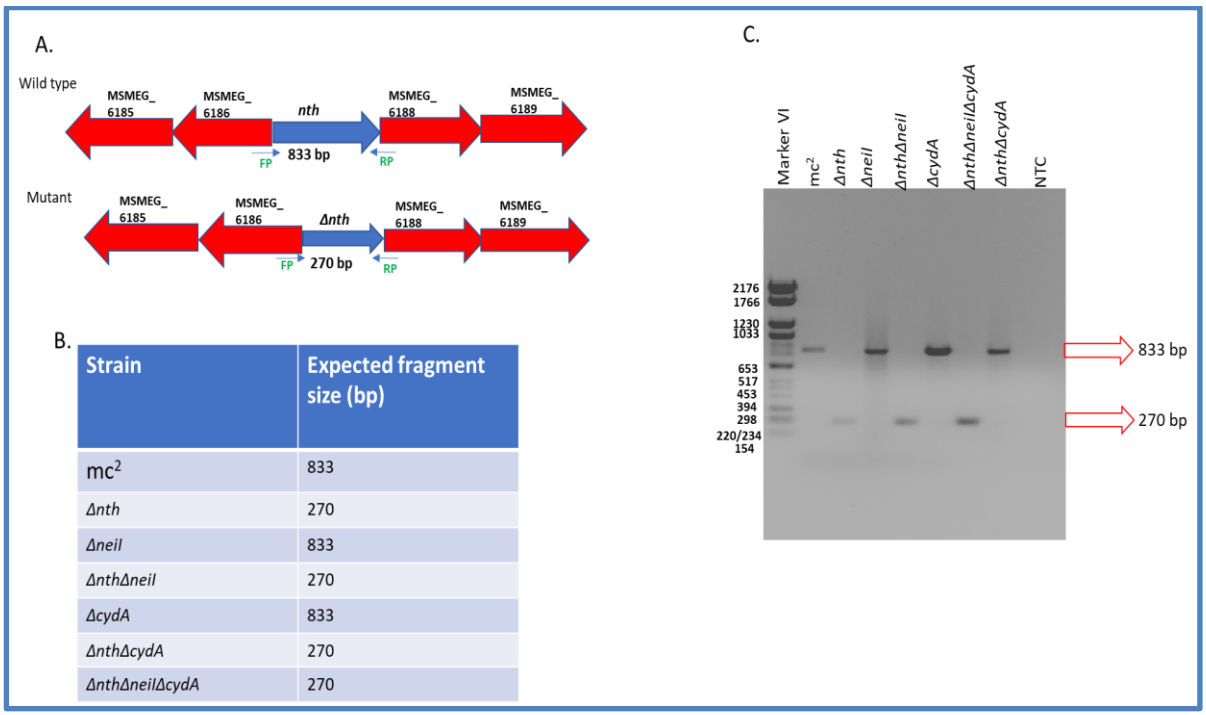


| Strain | Expected fragment size (bp) |
|---|---|
| mc² | 833 |
| *Δnth* | 270 |
| *ΔneiI* | 833 |
| *ΔnthΔneiI* | 270 |
| *ΔcydA* | 833 |
| *ΔnthΔcydA* | 270 |
| *ΔnthΔneiIΔcydA* | 270 |

**Figure 14. PCR screening with *nth* primers. (A)** Genomic map showing the wild type and mutant band sizes generated using clone manager software. **(B)** A table showing strains and the expected fragment sizes. **(C)**. 1% agarose gel electrophoresis showing the expected band sizes for each strain. The expected wild type allele is 833 bp whilst the mutant allele is 270 bp with the *nth* primers. The forward and reverse primer are notated with FP and RP, respectively.

### 3.2 Confirmation of the *pcydAaphKO* vector by restriction digest analysis

For generation of the *ΔnthΔcydA* mutant, the *cydA* deletion vector *pcydAaphKO* (Kana *et al*., 2001) was used. Plasmid DNA was extracted from *PcydA* strain using the NucleoBond Xtra Midi/Maxi kit. The vector was profiled with various restriction enzymes to ensure that it had not undergone any genetic rearrangement before use (Figure 15A). The plasmids digested as expected with Acc65, PstI, SmaI, and PvuII enzymes and showed all the expected band fragments as shown in Figure 15B. However, the SphI enzyme showed a similar fragment pattern to the uncut DNA indicating that the enzyme did not cut the DNA (Figure 15C). The HindII enzyme partially digested the DNA as an extra band between the sizes 1902 bp and 1080 bp was observed (Figure 15C). The BamHI digest also did not show 2654 bp and 2212 bp fragments suggesting that the DNA was also partially cut (Figure 15C). In these instances,

it could be that the digestion conditions for the SphI, HindII and BamHI enzyme digests were not conducive. However, as five out of the seven enzymes showed the correct banding pattern, the suicide vector was deemed to be correct.

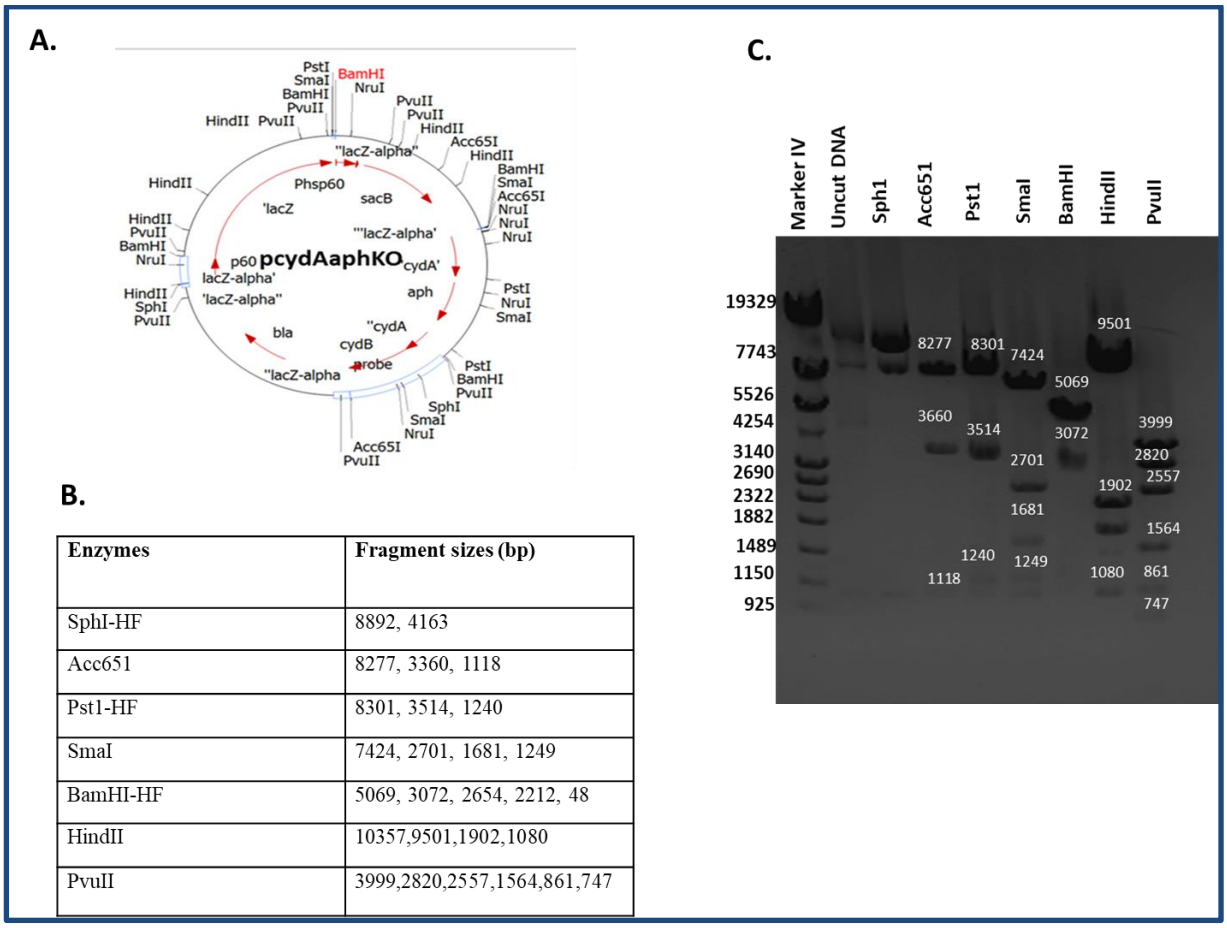


| Enzymes | Fragment sizes (bp) |
|---|---|
| SphI-HF | 8892, 4163 |
| Acc651 | 8277, 3360, 1118 |
| Pst1-HF | 8301, 3514, 1240 |
| SmaI | 7424, 2701, 1681, 1249 |
| BamHI-HF | 5069, 3072, 2654, 2212, 48 |
| HindII | 10357,9501,1902,1080 |
| PvuII | 3999,2820,2557,1564,861,747 |

**Figure 15. Restriction profile of the *pcydAaphKO* vector**. (**A**) The *pcydAaphKO* vector map generated using the Clone manager software. The vector was digested with 7 different enzymes. **(B)** Expected fragment sizes for each of the enzymes used to digest the plasmid DNA. (**C**) 1 % agarose gel indicating the expected DNA band sizes; lane 1(Marker IV), lane 2 (SphI), lane 3 (Acc651), lane 4 (PstI), lane 5 (SmaI), lane 6 (BamHI), lane 7 (HindII) and lane 8 (PvuII).

As both the DNA repair deficient mutant strains and the *cydA* deletion vector were confirmed to be correct, generation of combinatorial mutant strains lacking both the *nth and cydA* genes was pursued.

### 3.3 Generation of the *ΔnthΔcydA* mutant using homologous recombination.

The two-step homologous recombination method was used to generate the Δ*nth*Δ*cydA* deletion mutant as described by Gordhan and Parish (Gordhan and Parish, 2001). An illustration of the homologous recombination technique is shown in section 2.3. The suicide vector (*pcydAaphKO*) containing a non-functional copy of *cydA* disrupted by the *aph* gene encoding

for kanamycin and selectable marker genes (*lacZ*, and *sacB*) (Kana *et al*., 2001) was electroporated at various concentrations (5 µg, 10 µg, 20 µg, 30µg, and 40µg) into electrocompetent cell generated for the Δ*nth* DNA glycosylase deficient strain as described in section 2.3.1 and 2.3.2. Post electroporation after phenotypic expression the cells were spread on 7H10 media supplemented with 25 µg/ ml kan and 2% X-gal to identify clones that had undergone a single cross over event. These clones are identified as blue colonies because of the *lacZ* gene which encodes for beta-galactosidase breaking down X-gal to 5-bromo-4-chloro-indoxyl. The single cross-over strain (SCO) has both the wildtype and truncated Δ*cydA* genes together with the selectable marker genes (*lacZ*, and *sacB*). A positive control plasmid (*pTweety*) was used to assess the transformation efficiency which was approximately $5x10^7$ transformants/µg of DNA. Due to the white background of the picture in Figure 16A, the colonies on the positive control plate were not visible as they were also white. As the negative control electrocompetent cells with no plasmid was used to assess sensitivity of the cells to kan and rule out contamination with any plasmid. The plates from the electroporation are shown in Figure 16A.

The blue single cross over colonies were grown in the absence of Kan and counter screened by spreading serial dilutions of the cultures ($10^{-1}$ -$10^{-7}$) on 7H10 plates supplemented with 2% X-gal and 75% sucrose to select for the double crossover mutants. The *sacB* gene encodes for levansucrase, an enzyme that breaks down sucrose to levan which is toxic to cells and results in cell death. Hence, only colonies that lost the *sacB* and the *lacZ* genes during the double cross-over event would be white and resistant to sucrose. Blue/white colonies were identified indicating that the single cross of colonies underwent a second cross over event (Figure 16B).

To further confirm that the white colonies had lost the vector sequence together with the marker genes, these white colonies were spotted onto 7H10 plates supplemented with X-gal, kan and plus/minus sucrose. This selection process ensured that only colonies that have lost the *sacB* cassette are able to survive in the presence of sucrose (Figure 16C). About 21 white sucrose resistant clones were identified as possible *ΔnthΔcydA* double deletion mutants.

These colonies were then screened by PCR using primers listed in Table 3 and Southern blot analysis to identify the possible deletion mutants.

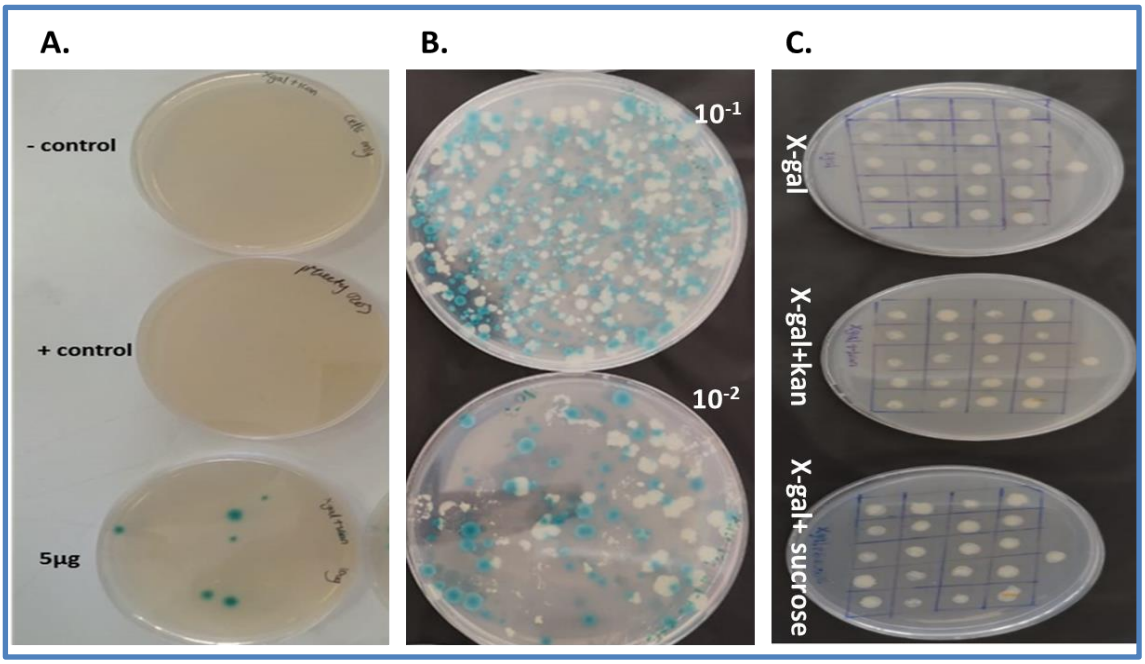


**Figure 16. Plate showing the knock-out mutant process carried out by two step-allelic exchange (A)** Electrocompetent Δ*nth* cells were transformed with the *pcydAaphKO* plasmid and were selected on 7H10 plates supplemented with 2% X-gal and 25 µg/ ml kanamycin. Negative control contains cells only (Δ*nth*), positive control (*pTweety*) and blue colonies were obtained for all concentrations of DNA electroporated (5, 10, 20 and 30 µg, but only the plate for 5 µg is shown). (**B**) Clones selected on 7H10 plates supplemented with 2% X-gal and 75% sucrose to identify DCOs. Different dilutions of the blue colony suspension were plated from $10^{-1}$ to $10^{-7}$ (only $10^{-1}$-$10^{-2}$ is shown) (**C**) The counter selection clones that underwent the second crossover event were spotted on 7H10 plates supplemented with X-gal plus Kan and X-gal plus sucrose to confirm the vector backbone had been lost during the second cross over event. Growth of the white colonies on the X-gal plus sucrose plate confirmed that the second cross over event was successful.

### 3.4 Confirmation of newly generated double deletion mutant by PCR screening

Five white, sucrose resistant clones were screened using PCR to identify the deletion mutants for *cydA* in the *nth* mutant background.

#### 3.4.1. PCR screening with *nth* primers

The *nth* primers were used to amplify the *nth* gene in the 5 possible mutant strains together with the wild type strain. As expected, the wild type strain showed the expected full-length amplicon of 833 bp and the mutant allele of 270 bp for clones 1-5. The non-template control was included to rule out contamination. These data confirmed that the Δ*nth* mutation is still retained in the double deletion mutant (Figure 17).

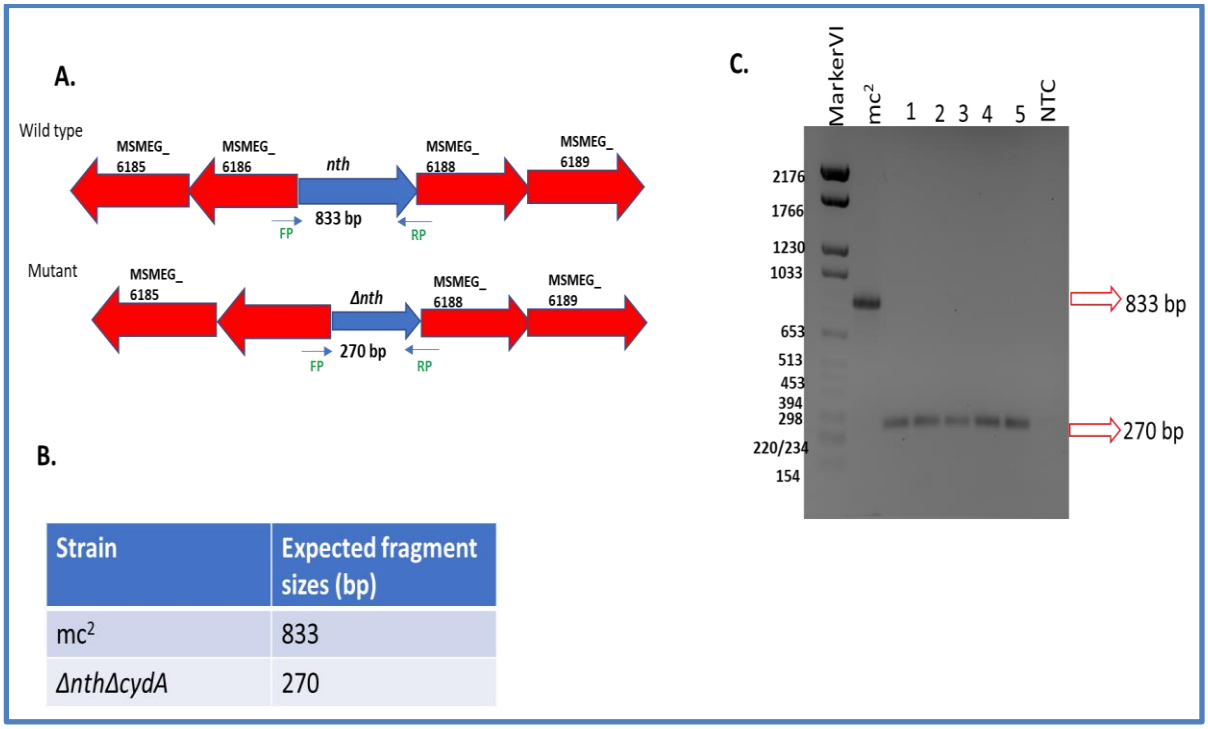


B.

| Strain | Expected fragment sizes (bp) |
|---|---|
| $mc^2$ | 833 |
| *ΔnthΔcydA* | 270 |

**Figure 17. PCR screening with *nth* primers** **(A)** Genotypic map that shows the expected fragment sizes of the mutant and wild type strain generated using clone manager software. **(B)** Table showing the expected fragment sizes for the possible *ΔnthΔcydA* positive mutants. **(C)** 1% agarose gel showing the confirmation by PCR of clone 1-5 using the *nth* primers. The parental strain, $mc^2$ showed the expected wild type band (833bp), all possible mutant clones showed the expected mutant band (270bp). The no template control in lane 8 showed no amplification confirming the absence of contamination. The forward and reverse primer are represented by FP and RP.

### 3.4.2 PCR screening with *cydA* primers

The 5 possible mutant clones were also screened with the *cydA* primers. For the wild type allele an amplicon of 157 bp was expected while for the mutant allele 1400 bp was expected. All 5 clones screened amplified the expected 1400 bp fragment and the wild type strain the 157 bp fragment whilst the non-template control showed no amplification confirming that there was no contamination in the PCR reaction (Figure 18).

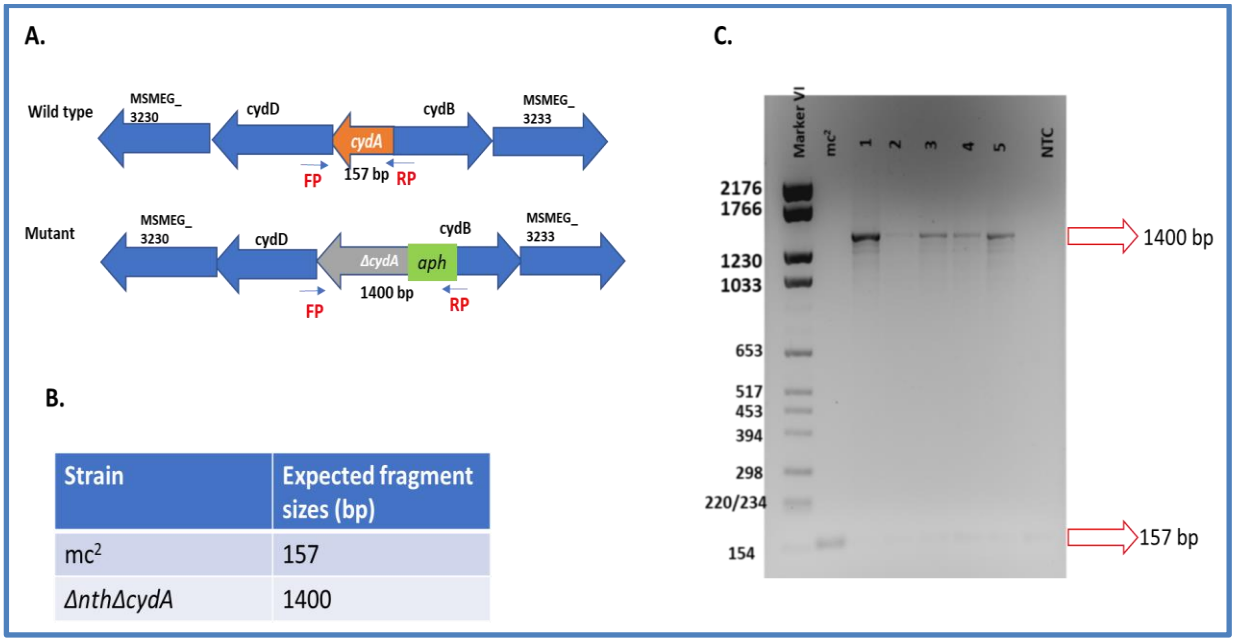


| Strain | Expected fragment sizes (bp) |
|---|---|
| mc$^2$ | 157 |
| *ΔnthΔcydA* | 1400 |

**Figure 18. PCR screening with *cydA* primers A.** Genotypic map that shows the expected fragment sizes of the mutant and wild type strain generated using clone manager software. **B.** Table showing the expected fragment sizes for the 5 clones and the parental strain**. C.** 1% agarose gel showing confirmation by PCR of clone 1-5 using *cydA* primers. The parental strain mc$^2$ showed the expected wild type band (157 bp) and the five mutant clones showed the expected mutant band (1400 bp) with the *cydA* primers. No template control showed no band confirming no contamination. FP and RP indicate forward primer and reverse primer, respectively.

### 3.5 Genotypic confirmation of the various mutants by Southern blot analysis

Once the Δ*nth*Δ*cydA* double deletion mutants were confirmed by PCR they were further confirmed by Southern blot together with Δ*nth*Δ*cydA*SCO. The parental strain (mc$^2$) and previously generated mutant strains (*Δnth, ΔneiI*, *ΔcydA*, Δ*nth*Δ*neiI*Δ*cydA*SCO and Δ*nth*Δ*neiI*Δ*cydA*) were also rescreened to ensure that all strains were genotypically correct. Genomic DNA was digested overnight at 37℃ with PstI and screened the *nth* probe (Figure 19) whilst genomic DNA digested with KpnI was screened with the *cyd* probe (Figure 20).

#### 3.5.1 Southern blot analysis of the various deletion mutants with the *nth* probe

Southern blot analysis was conducted to confirm positive mutants. Genomic DNA of the strains was digested with the PstI enzyme and the rest of the steps were performed as per method in section 2.9. The wild type allele was expected to be 5315 bp while the mutant allele was expected to be 4745 bp. The wild type strain (mc$^2$) displayed 5315 bp while the mutant strains *Δnth* (4745 bp), *ΔneiI* (5315 bp), *ΔnthΔneiI* (4745 bp), *ΔcydA* (5315 bp), *ΔnthΔcydA* (4745 bp), Δ*nthcydASCO* (4745 bp) and *ΔnthΔneiIΔcydA* (4745 bp) displayed the expected mutant bands, respectively. However, with the *ΔnthΔneiIΔcydASCO* mutant the expected band size 5315 bp

was seen except there was also an extra band (yellow arrow in figure 19C) which was higher than expected which would account for unspecific binding of the probe for this mutant.

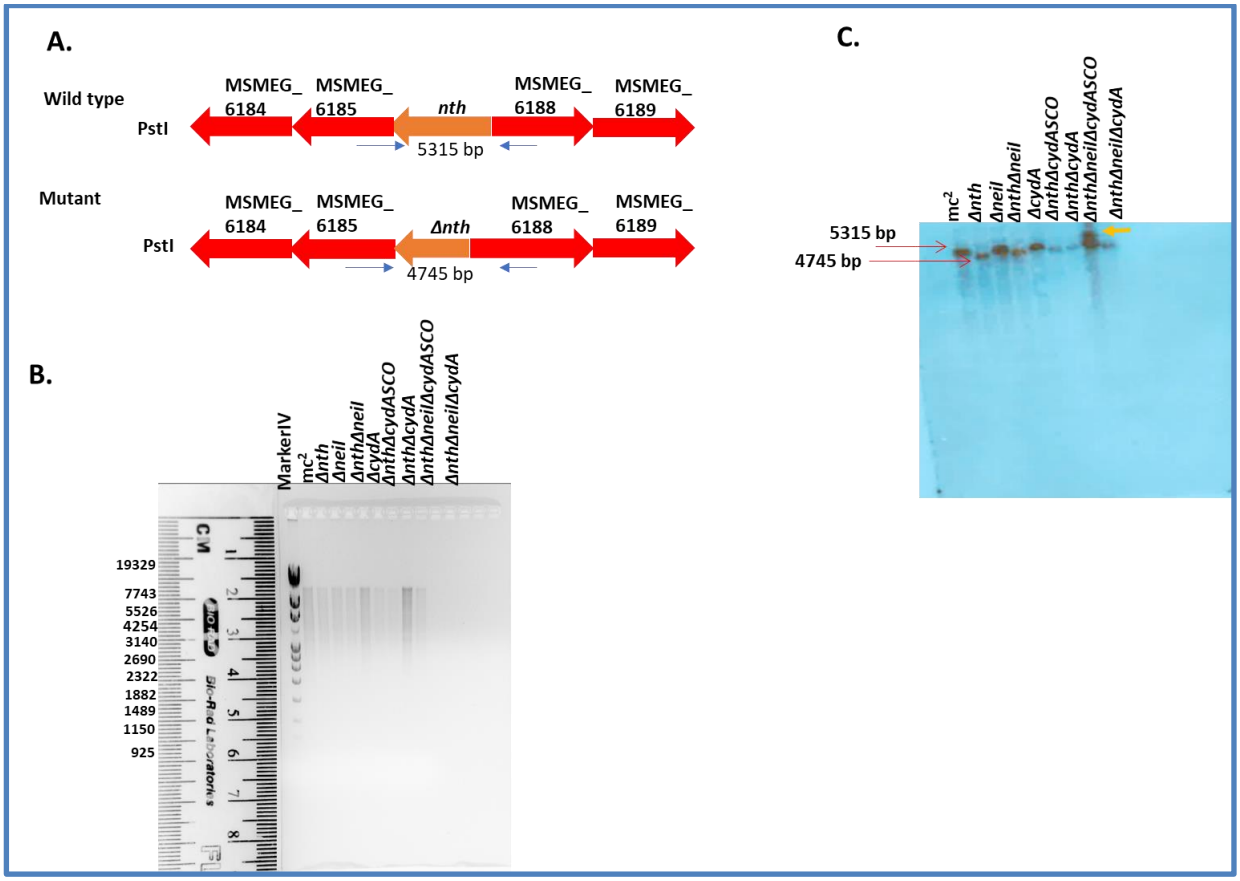


**Figure 19. Illustration of the southern blot analysis with *nth* probe (A).** Clone manager map with PstI restriction enzyme showing the expected band sizes for mutant and wild type allele. (**B**). 0.9% agarose gel showing the restriction profile of the *nth* gene cut with the PstI enzyme overnight. (**C**). Southern blot analysis with 5351 bp band for wild type and 4745 bp for the mutant allele band.

### 3.5.2 Southern blot analysis of the various deletion mutants with the *cydA* probe

Moreover, with southern blot analysis with the *cydA* probe the expected band size for the wild type allele was 2420 bp while for the mutant allele was 3360 bp with the KpnI enzyme digestion. The wildtype strain ($mc^2$) displayed 2420 bp while the mutant strains *Δnth* (2420 bp), *ΔneiI (*2420 bp), *ΔnthΔneiI* (2420 bp), *ΔcydA* (3360 bp), *ΔnthΔcydA* (3360 bp), Δ*nthcydASCO* (3360, 2420 bp), *ΔnthΔneiIΔcydASCO (*2420,3360 bp) and *ΔnthΔneiIΔcydA* (3360 bp) displayed the expected mutant bands, respectively. However, the *ΔnthΔneiI* and *ΔnthΔcydA*, and *ΔnthΔcydASCO* bands were faint. This was due to low signal of the probe during exposure of the nitrocellulose membrane to the x-ray film. Overall, genotypic confirmation of strains was considered correct.

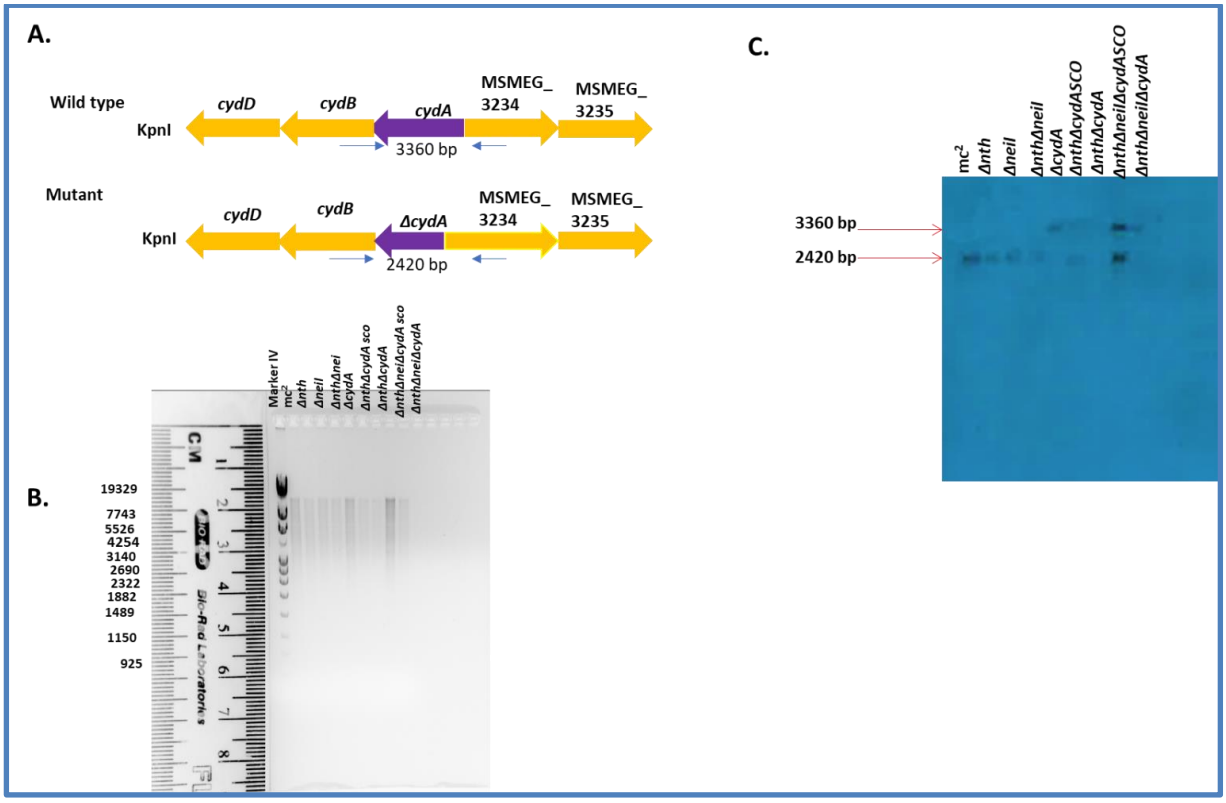


**Figure 20. Illustration of the southern blot analysis with *cydA* probe (A).** Clone manager map with KpnI restriction enzyme showing the expected band sizes for mutant and wild type allele. (**B**). 0.9% agarose gel showing the restriction profile of the *cydA* gene cut with the KpnI enzyme overnight. (**C**). Southern blot analysis with 3360 bp band for wild type and 2420 bp for the mutant allele band.

Southern blot analysis with the *neiI* probe was previously done at the CBTBR lab (Rantsi, unpublished 2017), thus repetition was not necessary as the strains had been confirmed with PCR and are correct.

**PHENOTYPIC CHARACTERISATION**

Once the double and triple deletion mutants (*ΔnthΔcydA* and *ΔnthΔneiIΔcydA*) were genotypically confirmed to be correct they were phenotypically characterized and compared to the respective parental, single and double deletion mutant strains devoid in enzymes from the BER and ETC pathways. The growth kinetics of the mutants was assessed under normal culture conditions and under hypoxic conditions as generated by biofilm cultures. Microscopic analysis was conducted on bacteria grown in biofilms to assess for changes in morphology. The mutant strains were also assessed for, survival under oxidative stress conditions as generated by hydrogen peroxide and menadione. In addition, the fluctuation assay was used to assess the mutation rates of each strain and compared to the parental strain to determine if deletion of genes in the BER and ETC pathways led to increased mutagenesis. These analyses are discussed in detail below.

### 3.6 Growth kinetics assessment of strains

The growth kinetics of all the strains ($mc^2$, Δ*nth,* Δ*nei1,* Δ*nth*Δ*neiI,* Δ*cydA,* Δ*nth*Δ*cydA,* Δ*nth*Δ*neiI*Δ*cydA*) was assessed under normal culture conditions to assess if the growth rate of the various strains was comparable. This was important to validate the interpretation of all downstream phenotyping. An overnight pre-culture of the various strains was diluted to an $OD_{600nm}$ = 0.01 in 10 ml 7H9 media supplemented with the appropriate antibiotic where necessary and incubated at 37 °C with shaking at 100 rpm. Thereafter, the growth rate was determined by monitoring the $OD_{600nm}$ at 3-hour intervals for 24 hours. In addition, at each time point viability of the cells was measured as CFU/ml as it is a far more accurate measure of growth rates. The data for both experiments is presented as the average of three experiments.

The $OD_{600nm}$ measurements showed that the wild type and the mutant strains deficient in the BER genes (*Δnth*, *ΔneiI*, *ΔnthΔneiI*) grew at a faster rate compared to strains with the *cydA* deletion (*ΔcydA, ΔnthΔcydA* and *ΔnthΔneiIΔcydA)* regardless of the background deletions (Figure 21A). Statistical analysis using the two tailed t test in Graph pad prism 8 software was done to assess the correlation between the *cydA* deletion mutant strains and the parental and DNA repair deficient mutant strain. The mutants with the *cydA* deletion showed a significant difference as the p-value was less than 0.05 ($p<0.001$) for all strains (Figure 21A). In contrast, the CFU data displayed a same growth pattern, and no significant difference was observed between the parental and mutant strains as the p-value was greater than 0.05 (Figure 21B). As

CFU measurements are far more accurate it was concluded that deletion of genes in the BER and/or the ETC pathways does not impact the growth kinetics of *M. smegmatis*.

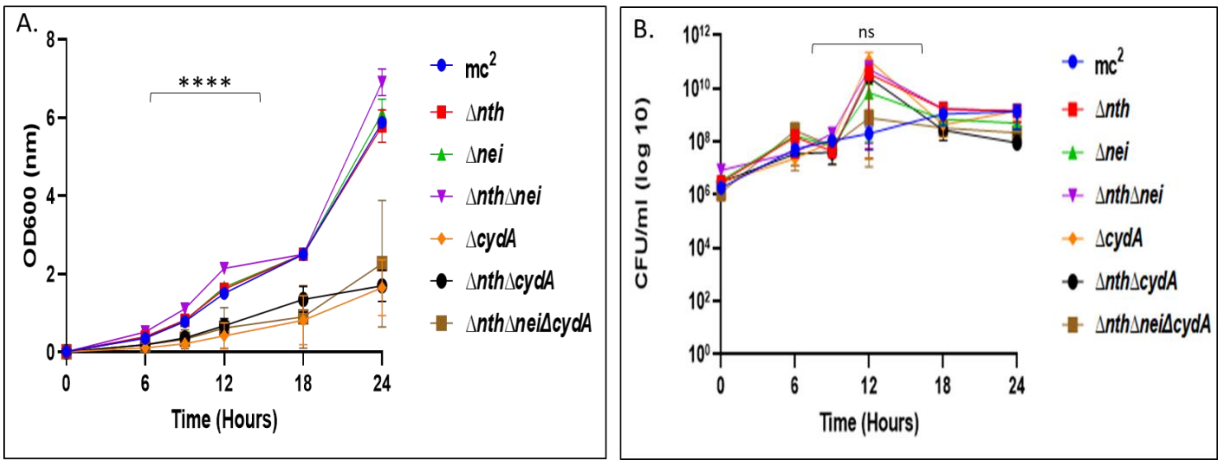


**Figure 21**. **Line graphs showing the growth kinetics for the parental and the various deletion mutant strains** ($mc^2$, Δ*nth*, Δ*nei1*, Δ*nth*Δ*neiI*, Δ*cydA*, Δ*nth*Δ*cydA*, Δ*nth*Δ*neiI*Δ*cydA*). Growth was monitored at 3-hour intervals over a period of 24 hours by measuring the $OD600_{nm.}$ For CFU/ml evaluation growth was monitored at 3-hour intervals over a period of 24 hours by spreading appropriate dilutions of each of the strains in duplicate on 7H10 media. Plates were incubated for 3-4 days before colonies were counted. Error bars represent the standard error of the mean (SEM) for three biological replicates. **A.** The $OD600_{nm}$ measurements showed a significant difference in the growth pattern for the mutants containing the *cydA* deletions compared to the mutants containing only deletions in the DNA repair genes and the wild type strain ($p<0.0001$). **B.** CFU/ml data showed no significant difference in the growth rate of all the strains ($p>0.05$). ******** is the p-value representing significance while **ns** is the p-value for non-significance.

### 3.7 Assessment of the sensitivity of the various mutant strains to hydrogen peroxide

In this experiment the viability of the various bacterial strains was assessed under oxidative stress conditions as generated by hydrogen peroxide. The oxidative stress conditions were optimized with the parental strain before testing the various strains to ensure the correct conditions to measure survival were established.

Based on the $OD_{600nm}$ values hydrogen peroxide was effectively killing the parental strain as the growth declined over the 6-hour period (Figure 22A). However, when CFU's were evaluated at the same time points, the hydrogen peroxide killed the strains within the first 2 hours of incubation after treatment (Figure 22B). These conditions were applied to test the mutant strain under oxidative stress conditions.

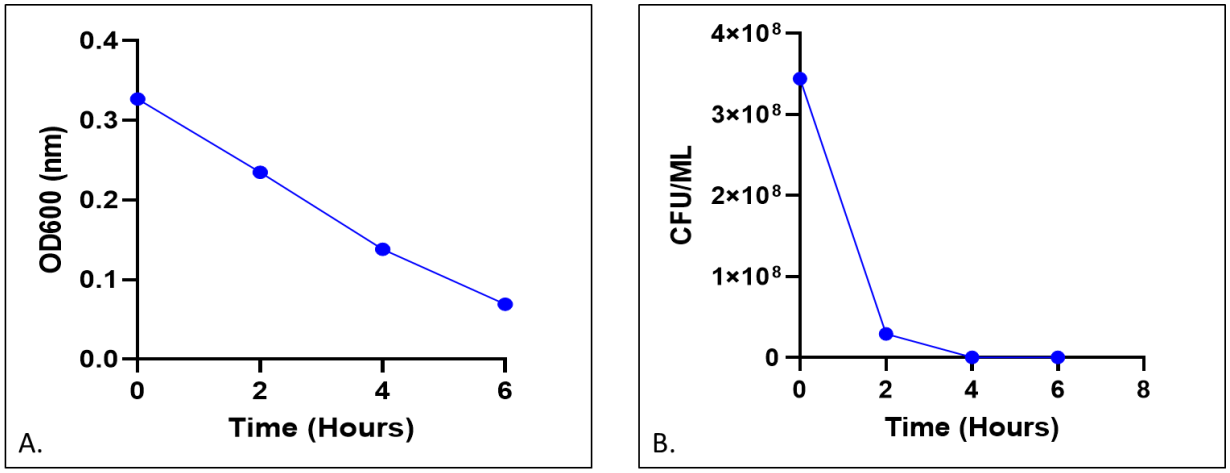


**Figure 22. Line graphs showing the $OD_{600nm}$ and CFU/ml values of the parental strain under oxidative stress conditions with hydrogen peroxide (2,5mM). A.** Hydrogen peroxide showed a steady decline in survival over the 6-hour period. **B.** Hydrogen peroxide showed a decline in growth within the first 2 hours of treatment.

Next these conditions were applied to test all the other mutant strains under oxidative stress. Exponentially growing wild type and mutant strains were exposed to hydrogen peroxide (2.5 mM) and at 2-hour intervals over a period of 6 hours the $OD6_{00nm}$ and CFU/ml was measured and enumerated respectively for each strain.

Based on the $OD_{600nm}$ readings the DNA repair deficient mutants (*Δnth*, *ΔneiI*, *ΔnthΔneiI*) showed decreased survival compared to the wild type strains and the single *cydA* deletion mutant. However, in contrast the *ΔnthΔcydA* and *ΔnthΔneiIΔcydA* strains appeared to be resistant to hydrogen peroxide treatment as they displayed an ascending growth pattern compared to the parental strain (Figure 23A).

Subsequently when the CFUs are analysed, as observed with the parental strain, all the mutant strains showed complete killing within 2 hours of exposure except the Δ*nth*Δ*cydA* mutant that did not have any colonies observed for all the time points (Figure 23B). This could have been due to experiment technicalities when growing the strain *(*Δ*nth*Δ*cydA*). As hydrogen peroxide is a highly unstable compound it poses several challenges for reproducibility. This data was not useful in dissecting out the growth kinetics of each of the strains under oxidative stress conditions and therefore, a more stable compound, menadione was used to assess the survival of the various strains to oxidative stress.

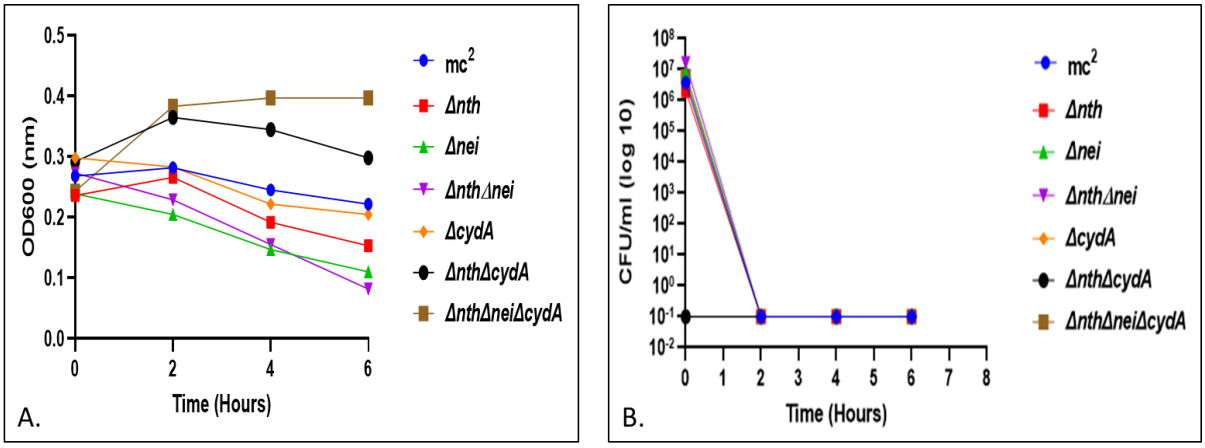


**Figure 23. Line graph showing the viability of the various mutant and parental strains under oxidative stress conditions with hydrogen peroxide (2, 5 mM). A.** The wild type strain, *ΔcydA* and the DNA repair deficient mutants (*Δnth, ΔneiI, ΔnthΔneiI*) are susceptible to hydrogen peroxide whilst *ΔnthΔcydA* and *ΔnthΔneiIΔcydA* strains are resistant. **B.** Line graph showing the viability of the various mutant and parental strains under stress conditions by hydrogen peroxide. Log phase cultures were treated with hydrogen peroxide (2.5 mM) and viability was assessed by plating appropriate dilutions at each time point. All the strains died after 2 hours of exposure to hydrogen peroxide. For presentation purposes all strains that had zero colonies were changed to 0.1 on the log scale.

### 3.8 MIC determination with menadione

The susceptibility of the strains to menadione was assessed using the broth dilution minimum inhibitory concentration (MIC) procedure. This compound as mentioned before is more stable in comparison to hydrogen peroxide so we anticipated that it would better delineate the survival kinetics of the various strains under oxidative stress.

First the MIC of the parental strain to menadione was assessed to obtain a baseline value for comparison of the MIC of the various mutants (Figure 24). Using the broth microdilution method, in a 96 well plate the menadione was diluted 2-fold twelve times and then all the wells in the plate inoculated with a diluted culture of the parental strain. After overnight incubation Alamar blue which is used to determine the viability of cells was added to the entire plate and growth was measured using a plate reader. Alamar blue is a resazurin-based solution that quantitatively measures viability by using the reducing power of living cells. Hence, growing cells will reduce the resazurin from a purple color to pink whilst no growth no convert to the purple dye. The data from three replicate experiments were analyzed and plotted as a graph which showed an MIC 0.01560 mg/ml for the parental strain against menadione (Figure 24).

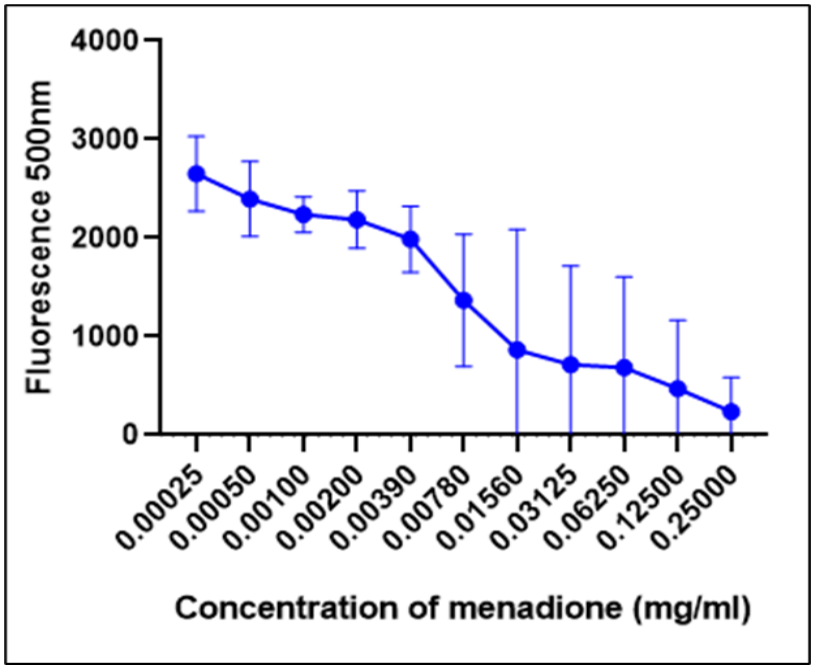


**Figure 24. Graph showing the MIC of menadione required to kill *M. smegmatis* wild type strain.** The parental strain was exposed to menadione for one day in a 96 well plate and then exposed to Alamar blue for 3 hours before the MIC was determined at wavelength 500 nm on a plate reader. The MIC was calculated as the average from three experiments and was taken as 0.01560 mg/ml.

Next the MIC of the various mutant strains (*Δnth, Δnei1, ΔnthΔneiI, ΔcydA, ΔnthΔcydA* and *ΔnthΔneiIΔcydA*) against menadione was assessed and compared to the parental strain (Figure 25). All the mutant strains displayed an MIC of 0.00780 mg/ml against menadione except for the *ΔcydA* mutant strain which showed a 2-fold lower MIC of 0.00390 mg/ml to this compound. Most of the mutant strains showed a two 2-fold difference in MIC compared to the parental strain which is considered insignificant. However, the 4-fold difference in MIC observed for the *cydA* deletion mutant may be because of oxidative stress condition generated by menadione. Why this effect was not seen for strains in which *cydA* was deleted in combination with the DNA repair enzymes is unknown and needs further investigation.

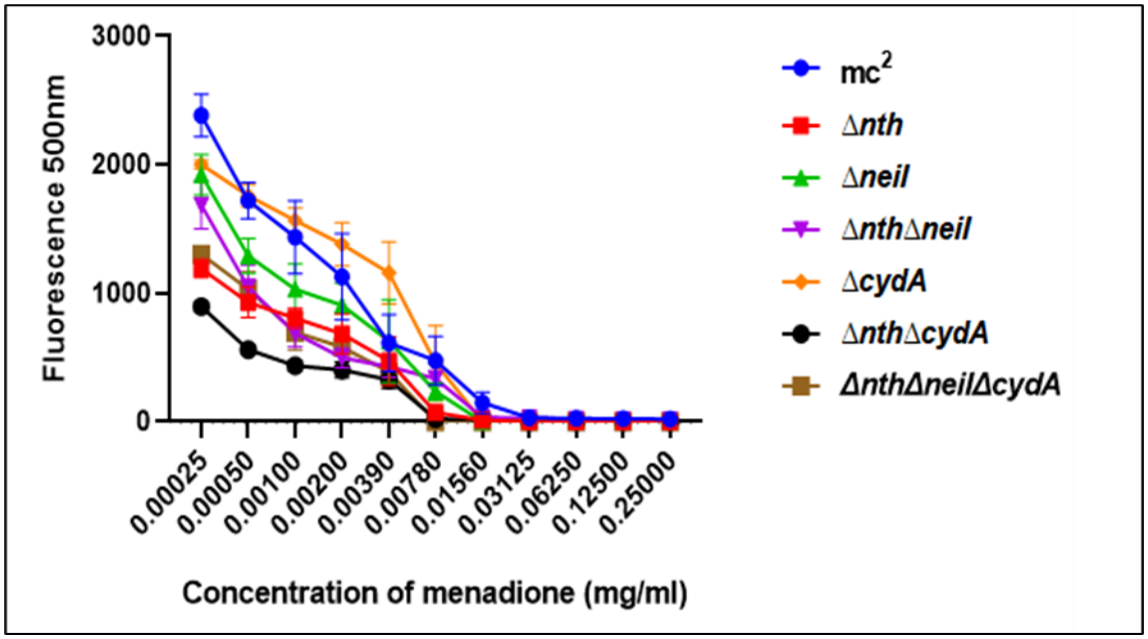


**Figure 25. Graph showing the MIC of menadione required to kill *M. smegmatis* wild type and the various mutant strains**. The strains were exposed to menadione for one day then exposed to Alamar blue for 3 hours before the MIC was determined at wavelength 500 nm using a plate reader. The MIC is the point before the growth drops to zero. The MIC for all strains was approximately 0.00780 mg/ml except for the Δ*cydA* mutant which showed a 4-fold lower MIC 0.00390 mg/ml compared to the parental strain (0, 01560 mg/ml).

As the MIC of all the strains was similar, we next checked whether treatment of the various strains with menadione results in redox heterogeneity. This assessment was important since hydrogen peroxide killed all the strains after 2 hours**.**

### 3.9 Measurement of redox heterogeneity of the wild type and mutant strains with cumene hydroperoxide, dithiothreitol and menadione treatment

The parental and *M. smegmatis* mutant strains were marked with a GFP reporter to gauge the oxidative stress response to cumene hydroperoxide (CHP) oxidant, dithiothreitol (DTT) reductant and menadione. The two compounds were included in this experiment as controls to calibrate the response of all the strains to either a 100% reduced (DTT) or 100% oxidized (CHP) environment. Moreover, GFP is a sensitive reporter for gene expression in cells as measured by fluorescence by flow cytometry (Soboleski *et al*., 2005). Flow cytometry quantitively analyses the fluorescent intensity where the intensity of the GFP reporter is directly proportional to the GFP fluorescent in the marked cells (Soboleski *et al*., 2005). In this experiment, the reporter served as a signal when oxidative stress results in fluorescence. The signal would show redox heterogeneity of either oxidation or reduction.

*M. tb* during oxidative stress conditions produces millimolar concentrations of mycothiol (MSH), which acts as a cytoplasmic redox buffer (Bhaskar *et al*., 2014). Thus, to measure the redox potential ($E_{MSH}$) of strains various gating options on the flow cytometer were used. The strains were grown to the exponential phase and treated with the different compounds. After treatment, the cells were resuspended in PBS before analysis with flow cytometry. The $GFP^+$ population of the strains were divided into three sub-populations: $E_{MSH}$-oxidized, $E_{MSH}$-reduced, and $E_{MSH}$-basal. The number of events per population was represented as the percentage of each sub-populations (displayed as bar graphs in Figure 26). Analysis is presented as the sum of the redox (oxidization and reduction) potential of each compound treatment for all the strain. In addition, dot plots were also used to represent the shift in each population towards oxidized or reduced conditions after treatment with the CHP, DTT and menadione, respectively and these are shown in Appendix C.

**A. Untreated cells**

When the cells containing the GFP reporter were untreated, their response to the redox reaction system varied. The wild type GFP marked strain gave a fully reduced signal (Figure 26A). Some of the mutants (*Δnth*-GFP, *ΔneiI*-GFP, *ΔnthΔcydA*-GFP) consist of cells mostly in the reduced state with a small portion in the oxidized state (Figure 26B, C, and F). The remaining mutants (*ΔnthΔneiI*-GFP, *ΔcydA*-GFP and *ΔnthΔneiIΔcydA*-GFP) showed both reduced and oxidized cells, along with cells in a basal redox state (Figure 26D, E and G). Conclusively, these findings indicate that untreated cells for all the strains were in a reduced state. These data are also summarized in Figure 27 using the GFP marked parental strain as a control to confirm the conclusion drawn.

**B. CHP treatment**

With the CHP treatment, as expected the $mc^2$-GFP strain was fully oxidized (100%) as well as the *ΔneiI*-GFP and *ΔnthΔcydA*-GFP mutant strains whilst the *Δnth*-GFP and *ΔnthΔneiI*-GFP were 98% oxidized (Figure 26A, B, C, D and F). Lastly the *ΔnthΔneiIΔcydA*-GFP was oxidized at 99% (Figure 26G). In the *ΔcydA*-GFP cells only 61% oxidation was measured (Figure 26E) suggesting that this strain is resistant to change it redox state, even if an oxidant is used for treatment.

**C. DTT treatment**

DTT treatment, displayed a 98-100% reduction rate for all strains except for the *cydA*-GFP strains. The $mc^2$-GFP, *Δnth*-GFP, *ΔneiI*-GFP, *ΔnthΔcydA*-GFP and *ΔnthΔneiIΔcydA*-GFP strains were fully reduced (100%) whilst *ΔnthΔneiI*-GFP was reduced at 99% and the *ΔcydA*-

GFP was reduced at 98%. These results are shown in Figure 26 under the DTT treatment label in all panels.

**D. Menadione**

Treatment of the various strains with menadione resulted in 100% oxidation in strains $mc^2$-GFP, *Δnth*-GFP, *ΔneiI*-GFP, *ΔnthΔneiI*-GFP, *ΔnthΔcydA*-GFP and *ΔnthΔneiIΔcydA*-GFP (Figure 26A, B, C, D, F and G). However, the *ΔcydA*-GFP cells were oxidized at an 80% rate (Figure 26E). The reduced response of this strain to menadione was like that observed with CHP indicating that deletion of the *ΔcydA* induces other compensatory respiratory genes/pathways that controls the oxidative stress.

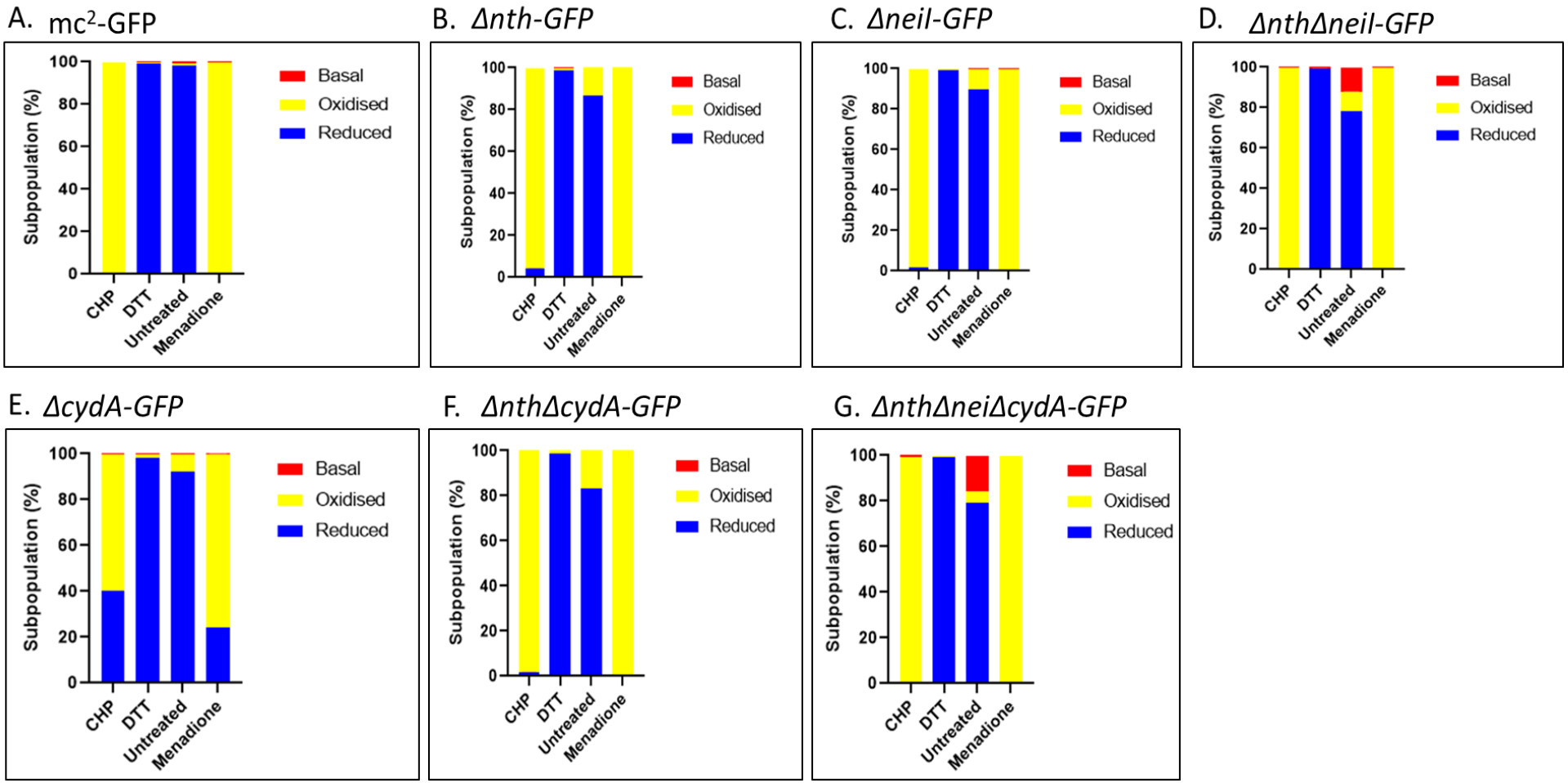


**Figure 26. Bar graphs illustrating the redox heterogeneity of seven GFP marked strains.** Strains (mc²-GFP, Δ*nth-GFP*, Δ*neiI-GFP*, Δ*nth*Δ*neiI-GFP*, Δ*cydA-GFP*, Δ*nth*Δ*cydA-GFP* and Δ*nth*Δ*neiI*Δ*cydA-GFP*) were grown to exponential phase ($OD_{600nm}$=0.5-0.8) and treated with different concentrations of CHP

(10mM), DTT (40mM) and menadione (1mg/ml)**.** The program FCSalyzer was used to analyse and categorise each population (basal, oxidized and reduced). The bar graphs represent the percentage of cells that fall into each of the subpopulations. The data showed that the CHP oxidant and menadione compound were able to oxidise all strains at a (99-100%) rate except the Δ*cydA*-GFP mutant. DTT reductant, reduced the strains at a (98-100%) rate. The untreated strains were reduced at the same rate (80-100%) as the DTT compound indicating that the *M. smegmatis* strains are in a reduced state.

This experiment clearly shows that CHP and menadione can induce oxidative stress at a 99-100% rate in all the mutant strains except the Δ*cydA*-GFP mutant. Moreover, the data show that even though the strains succumb to oxidative stress conditions, some cells can shift to a reduced or basal state most likely as a survival strategy. As the strains in their untreated state show a reduced phenotype ranging from 80-100% rate they validate the oxidation measurements (Figure 27) and these finding were explored further as discussed in section 3.9.1.

### 3.9.1 Confirmation of the redox heterogeneity system of the *M. smegmatis* mutants

To show that the results achieved in section 3.9 are reversible, we used the wild type strain ($mc^2$-GFP) as a control to show how these *M. smegmatis* strains respond to successive menadione and DTT treatments. As our assumption based on the above data was that the strains are originally in a reduced state, treatment with both menadione and DTT should cause a redox shift from oxidised to a reduced state. In the bar graph as expected there is a redox shift response from reduction to oxidation when the cells are treated with menadione and then back to the reduced state when treated with DTT (MenDTT) (Figure 27). These data also suggest that mycobacteria after being exposed to oxidative stress conditions can survive in the cell and recover by shifting to their original state (reduced).

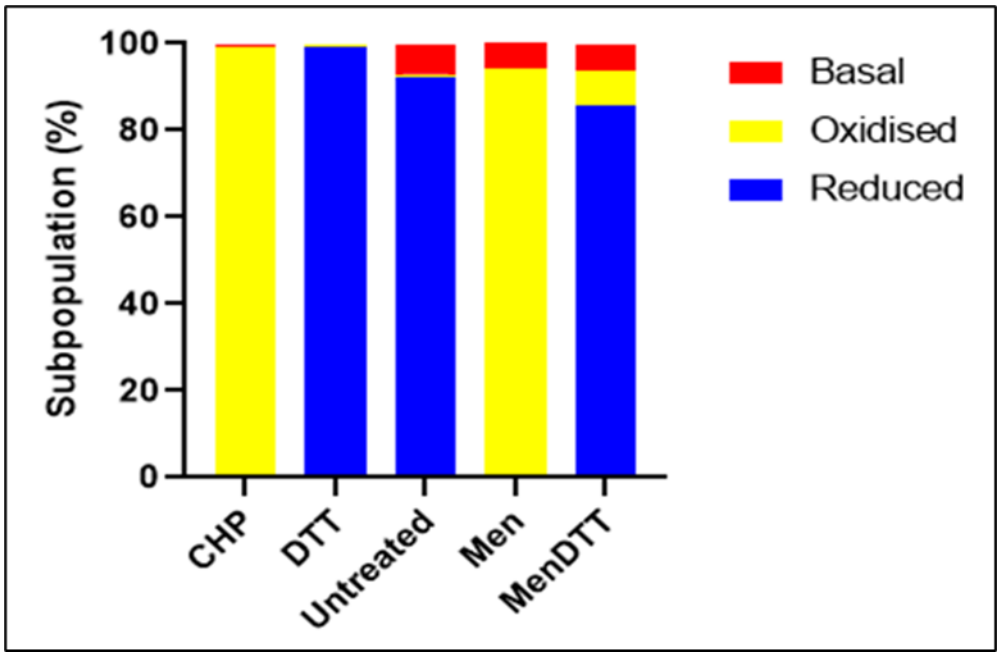


**Figure 27. Bar graphs illustrating the redox heterogeneity of wild type GFP marked strain.** The parental strain was grown to log phase of 0.5 in $OD_{600nm.}$, thereafter it was treated with CHP (10mM), DTT (40mM), menadione (1mg/ml) and menadione (1mg/ml) followed by DTT (40mM) to assess if overwhelming of the cells with compounds will enhance their redox state or not. CHP oxidant oxidizes the strain fully (100%), DTT fully reduces the strain as expected, untreated cells displayed both reduced and basal states. Menadione alone oxidized the strain and the menadione and DTT treatment demonstrated the reversal of the oxidized state.

Based on these data, menadione is a useful oxidative generating compound and should be optimized to further analyse the various mutant strains. Unfortunately, due to time constraints this could not be explored further in this study.

### 3.10 Assessment of mutation rates with the fluctuation assay.

To determine the mutation distribution of each mutant and parental strain, mutation rates were evaluated using the fluctuation assay. The fluctuation assay uses parallel cultures to determine the mutational events in a population of each strain. Three different methods were employed in this study including the Luria-Delbrück, Jones Median estimator, and the Quartiles Koch method to assess the mutation rates, respectively. This was to account for any limitations that each method has and to get accurate data as possible. Thereafter analysis was done by calculating the fold change of each mutant strain relative to the parental strain. Previously Moolla and colleagues showed that deletion of the DNA repair genes (*nth* and *nei*) increases mutagenesis (Moolla *et al*., 2014). In this study we investigated the impact of deletion of genes from both the BER and ETC pathway on mutagenesis.

**Luria-Delbrück fluctuation method**

The mutation rates were calculated using the Luria-Delbrück fluctuation method for the wild type and mutant strains (*ΔnthΔneiI, ΔcydA, ΔnthΔcydA* and *ΔnthΔneiIΔcydA).* The Luria Delbrück method follow certain assumptions to draw conclusions for a successful experiment which includes (a) the likelihood of mutation is constant throughout the cell's lifetime, (b) the probability of mutation during the lifetime of the cell does not vary during the growth of the culture, (c) the proportion of mutants is always small, (d) the initial number of cells is negligible in comparison to the final number of cells, (e) the growth rates of mutants and non-mutants are similar, (f) the reverse mutations are minor, (g) death is insignificant, (h) all mutants are detected and (ix) no mutants occur after selection (Rosche and Foster, 2000).

The mutation rates (μ) are dependent on the distribution of mutations (m) in the entire population (*Nt*) (Rosche and Foster, 2000). The mutation events for this method should be between 0.3 and 2.3 for mutation rate to be considered correct. In this case, an excel spreadsheet created at the CBTBR was used to generate the maximum likelihood curve to estimate the *m* value required to calculate the mutation rates (Machowski *et al*., 2007). The fluctuation assay was conducted in three independent experiments for all the strains and the wild type strain was used as an example to illustrate how the MSS-Maximum likelihood curve is analysed. This method computes the Luria Delbruck distribution by calculating the mean number of observed mutants. Using the excel spreadsheet, the m-value was calculated at 1.61 (red arrow in Figure 28), the final number of cells ($N_t$) was $2.10\times10^7$, and thus inserting these values in the formulae $\mu=\ln 2 \times m / N_t$ (Luria and Delbrück, 1943) the (μ) was calculated as $5.31\times10^{-8}$ for the parental strain in experiment 1.

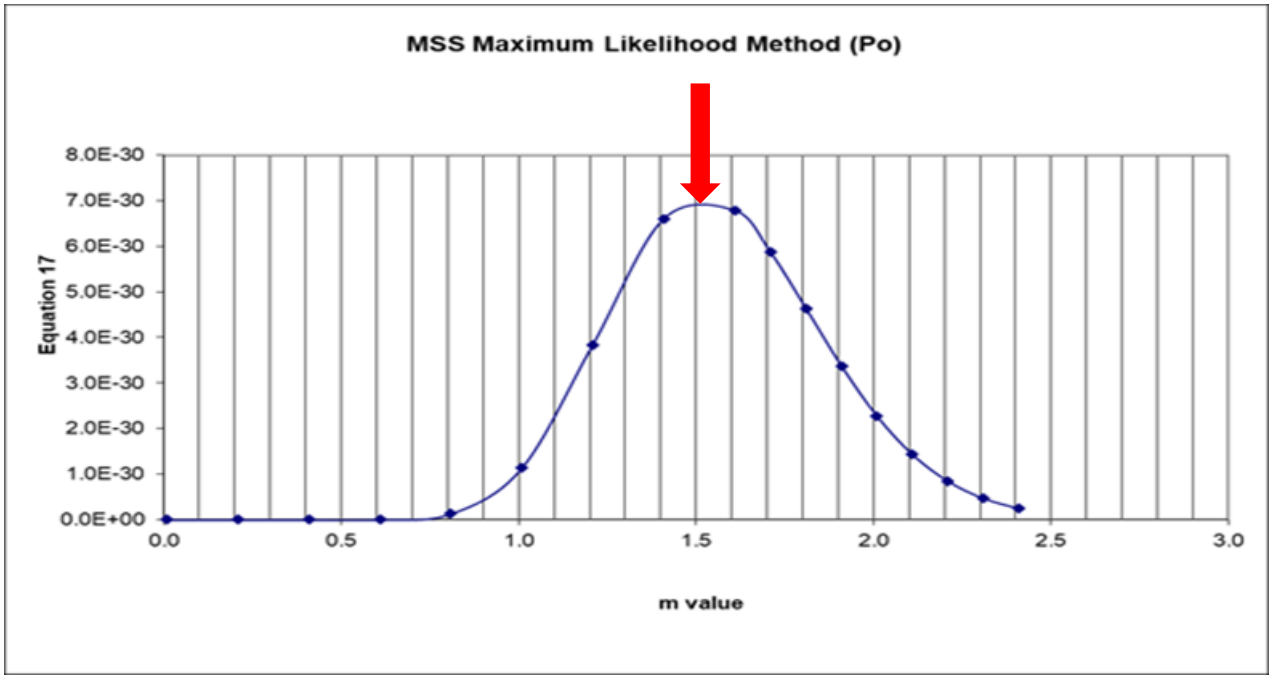


**Figure 28**. **MSS distribution LC curve used to estimate the mutation rate for the parental strain**. This graph shows the peak at which the m-value for the wild type strain is determined. The m value represents the distribution of the mutations and it was used to calculate the mutation rate for the parental strain by the use the excel spreadsheet created at the CBTBR lab (Machowski *et al*., 2007). In this spreadsheet, the possible values of m were plotted on the x-axis and equation 17 data was plotted on the y-axis (Machowski *et al*., 2007) . The peak on the graph (red arrow) is the most probable m value (1.61).

Similarly, the mutation rates of all the mutant strains and the parental strain for the three independent experiments was calculated and relative fold changes in mutation rates was calculated for each strain in relation to the wild type strain for each independent experiment (Table 4).

**Table 4. Analysis of mutation rates by comparing the relative fold changes with Luria-Delbruck method.**

| Strains | Mutation rates per experiment ($10^{-8}$) | | | Relative fold change relative to wild type strain ($mc^2$) | | |
|---|---|---|---|---|---|---|
| Experiment | **1** | **2** | **3** | **1** | **2** | **3** |
| $mc^2$ | 5.17 | 1.70 | 7.93 | 1.0 | 1.0 | 1.0 |
| Δ*nth* | 6.08 | 14.1 | 1.65 | 1.71 | 8.29 | 0.208 |
| Δ*neiI* | 0.403 | 14.0 | 6.44 | 0.078 | 8.24 | 0.812 |
| Δ*nth*Δ*neiI* | 0.658 | 230 | 2.79 | 0.127 | 135.3 | 0.351 |
| Δ*cydA* | 0.183 | 1.03 | 1.92 | 0.035 | 0.605 | 0.242 |
| Δ*nth*Δ*cydA* | 90.6 | 12.0 | 2.33 | 17.5 | 7.05 | 0.293 |
| Δ*nth*Δ*neiI* Δ*cydA* | 0.355 | 9.44 | 0.315 | 0.069 | 5.55 | 0.039 |

### 3.10.1 Analysis of mutation rates by comparing the relative fold changes.

Based on the data the mutation rates between the three experiments were not consistent. Only experiment 2 showed a shift in mutation rates for all the strains except for Δ*cydA.* The single DNA repair deficient (*Δnth* and *ΔneiI*) mutants showed 8-fold increase in mutation rate *w*hilst the *ΔnthΔneiI* combinatorial mutant showed a massive increase (yellow highlight) in mutations (Table 4) which agreed with the observations of Moola et al (Moolla *et al*., 2014) Plates with $Rif^R$ colonies greater than 150 and vary from the rest of the data were considered jackpots and therefore, were excluded from the calculations. Deletion of the *cydA* gene is from the ETC pathway (*ΔcydA*), show no increase in spontaneous mutations however, when genes from both the ETC and BER pathway are missing (*ΔnthΔcydA* and the *ΔnthΔneiIΔcydA*) there is an increase in the mutation rates (Table 4). These data show that under spontaneous oxidative stress conditions, the absence of genes in both the BER and ETC pathways leads to increased mutagenesis suggesting that the cell in the absence of *cydA* gene is experiencing higher levels of oxidative stress leading to increased DNA damage which in the absence of the DNA repair enzymes is struggling to maintain genome stability and eventually the cell will die. These data show the importance of the both the ETC and BER pathways in maintaining cell viability under oxidative stress conditions however, this experiment will need to be repeated as these

conclusions are based on one experiment only. The reason for the low mutation rates for most of the strains in experiments 1 and 2 may be due to technical errors and therefore, requires further experimentation.

**The Quartiles Koch method**

The quartiles Koch method uses the upper and lower quartiles with the median to determine the mutation rates. To get the number of mutational events, the number of $Rif^R$ colonies were used to calculate the median which was then used to determine the mutation rates based on the position of the r (median number of mutants in a culture) whether it falls under the upper or lower quartile. According to Foster, the values of m should be between 2 and 14 for the method to be correct for use (Rosche and Foster, 2000, Foster, 2006). If not, the method is considered undefined.

This analysis also showed increased mutagenesis for the *ΔnthΔneiI* mutant (Table 5, green highlight) compared to the individual deletion mutants (Δ*nth* and Δ*nei1*) as observed with the in the Luria Delbruck analysis (Table 4, yellow highlight). Similarly, the *cydA* deficient mutant did not show any distinguishable variation in mutation rates (Table 5). However, deletion of *cydA* in combination with the BER enzymes (Δ*nthΔcydA* and Δ*nth*Δ*neiI*Δ*cydA*) showed an increase in mutation rates (Table 5).

**Table 5. Analysis of mutation rates by comparing the relative fold changes with the Koch quartiles method.**

| Strains | Mutation rates per experiment ($10^{-8}$) | | | Relative fold change relative to wild type strain ($mc^2$) | | |
|---|---|---|---|---|---|---|
| Experiment | **1** | **2** | **3** | **1** | **2** | **3** |
| $mc^2$ | 6.15 | 2.55 | 16.8 | 1.0 | 1.0 | 1.0 |
| Δ*nth* | 9.40 | 24.0 | 5.37 | 1.52 | 9.41 | 0.319 |
| Δ*neiI* | 0.415 | 62.9 | 20.4 | 0.067 | 2.46 | 1.21 |
| Δ*nth*Δ*neiI* | 1.97 | 504 | 6.27 | 0.320 | 197.6 | 0.372 |
| Δ*cydA* | 0.965 | 2.95 | 10.4 | 0.156 | 1.15 | 0.619 |
| Δ*nth*Δ*cydA* | 23.1 | 16.3 | 12.2 | 37.5 | 6.39 | 0.73 |
| Δ*nth*Δ*neiI* Δ*cydA* | 1.05 | 15.2 | 2.87 | 0.170 | 5.96 | 0.170 |

**The Jones median Estimator method**

Lastly the Jones median estimator method was explored for analysis of the mutation rates in these experiments. The Jones estimator method is normally used when m is between 1,5 and 10 or when the median is 0,5 (Jones *et al*., 1994). If these criteria are not met then the method is considered unreliable and inefficient (Jones *et al*., 1994). As shown in table most of the mutation rates across the 3 experiments were undefined (UD) because the median was 0 which made the m value undefined and thus the mutation rates could not be determined. Hence, this method was not useful in calculating the mutation rates for most of the strains but does maintain like the previous two methods that the double deletion mutant (*ΔnthΔneiI*) displays greater mutagenesis (experiment 1 and 2 in Table 6, highlighted in blue). In this analysis the *cydA* deletion mutants did not yield comparable mutation rates as the previous 2 methods.

**Table 6. Analysis of mutation rates by comparing the relative fold changes with Jones median estimator method.**

| Strains | Mutation rates per experiment ($10^{-8}$) | | | Relative fold change relative to wild type strain ($mc^2$) | | |
|---|---|---|---|---|---|---|
| Experiment | **1** | **2** | **3** | **1** | **2** | **3** |
| $mc^2$ | 4.64 | 1.55 | UD | 1.0 | 1.0 | UD |
| Δ*nth* | 5.19 | 15.1 | UD | 1.12 | 9.74 | UD |
| Δ*neiI* | 0.236 | UD | 13.8 | 196 | UD | UD |
| Δ*nth*Δ*neiI* | 1.03 | 134 | 4.40 | 4.50 | 86.4 | UD |
| Δ*cydA* | UD | UD | UD | UD | UD | UD |
| Δ*nth*Δ*cydA* | UD | 14.5 | UD | UD | 0.106 | UD |
| Δ*nth*Δ*neiI*Δ *cydA* | 0.431 | 11.09 | UD | 1.076 | 0.139 | UD |

UD = undefined

Overall, the comparative analysis for calculating mutation rates suggest that the Luria-Delbrück method may be the most accurate.

### 3.10.2 Determining the morphologies of spontaneous rifampicin resistant mutants.

As there was a change a mutation rates between the various mutant strains, it was interesting to determine if the morphology of the $Rif^R$ was different for the various strains. The colonies obtained on the Rif plates for the various mutant and parental strains were viewed under the Zeiss Stemi 2000 stereomicroscope and analyzed using the Zen software.

Microscopic analysis was done at three different magnifications, 0.65x, 1x and 1.25x at a scale bar of 100 pixels for each strain (Figure 29). The wild type strain displayed a bulgy cord morphology, which was also observed for the DNA repair single deletion mutants *Δnth* and *ΔneiI* (Figure 29). The double deletion *ΔnthΔneiI* mutant showed a slightly bulgier cording morphology around the periphery of the colony. This showed that with increased loss of genes from the BER pathway results in an exaggerated phenotype. This result is consistent with the mutation rates data that displayed increased mutagenesis in the *ΔnthΔneiI* strain. The energy metabolism deficient mutant displayed a very different morphology compared to the parental or the DNA deficient mutant strains. The colonies were flat, shiny, and displayed no cording. (Figure 29). However, when the DNA repair genes are also deleted with the *cydA* gene in the *ΔnthΔcydA and ΔnthΔneiIΔcydA* mutants, the mutants start to regain the cording effect which is more pronounced when both the repair genes are deleted (*ΔnthΔneiIΔcydA*) (Figure 29). However, the cording is not the same as observed for the parental strain and the BER deletion mutants suggesting that deletion of the *cydA* gene in the background of the BER genes does have an impact in maintaining cell fidelity. These data also correlate well with the oxidative stress survival and mutagenesis observations as in all these experiments the *ΔnthΔneiI* double deletion mutant showed a more exaggerated phenotype compared to the individual single mutants. The *cydA* single deletion mutant does not display a dramatic phenotype but combinatorial deletion of this gene together with BER genes results in an exaggerated phenotype of an increased mutagenesis. These observations point to the fact that both the BER and ETC pathways work in synergy in DNA damage tolerance and survival under hostile conditions.

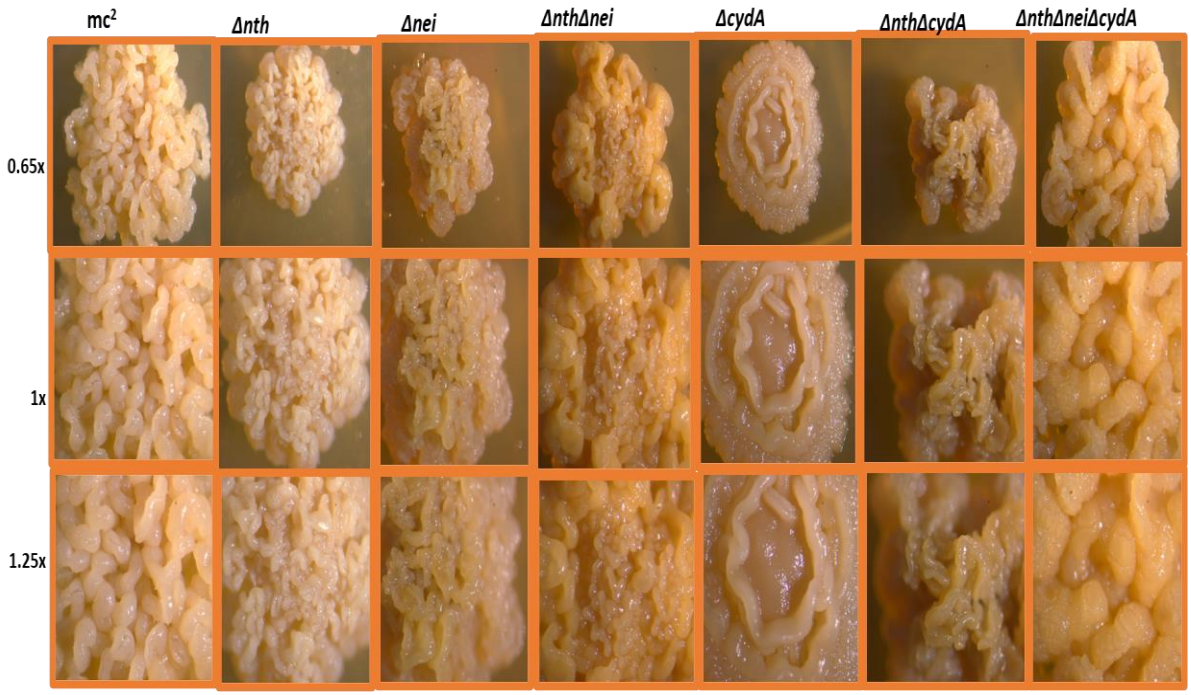


**Figure 29. Microscopic analysis of the parental and mutant strains colonies under rifampicin treatment.** Colonies were viewed using 3 different magnifications; first row represents 0.65x, second row represents 1x and 1.25x is represented by the third row for each strain. The parental $mc^2$ strain and the single DNA repair gene deletion mutants (*Δnth* and *ΔneiI*) displayed a bulgy cording morphology. The *ΔnthΔneiI* mutant showed a bulgier phenotype compared to the single deletion mutant strains. The *ΔcydA* displayed a distinct flat and shiny phenotype compared to all the strains but this phenotype is lost as strains deficient in genes from both the BER and ETC pathway show a recovery effect in that these combinatorial mutants start regaining the cording morphology which is more pronounced with loss of both the DNA repair genes.

### 3.11 Biofilms

In addition to oxidative stress, the various mutants were also assessed under oxygen limiting conditions as created by biofilms. During infection, the mycobacteria are engulfed by the alveolar macrophages as a host immune response. This process can result either in some bacilli developing into active TB disease or most bacilli progressing to develop latent TB. The latent TB state renders the tubercle bacilli inactive and contains it in a granuloma where the bacteria can survive under oxygen limiting conditions. Thus, to understand the adaption of mycobacterial cells under hypoxia conditions these various mutant strains together with the parental strain was assessed for survival under biofilm conditions.

Bacteria on biofilm surfaces consume oxygen creating an oxygen-depleted (hypoxic) environment. The generated biofilms were quantified for biomass and cell adherence as well

as microscopic assessment to identify any differences between the various mutant strains and the parental strain.

### 3.11.1 Microscopy analysis of biofilms for wild type and mutant strains

Once the biofilms were grown, the Zeiss Stemi 2000 stereomicroscope was used to capture images of the biofilms for the wild type and mutant strains at two different magnification (1X and 1.25X) to identify any morphological changes due to deletion of the various BER and ETC enzymes.

Biofilms of both the wild type and *Δnth* strain showed a thick, ruffled, and intact morphology whilst the *Δnei1* mutant strain showed a more tubular and granular morphology but biofilm was still intact (Figure 30). This phenotype was further enhanced in the double deletion mutant *ΔnthΔneiI* (Figure 30) suggesting that deletion of both the *nth* and *nei* genes affects bacterial growth and survival as previously observed (Moolla *et al*., 2014). The *ΔcydA* deletion mutant was unable to form a biofilm but instead showed a sediment of cells at the bottom of the well. The inability of the Δ*cydA* mutant to form biofilms was also observed by N. Narrandes (unpublished, 2018). In contrast deletion of the *cydA* gene in combination with the BER enzymes Nth and/or Nei resulted in strains *ΔnthΔcydA* and *ΔnthΔneiIΔcydA* forming biofilms that displayed a rather smooth, thin, and flat morphology. This recovery in biofilm formation which despite not being as robust as the parental strain suggested that other repair enzymes in the BER pathway for example the second Nei homologue maybe having a compensatory role allowing the *ΔnthΔcydA* and Δ*nthΔneiIΔcydA* to tolerate hypoxic conditions.

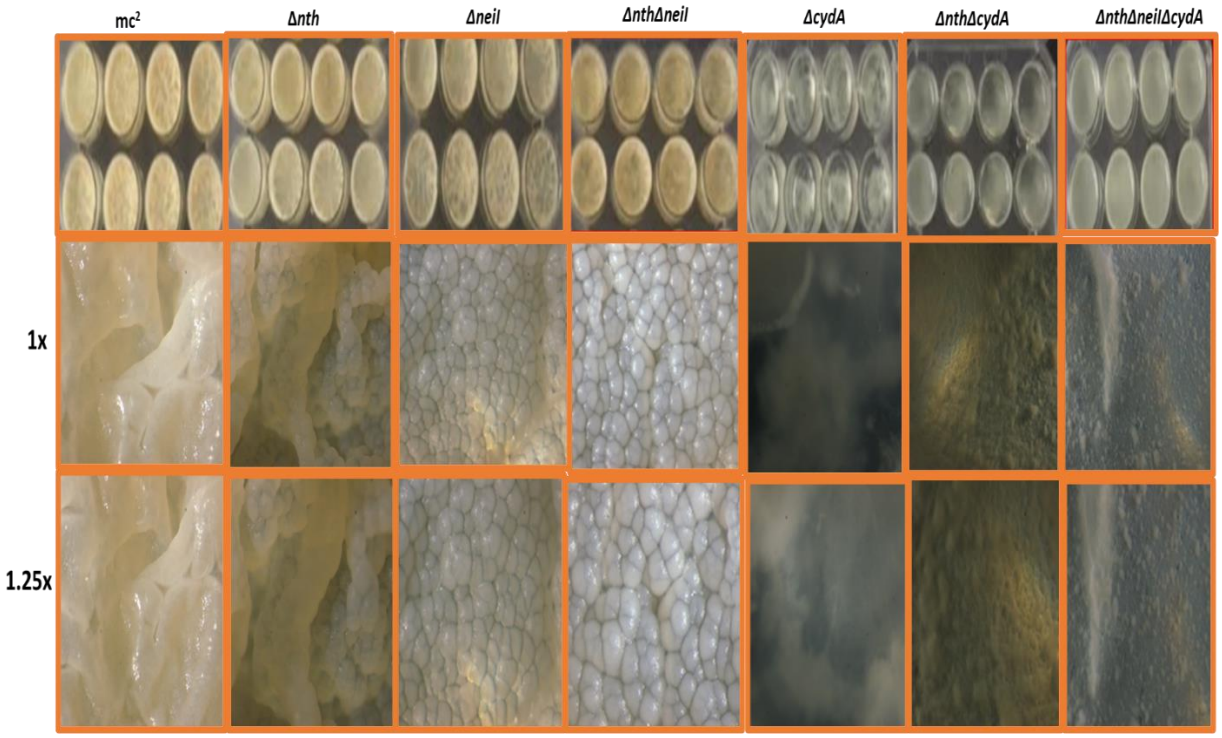


**Figure 30. Microscopy analysis of biofilm formation in the parental *M. smegmatis* and the various mutant strains.** Once the biofilms were grown, they were examined under the microscope at two magnifications (1x and 1.25x) under the microscope. The second row represents the 1x magnification while the third row is the 1.25x. The wild type strain and the DNA repair deficient mutant strains (*Δnth, ΔneiI, ΔnthΔneiI*) were able to form solid biofilms that displayed some morphological difference as multiple repair genes were deleted. In contrast the *ΔcydA* mutant was unable to form intact biofilms but mutants deficient in genes from both pathways (*ΔnthΔcydA* and *ΔnthΔneiIΔcydA*) showed a slight recovery in biofilm formation which was flat and thinner in comparison to the parental and the DNA repair deficient mutants.

### 3.11.2 Biomass quantification of biofilms

Crystal violet staining was used to quantify the biofilm biomass. The cells beneath the biofilm were removed with a pipette without disrupting the biofilms and stained. Each sample was diluted to 1:100 and the $OD_{600nm}$ was measured.

The data showed that the wild type strain and the DNA repair deficient mutant strains had a higher biomass whilst, as expected the *ΔcydA* mutant had a lower biomass due its inability to produce intact biofilms. Statistically, the *ΔcydA* mutant was significantly different from *ΔnthΔcydA* which could form smooth, flat moderate biofilms (Figure 31) as the p- value was less than 0.05 ($p<0.001$). However, there was no significant difference ($p>0.05$) between all the other mutant strains and the parental strains (Figure 31). These preliminary data suggests that with the incremental loss of DNA repair enzymes together with deficiency in the

respiratory gene perhaps results in a critical level of hypoxic stress that forces other genes in the repair pathway to be activated for DNA repair to occur for cell survival.

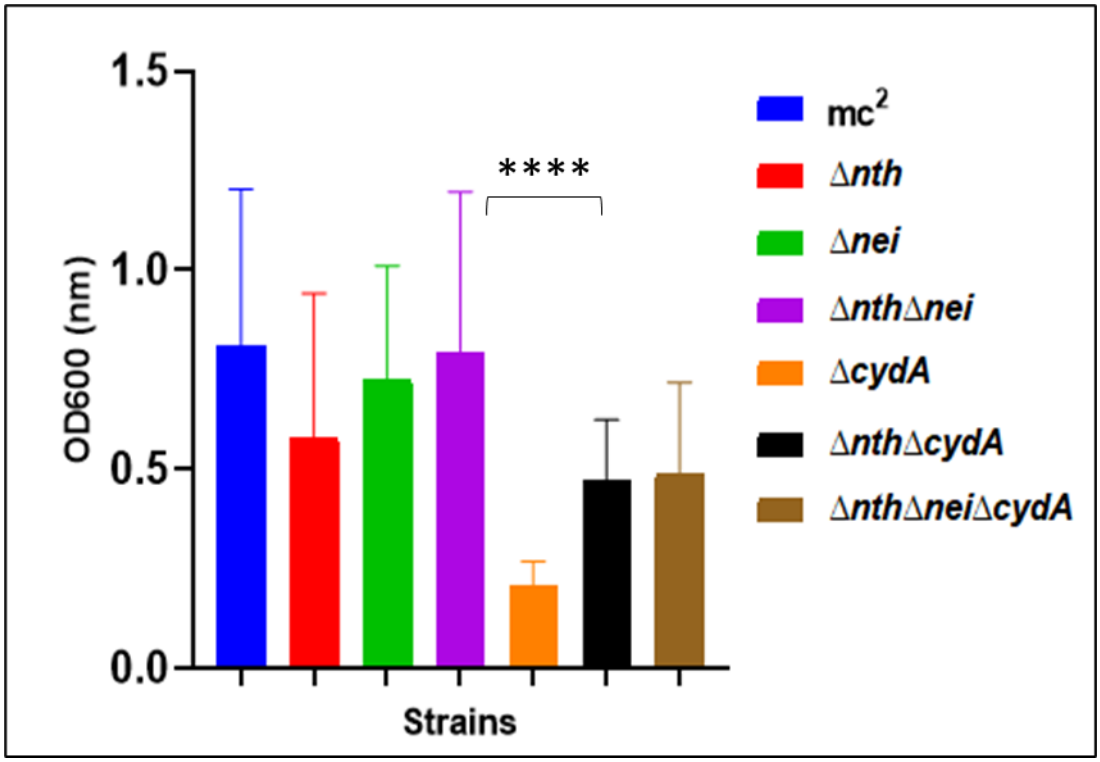


**Figure 31**. **Bar graph showing the biomass quantification of the *M. smegmatis* parental and mutant strains.** Wild type strain and the DNA repair deficient mutant strains had a higher biomass compared to the *ΔcydA* mutant due to its inability to produce intact biofilms. Error bars represent the standard error of the mean (SEM) for three biological replicates. The t-test was used for the statistical analysis on the GraphPad 8 software. ***represents the p-value of significance of 0.05.

### 3.11.3 Cell adherence quantification of formed biofilms

The ability of the parental and the mutant biofilms to attach to the plate surfaces was measured Contents of the formed biofilm were poured out and the remaining cells were stained then quantified. Each sample was diluted to 1:100 and the $OD_{600nm}$ was measured.

Wild type strain and the DNA repair deficient mutant strains had a higher cell adhesion ability (Figure 32) whilst the *ΔcydA* had a lower cell adherence due to the strains inability to produce intact biofilms (Figure 32). Statistical analysis showed no significant difference between all the strains and the wild type strain as the p-value was greater than 0.05. These data indicate that even though the strains are exposed to hypoxic conditions they are still able to survive and adhere to the surface (Figure 32).

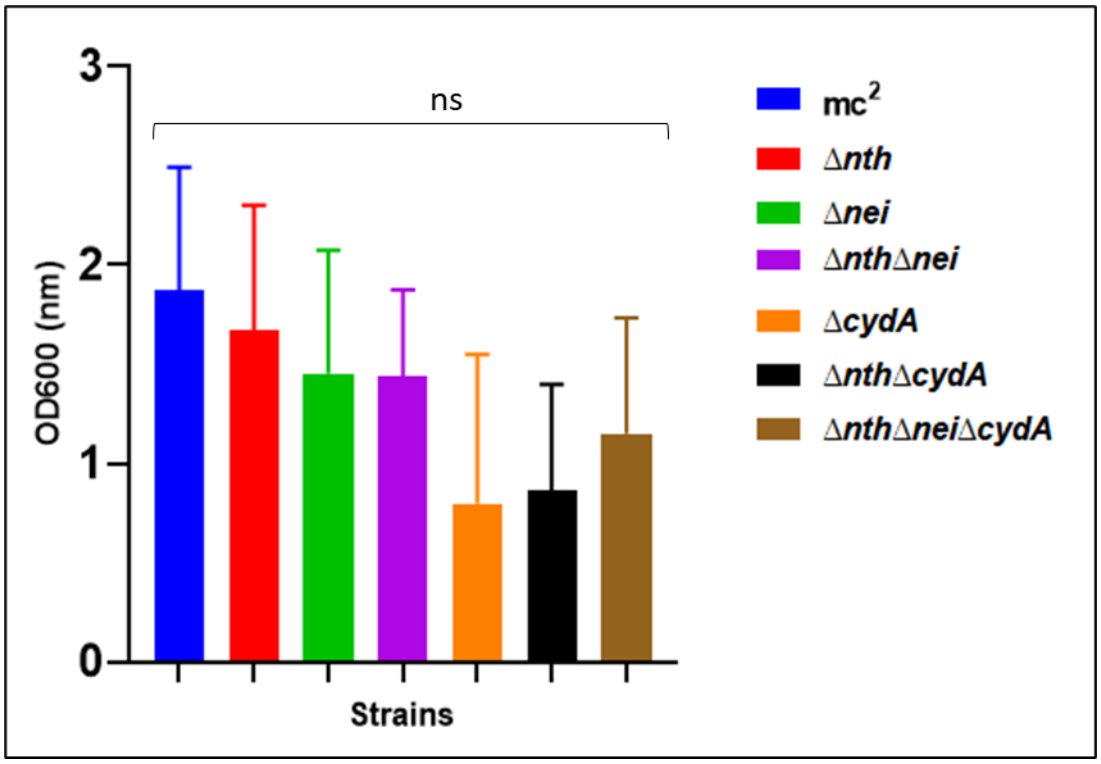


**Figure 32**. **Bar graph showing the cell adhesion quantification of the *M. smegmatis* parental and mutant strains**. Wild type strain and the DNA repair deficient mutant strains had higher cell adhesion whilst the *ΔcydA* had a lower cell adherence due to the strains inability to produce intact biofilms. Error bars represent the standard error of the mean (SEM) for three biological replicates. GraphPad 8 software was used to calculate the data and analysis was done by the t-test. The p value was not significant (ns).

Our phenotypic analysis of mutants shows that increasing the oxidative stress by deleting the *cydA* mutants in the background of BER pathway genes results in increased mutagenesis

suggesting that these genes in these two pathways are crucial for the maintenance of DNA integrity and cell survival.

**DISCUSSION**

TB continues to be a global threat despite the efforts to combat the disease through TB treatment and better accurate diagnostic techniques to detect the disease rapidly. However, the surge in drug and intrinsic resistance of mycobacteria to antimicrobial agents has exacerbated the challenges in TB treatment. Since mycobacteria are constantly exposed to DNA damaging conditions, understanding the different methods that the cellular machinery uses to repair DNA damage is also crucial as a key feature of virulence for the pathogen. Hence, in this study we aimed to understand the interaction between genes involved in the BER and ETC pathways and elucidate their effects on cell survival under unfavorable growth conditions.

The significance of DNA repair enzymes in the survival of *M. smegmatis* under oxidative stress conditions has been previously discussed ((Moolla *et al*., 2014) (Tebogo Rantsi, unpublished 2017). Moolla and colleagues showed that *nth* displays antimutator properties as deletion of the *nth* gene resulted in increased spontaneous mutation rates against rifampicin and decreased survival under oxidative stress conditions that were generated by hydrogen peroxide ($H_2O_2$) (Moolla *et al*., 2014). Combinatorial deletion of the *nth*/*nei* genes further exacerbated this phenotype, suggesting that both *nth* and *nei* play a crucial synergistic role in the maintenance of genome integrity in *M. smegmatis* under oxidative stress conditions.

Mycobacteria respire by oxidative phosphorylation that terminates with two branches; cytochrome bd-type quinol oxidase and cytochrome bc1-aa3 type oxidase (Lu *et al*., 2015b). *M. smegmatis* mutants lacking bc1/aa3 cytochrome oxidase results in decreased growth compared to the parental strain but showed up-regulation of cytochrome bd (Lu *et al*., 2015b) suggesting that mycobacteria have the ability to shift to an alternative respiratory pathway when bc1/aa3 cytochrome is absent, ensuring the survival success of the bacteria under unfavorable conditions (Kana *et al*., 2001). Since inhibition of energy metabolism and DNA repair pathways shows impaired functioning of *M. smegmatis* under anaerobic conditions and oxidative stress conditions respectively, it opens a unique avenue to simultaneously study these pathways to better understand the link between ROS and its impact on DNA damage and cell death. Our approach was to inhibit the ETC and BER pathway to examine if there would be an energy deficit that would lead to mutagenesis. This was investigated by generating mutant

strains deficient in select genes in these two pathways and analysis of these mutants under varying stress conditions.

### *M. smegmatis* wild type and mutant strains are not essential for growth activity under normal culturing conditions.

Comparison of the parental and mutant strains under normal culture conditions, displayed the same growth rate with no significant difference (Figure 21 B). This indicated that these genes do not play any crucial role in the growth activity of mycobacteria. Previously, Moolla and Goosen's studies showed that the single deletion mutants of the DNA glycosylases enzymes had no defects under normal growth conditions (Moolla *et al*., 2014, Goosens, 2009). Additionally, a study that investigated the role of BER genes in *Listeria monocytogenes* in survival and DNA damage repair, demonstrated that in *L. monocytogenes* deletion mutants growth was indistinguishable to that of the wild type indicating that these BER enzymes are not essential for growth (Zhang *et al*., 2020). Our data also showed that the ETC enzymes are not essential for growth confirming that loss of these genes has no effect on *M. smegmatis* growth.

### Sensitivity of *M. smegmatis* strains to hydrogen peroxide antibiotic

Hydrogen peroxide is a natural oxidant that causes oxidative damage to biological macromolecules leading to DNA mutations, drug resistance and cell death. Previously Moolla et al reported that combinatorial deletion of the *nth, fpg1* and *fpg2* lead to a marginal reduction in viability of strains under oxidative stress by hydrogen peroxide (Moolla *et al*., 2014) while sequential deletion of the *nth* gene in the *nei* deficient mutant background significantly reduced survival by 3–4 log after 4 hours of exposure to oxidative stress compared to the parental strain (Moolla *et al*., 2014). Additionally, Ping Lu and colleagues showed that the energy metabolism mutant's hypersensitivity to hydrogen peroxide is not due to a growth defect but the oxygen scavenging and catalyse activity that these enzymes display (Lu *et al*., 2015a) wherein the catalase activity of the cytochrome bd, directly metabolises peroxides providing a protective role against hydrogen peroxide stress conditions to prevent the production of ROS.

In this study, exposure of exponentially growing strains to hydrogen peroxide at 2.5mM concentration displayed a rapid decline in cell viability for all strains within the first 2 hours after treatment based on the CFU/ml measurement. The strains displayed a very high sensitivity response to the compound, such that we were unable to conclude the effect of ROS on the survival of these various mutant strains. However, because these strains were killed by the

compound it means the catalyse activity together with the oxygen scavenger roles were not activated. As hydrogen peroxide is a light sensitive and unstable compound a second more stable compound, menadione was used to assess oxidative stress in *M. smegmatis*.

**Susceptibility of *M. smegmatis* strains to menadione**

To get a better understanding of the survival kinetics of the *M. smegmatis* parental and mutant strains under oxidative stress conditions, their susceptibility to menadione was investigated using the MIC method. The MIC for the parental strain against menadione was 0.01560 mg/ml whilst for the mutant strains the MIC was 0.00780 mg/ml. The *ΔcydA* mutant showed a 4-fold difference in MIC compared to the wild type strain but deletion of *cydA* together with the DNA repair genes did not retain or exacerbate the MIC against menadione. The reason for this is unclear and future investigations are required.

**Sensitivity of *M. smegmatis* strains response with CHP, DTT and menadione treatment**

CHP is an organic hydroperoxide that chemically reacts with hydrogen atoms of the biological macromolecules and cause oxidative stress which eventually leads to the loss of cell viability (Patel and Mehra, 2017, Akaike *et al*., 1992). A previous study investigated oxidative stress in *M. smegmatis*, cells treated with a sub-inhibitory concentration of 152 mg/mL CHP and displayed no apparent effect on cell viability (Patel and Mehra, 2017). However, increasing the CHP to 380 mg/mL showed increased ROS levels (Patel and Mehra, 2017). These data shows that CHP oxidant can enhance stress levels in the cell by producing radicals.

DTT acts as a reducing agent and was used in the study as a control to calibrate the response of all the strains to a 100% reduced environment. Interestingly, the redox state of the untreated strains was not significantly different when compared to those treated with DTT. This hypothetically could mean that the strains that encompasses the GFP reporter are already in a reduced state which is why when they are treated with a reductant, they show no effect.

In this study we marked *M. smegmatis* mutant strains with a redox-sensitive GFP reporter to assess the redox heterogeneity in each strain. About 99-100% of the cells were oxidized by CHP which increases the likelihood that these strains will suffer damage from oxidative stress. However, the *ΔcydA-GFP* showed a resistance to changing its redox state from reduced to oxidised when treated with CHP. This means that the *cydA* protein has the potential to act as a reducing agent that protects the cell from radicals that seek to oxidise the cell. But with the constant presence of a strong oxidising agent, most cells end up being oxidised probably due to more radicals being produced in the cell since the ETC pathway (cytochrome bd) has been

disturbed. The essentiality of *cydA* is however, revealed that deletion of the *cydA* gene can cause the cell to be compromised to radicals leading to oxidative stress.

Moreover, menadione a compound that generates intracellular ROS at multiple cellular sites through redox cycling was also used to treat strains for an oxidative stress response (Loor *et al*., 2010). Previous studies have shown that high levels of menadione oxidants generates ROS which can lead to damage of macromolecules like DNA, RNA, and proteins, eventually this can trigger cell death. Furthermore, with low levels of menadione the oxidants act as active redox transduction signals which trigger protection of the cell against oxidative stress damage (Heinzel *et al*., 2005).

This study, menadione oxidized the strains at a (99-100%) rate except for the Δ*cydA*-GFP mutant. This result was the same as CHP treatment of strains. Overall, these strains showed a high sensitivity to menadione. However, to show that the redox environment is dynamic and that these treatments are reversible, we subjected the wild type strain to both menadione and DTT. The experiment displayed that *M. smegmatis* strains are originally in a reduced redox state, and after being exposed to harmful conditions they are still able to return to their initial reduced state. This mechanism showed that bacteria employ different ways to survive in the cell under oxidative stress.

**Increased mutation rates observed by Luria-Delbrück, Koch's quartiles, and Jones median estimator analysis under rifampicin treatment.**

Rifampicin is used as an assay drug because it targets the *rpoB* gene which is prone to approximately 95% of rifampicin resistance mutations occurring in the 81bp Rifampicin Resistance Determining Region (RRDR) (Ling *et al*., 2008). Single base mutations in the *rpoB* gene lead to the development of resistance against RIF making it suitable for mutation rates assessments (Zhang *et al*., 2020). Spontaneous mutations occur because of cellular processes that lead to DNA damage. Mutation rate is the expected number of mutations that occur per bacterial populations in a cell during its lifetime (Foster *et al*., 2015). Mostly, mutation rates are determined by the Luria and Delbruck method which was a model created for understanding the distribution of mutant clones per culture (Rosche and Foster 1943). However, for accurate calculation of mutation rates, the strength and limitations of the fluctuation assay should be optimised properly.

Although the fluctuation assay was carried out in triplicate only one experiment was useful for analysis. All the mutant strains displayed no increase in mutation rates relative to the wild type

strain except the *ΔnthΔneiI* mutant that showed a sharp increase compared to the individual mutants (Table 4, 5 and 6). The variations in mutant rates between the three experiments could be explained by technical variations of the fluctuation assay namely, inoculum size, initial number of cells undergoing multiplication which may result in differences in the total final number of viable cells that were plated on rifampicin. This data is comparatively like a study done by Tebogo Rantsi (unpublished, 2017) where the single mutant strains *(*Δ*nth,* Δ*nei1* and Δ*neiII*) displayed no change in mutation rates yet the combinatorial deletion mutants *(*Δ*nth*Δ*neiI*) displayed a 6-8-fold increase in mutation rates whilst the Δ*nth*Δ*nei1I* mutants showed a 2-fold increase in the mutation rates. Moolla and colleagues also showed that combinatorial deletion of the Δ*nth*/Δ*nei* genes displayed elevated spontaneous mutation frequencies compared to the wild type strain. This indicated that both Δ*nth* and Δ*nei* play a crucial synergistic role in the maintenance of genome integrity in *M. smegmatis* under oxidative stress conditions (Moolla *et al*., 2014).

The Δ*cydA* mutant did not show an increase in mutation rates suggesting that the disturbance in the energy metabolism pathway does not cause sufficient DNA damage that cannot be repaired by the BER genes. However, when *cydA* was deleted together with the DNA repair enzymes the mutation rate was elevated suggesting that that the DNA damage caused increased oxidative stress caused by the loss of the cydA gene is unable to be repaired in the absence of the key BER enzymes. These data indicated that both the ETC and BER pathways are important in maintaining cell viability under oxidative stress conditions.

**Microscopic analysis of *M. smegmatis* colonies under rifampicin treatment**

It has been previously outlined that the aggregation of mycobacterial cells that resemble cords is mostly associated with *Mycobacterium tuberculosis* complex and the *Mycobacterium marinum* species (Julián *et al*., 2010). Here we assessed whether the colonies for the various mutant strains exposed to rifampicin displayed any differences in morphology. Microscopic data displayed rough, bulgy cords morphology for the wild type strain, *Δnth, ΔneiI*, and *ΔnthΔneiI* mutants. The *ΔcydA* mutant did not display this morphology but rather a thin and flat colony but when genes in both the BER and ETC pathways were deleted the morphology is restored (*ΔnthΔcydA and ΔnthΔneiIΔcydA)* suggesting that there is some compensatory role in the DNA repair pathway for mycobacteria.

**Survival of *M. smegmatis* strains under oxygen limiting conditions.**

Biofilms are surfaces known to protect pathogens from phagocytosis and other adverse conditions by creating an oxygen depleted environment. Previously, *M. smegmatis* has been reported to have the ability to survive in hypoxic conditions and in this study this phenotype was explored for the different mutant strains of *M. smegmatis*.

Exponentially growing strains which were washed and grown to biofilms for 7 days with incubation at 37°C displayed varying phenotypes under the stereo microscope. The wild type strain was able to form intact and ruffled biofilms which confirms that *M. smegmatis* can survive under oxygen depleted environments. Under a scanning electron microscopy, a strong cellular aggregation with dense matt biofilm formation was discovered in *M. smegmatis* (Abidi *et al*., 2014). These results correlate to our findings that for growth and survival under unfavourable conditions, biofilms can be a protective system for bacteria. DNA glycosylases deficient mutants were also characterised for biofilm formation and *Δnth* strain showed ruffled, thick, and intact morphologies of biofilms. While the *ΔneiI* and *ΔnthΔneiI* strains displayed a tubular, ruffled, and intact morphology. This indicate that loss of these DNA repair genes does not impair growth and survival of these strains as they are able to form the biofilm phenotype and still survive hypoxic conditions.

The energy metabolism cytochrome bd gene *cydA* has been reported to be unable to form intact biofilms by N. Narrandes (unpublished, 2018) and the same findings were observed in this study. Lack of the *cydA* gene displayed a phenotypic defect in biofilm formation showing sediments of cells at the bottom of the well rather than intact biofilms. However, when genes from the BER pathways was deleted together with the *cydA* gene, (*ΔnthΔcydA* and *ΔnthΔneiIΔcydA*) the strains were able to form biofilms and this a recovery could be due to compensation by other DNA repair genes in the BER pathway.

Further, quantification of biofilms (biomass and cell adherence) displayed the same phenotype due to the *ΔcydA* mutant unable to form biofilms, which resulted in the low efficiency for the cells to adhere to surfaces and the reduced cell quantity compared to the parental strain and other mutants. However, the *ΔnthΔcydA* and *ΔnthΔneiIΔcydA* mutant strains increased biomass and cell adherence of the cells, once again suggesting that other DNA repair enzymes of the BER are most likely compensating for the loss of the Nth and Nei homologues for survival under hypoxic conditions.

## CONCLUDING REMARKS

Overall, the aim and objectives of this study were achieved in evaluating the phenotypes displayed by *M. smegmatis* parental and mutant strains under standard and unfavourable conditions. A better understanding of how the BER and ETC interplay in aiding the survival of the cell and maintenance of the bacterial genome integrity under harsh environments was also achieved. It is important to note that phenotypic analysis highlighted that single deletion mutants were more prone to be affected by the unfavourable conditions. However, when the double or triple mutants are exposed to the stress conditions, they were resistant and revealed a recovery role in enhancing survival of the cell. Mutagenesis was also assessed, and it was confirmed that when essential genes from the DNA repair pathway and ETC are deleted it led to a high rate of mutations which could lead to resistance and eventually cell death if they are not rectified. Therefore, the finding of this study indicates that that the two pathways (ETC and BER) has contributed substantial information which can be applied to *M. tb* to better understand the development of resistance and how the bacterium is able to persist and maintain genome integrity under oxidative and hypoxic conditions.

## FUTURE STUDIES

The redox potential system, would be useful to assess mutagenesis of the GFP marked mutant strains after the strains have been exposed to oxidative stress conditions. This assay system provided a much better and stable assay to measure mutagenesis in comparison to measuring survival under oxidative stress conditions as generated by hydrogen peroxide. Due to the instability and light sensitivity of hydrogen peroxide it poses several technical challenges for reproducibility and robustness of data.

## REFERENCES


Abidi SH, Ahmed K, Sherwani SK, Bibi N & Kazmi SU (2014) Detection of Mycobacterium smegmatis biofilm and its control by natural agents. *Int J Curr Microbiol App Sci* **3**: 801-812.

Acuña-Villaorduña C, Jones-López EC, Fregona G, Marques-Rodrigues P, Gaeddert M, Geadas C, Hadad DJ, White LF, Molina LPD & Vinhas S (2018) Intensity of exposure to pulmonary tuberculosis determines risk of tuberculosis infection and disease. *European Respiratory Journal* **51**: 1701578.

Aguiar PH, Furtado C, Repolês BM, Ribeiro GA, Mendes IC, Peloso EF, Gadelha FR, Macedo AM, Franco GR & Pena SD (2013) Oxidative stress and DNA lesions: the role of 8-oxoguanine lesions in Trypanosoma cruzi cell viability. *PLoS neglected tropical diseases* **7**: e2279.

Ahmad S (2010) Pathogenesis, immunology, and diagnosis of latent Mycobacterium tuberculosis infection. *Clinical and Developmental Immunology* **2011**:

Akaike T, Sato K, Ijiri S, Miyamoto Y, Kohno M, Ando M & Maeda H (1992) Bactericidal activity of alkyl peroxyl radicals generated by heme-iron-catalyzed decomposition of organic peroxides. *Archives of biochemistry and biophysics* **294**: 55-63.

Alemu J, Mamo G, Ameni G & Pal M (2016) Molecular Epidemiology of Bovine Tuberculosis in Cattle and its Public Health Implications in Gambella Town and its Surroundings, Gambella Regional State, Ethiopia. *Global Journal of Medical Research*

Annabel B, Anna D & Hannah M (2019) Global tuberculosis report 2019. *Geneva: World Health Organization* 7-9.

Barberis I, Bragazzi NL, Galluzzo L & Martini M (2017) The history of tuberculosis: from the first historical records to the isolation of Koch's bacillus. *Journal of preventive medicine and hygiene* **58**: E9.

Berney M & Cook GM (2010) Unique flexibility in energy metabolism allows mycobacteria to combat starvation and hypoxia. *PloS one* **5**: e8614.

Bhaskar A, Chawla M, Mehta M, Parikh P, Chandra P, Bhave D, Kumar D, Carroll KS & Singh A (2014) Reengineering redox sensitive GFP to measure mycothiol redox potential of Mycobacterium tuberculosis during infection. *PLoS Pathog* **10**: e1003902.

Bloom DE, Cafiero E, Jané-Llopis E, Abrahams-Gessel S, Bloom LR, Fathima S, Feigl AB, Gaziano T, Hamandi A & Mowafi M 2012. The global economic burden of noncommunicable diseases. Program on the Global Demography of Aging.

Boshoff HI & Barry CE (2005) Tuberculosis—metabolism and respiration in the absence of growth. *Nature Reviews Microbiology* **3**: 70-80.

Cadet J & Davies KJ (2017) Oxidative DNA damage & repair: an introduction. *Free Radical Biology and Medicine* **107**: 2-12.

Candeias LP & Steenken S (2000) Reaction of HO. with Guanine Derivatives in Aqueous Solution: Formation of Two Different Redox-Active OH-Adduct Radicals and Their Unimolecular Transformation Reactions. Properties of G (-H). *Chemistry–A European Journal* **6**: 475-484.

Cheremisinoff P 2018. *Air pollution control and design for industry*, Routledge.

Costa RM, Chigançcas V, Da Silva Galhardo R, Carvalho H & Menck CF (2003) The eukaryotic nucleotide excision repair pathway. *Biochimie* **85**: 1083-1099.

Creswell JH 2015. *Early and increased tuberculosis case detection: Implementation, measurement, and evaluation*, Universiteit van Amsterdam [Host].

Cunningham RP & Weiss B (1985) Endonuclease III (nth) mutants of Escherichia coli. *Proceedings of the National Academy of Sciences* **82**: 474-478.

Darwin KH & Nathan CF (2005) Role for nucleotide excision repair in virulence of Mycobacterium tuberculosis. *Infection and immunity* **73**: 4581-4587.

Davis EO, Dullaghan EM & Rand L (2002) Definition of the mycobacterial SOS box and use to identify LexA-regulated genes in Mycobacterium tuberculosis. *Journal of bacteriology* **184**: 3287-3295.

Dianov G & Lindahl T (1994) Reconstitution of the DNA base excision—repair pathway. *Current biology* **4**: 1069-1076.

Dos Vultos T, Mestre O, Tonjum T & Gicquel B (2009) DNA repair in Mycobacterium tuberculosis revisited. *FEMS Microbiology Reviews* **33**: 471-487.

Flagan RC (2011) Electrical mobility methods for submicrometer particle characterization. *Aerosol Measurement: Principles, Techniques, and Applications* 339-364.

Flemming H-C & Wingender J (2010) The biofilm matrix. *Nature reviews microbiology* **8**: 623.

Foster PL (2006) Methods for determining spontaneous mutation rates. *Methods in enzymology* **409**: 195-213.

Foster PL, Lee H, Popodi E, Townes JP & Tang H (2015) Determinants of spontaneous mutation in the bacterium Escherichia coli as revealed by whole-genome sequencing. *Proceedings of the National Academy of Sciences* **112**: E5990-E5999.

Foudah AI, Alam A, Soliman GA, Salkini MA, Ahmed EOI, Yusufoglu HS, Chanda S, Funk V, Bayer R & Keeley S (2014) Free radicals and oxidative stress in bacteria. *Asian Journal of Biological Sciences* **9**: 69-73.

Fromme JC, Banerjee A & Verdine GL (2004) DNA glycosylase recognition and catalysis.

*Current opinion in structural biology* **14**: 43-49.

Gedik CM & Collins A (2005) Establishing the background level of base oxidation in human lymphocyte DNA: results of an interlaboratory validation study. *The FASEB journal* **19**: 82 -84.

Gengenbacher M & Kaufmann SH (2012) Mycobacterium tuberculosis: success through dormancy. *FEMS microbiology reviews* **36**: 514-532.

Getahun H, Matteelli A, Chaisson RE & Raviglione M (2015) Latent Mycobacterium tuberculosis Infection. *New England Journal of Medicine* **372**: 2127-2135.

Goosens VJ. 2009. *The construction and phenotypic characterization of mycobacterial mutants deficient in DNA glycosylases.*

Gordhan BG & Parish T 2001. Gene replacement using pretreated DNA. *Mycobacterium tuberculosis protocols.* Springer.

Guirado E & Schlesinger L (2013) Modeling the Mycobacterium tuberculosis granuloma–the critical battlefield in host immunity and disease. *Frontiers in immunology* **4**: 98.

Guo Y, Bandaru V, Jaruga P, Zhao X, Burrows CJ, Iwai S, Dizdaroglu M, Bond JP &

Wallace SS (2010) The oxidative DNA glycosylases of Mycobacterium tuberculosis exhibit different substrate preferences from their Escherichia coli counterparts. *DNA repair* **9**: 177-190.

Gutierrez MC, Brisse S, Brosch R, Fabre M, Omaïs B, Marmiesse M, Supply P & Vincent V (2005) Ancient origin and gene mosaicism of the progenitor of Mycobacterium tuberculosis. *PLoS pathogens* **1**: e5.

Harding E (2020) WHO global progress report on tuberculosis elimination. *The Lancet Respiratory Medicine* **8**: 19.

Hassim F, Papadopoulos AO, Kana BD & Gordhan BG (2015) A combinatorial role for

MutY and Fpg DNA glycosylases in mutation avoidance in Mycobacterium smegmatis. *Mutation Research/Fundamental and Molecular Mechanisms of Mutagenesis* **779**: 24-32.

Heinzel FR, Luo Y, Li X, Boengler K, Buechert A, García-Dorado D, Di Lisa F, Schulz R & Heusch G (2005) Impairment of diazoxide-induced formation of reactive oxygen species and loss of cardioprotection in connexin 43 deficient mice. *Circulation research* **97**: 583-586.

Imlay JA & Linn S (1988) DNA damage and oxygen radical toxicity. *Science* **240**: 1302-1309.

Jones M, Thomas S & Rogers A (1994) Luria-Delbrück fluctuation experiments: design and analysis. *Genetics* **136**: 1209-1216.

Julián E, Roldán M, Sánchez-Chardi A, Astola O, Agustí G & Luquin M (2010) Microscopic cords, a virulence-related characteristic of Mycobacterium tuberculosis, are also present in

nonpathogenic mycobacteria. *Journal of bacteriology* **192**: 1751-1760.

Kana BD, Weinstein EA, Avarbock D, Dawes SS, Rubin H & Mizrahi V (2001) Characterization of thecydAB-Encoded Cytochrome bd Oxidase fromMycobacterium smegmatis. *Journal of Bacteriology* **183**: 7076-7086.

Kendall EA, Cohen T, Mitnick CD & Dowdy DW (2017) Second line drug susceptibility testing to inform the treatment of rifampin-resistant tuberculosis: a quantitative perspective. *International Journal of Infectious Diseases* **56**: 185-189.

Koch AL & Wang CH (1982) How close to the theoretical diffusion limit do bacterial uptake systems function? *Archives of Microbiology* **131**: 36-42.

Kropachev KY, Zharkov DO & Grollman AP (2006) Catalytic mechanism of Escherichia coli endonuclease VIII: roles of the intercalation loop and the zinc finger. *Biochemistry* **45**: 12039-12049.

Kurthkoti K, Kumar P, Jain R & Varshney U (2008) Important role of the nucleotide excision repair pathway in Mycobacterium smegmatis in conferring protection against commonly encountered DNA-damaging agents. *Microbiology* **154**: 2776-2785.

Kurthkoti K, Kumar P, Sang PB & Varshney U (2020) Base excision repair pathways of bacteria: new promise for an old problem. *Future Medicinal Chemistry* **12**: 339-355.

Kurthkoti K & Varshney U (2011) Base excision and nucleotide excision repair pathways in mycobacteria. *Tuberculosis* **91**: 533-543.

Kurthkoti K & Varshney U (2012) Distinct mechanisms of DNA repair in mycobacteria and their implications in attenuation of the pathogen growth. *Mechanisms of ageing and development* **133**: 138-146.

Ling DI, Zwerling AA & Pai M (2008) GenoType MTBDR assays for the diagnosis of multidrug-resistant tuberculosis: a meta-analysis. *European Respiratory Journal* **32**: 1165-1174.

Liu Y, Fiskum G & Schubert D (2002) Generation of reactive oxygen species by the mitochondrial electron transport chain. *Journal of neurochemistry* **80**: 780-787.

Lodish H, Berk A, Zipursky SL, Matsudaira P, Baltimore D & Darnell J 2000. Electron transport and oxidative phosphorylation. *Molecular Cell Biology. 4th edition.* WH Freeman.

Loor G, Kondapalli J, Schriewer JM, Chandel NS, Hoek TLV & Schumacker PT (2010) Menadione triggers cell death through ROS-dependent mechanisms involving PARP activation without requiring apoptosis. *Free Radical Biology and Medicine* **49**: 1925-1936.

Lu P, Heineke MH, Koul A, Andries K, Cook GM, Lill H, Van Spanning R & Bald D (2015a) The cytochrome bd-type quinol oxidase is important for survival of

Mycobacterium smegmatis under peroxide and antibiotic-induced stress. *Scientific reports* **5**: 1-10.

Lu P, Heineke MH, Koul A, Andries K, Cook GM, Lill H, Van Spanning R & Bald D (2015b) The cytochrome bd-type quinol oxidase is important for survival of Mycobacterium smegmatis under peroxide and antibiotic-induced stress. *Scientific reports* **5**: 10333.

Luca S & Mihaescu T (2013) History of BCG vaccine. *Maedica* **8**: 53-58.

Luria SE & Delbrück M (1943) Mutations of bacteria from virus sensitivity to virus resistance. *Genetics* **28**: 491.

Machowski EE, Barichievy S, Springer B, Durbach SI & Mizrahi V (2007) In vitro analysis of rates and spectra of mutations in a polymorphic region of the Rv0746 PE_PGRS gene of Mycobacterium tuberculosis. *Journal of bacteriology* **189**: 2190-2195.

Manuel RC, Czerwinski EW & Lloyd RS (1996) Identification of the structural and functional domains of MutY, an Escherichia coli DNA mismatch repair enzyme. *Journal of Biological Chemistry* **271**: 16218-16226.

Marti TM, Kunz C & Fleck O (2002) DNA mismatch repair and mutation avoidance pathways. *Journal of cellular physiology* **191**: 28-41.

Mascolo L & Bald D (2019) Cytochrome bd in Mycobacterium tuberculosis: A respiratory chain protein involved in the defense against antibacterials. *Progress in biophysics and molecular biology*

Matsoso LG, Kana BD, Crellin PK, Lea-Smith DJ, Pelosi A, Powell D, Dawes SS, Rubin H, Coppel RL & Mizrahi V (2005) Function of the cytochrome bc1-aa3 branch of the respiratory network in mycobacteria and network adaptation occurring in response to its disruption. *Journal of bacteriology* **187**: 6300-6308.

Miller M & Gennis RB (1985) The cytochrome d complex is a coupling site in the aerobic respiratory chain of Escherichia coli. *Journal of Biological Chemistry* **260**: 14003-14008.

Mittler R (2002) Oxidative stress, antioxidants and stress tolerance. *Trends in plant science* **7**: 405-410.

Mizrahi V & Andersen SJ (1998) DNA repair in Mycobacterium tuberculosis. What have we learnt from the genome sequence? *Molecular microbiology* **29**: 1331-1339.

Mohammadipanah F & Dehhaghi M 2017. Classification and Taxonomy of Actinobacteria. *Biology and Biotechnology of Actinobacteria.* Springer.

Moolla N, Goosens VJ, Kana BD & Gordhan BG (2014) The contribution of Nth and Nei DNA glycosylases to mutagenesis in Mycobacterium smegmatis. *DNA repair* **13**: 32-41.

Nardell EA (2016) Transmission and institutional infection control of tuberculosis. *Cold Spring Harbor perspectives in medicine* **6**: a018192.

Nicholas AB, Bishai WR & Jain SK 2016. Pathogenesis of Tuberculosis: New Insights. *Tuberculosis.* CRC Press.

Nimse SB & Pal D (2015) Free radicals, natural antioxidants, and their reaction mechanisms. *Rsc Advances* **5**: 27986-28006.

Olsen I, Balasingham SV, Davidsen T, Debebe E, Rødland EA, Van Soolingen D, Kremer K, Alseth I & Tønjum T (2009) Characterization of the major formamidopyrimidine-DNA glycosylase homolog in Mycobacterium tuberculosis and its linkage to variable tandem repeats. *FEMS Immunology & Medical Microbiology* **56**: 151-161.

Patel YS & Mehra S (2017) Synergistic response of rifampicin with hydroperoxides on mycobacterium: a mechanistic study. *Frontiers in microbiology* **8**: 2075.

Pethe K, Bifani P, Jang J, Kang S, Park S, Ahn S, Jiricek J, Jung J, Jeon HK & Cechetto J (2013) Discovery of Q203, a potent clinical candidate for the treatment of tuberculosis. *Nature medicine* **19**: 1157-1160.

Philips JA & Ernst JD (2012) Tuberculosis Pathogenesis and Immunity. *Annual Review of Pathology: Mechanisms of Disease* **7**: 353-384.

Rosche WA & Foster PL (2000) Determining mutation rates in bacterial populations. *Methods* **20**: 4-17.

Sarkar S, Ma W & Sandri GVH (1992) On fluctuation analysis: a new, simple and efficient method for computing the expected number of mutants. *Genetica* **85**: 173-179.

Sevilla IA, Molina E, Elguezabal N, Pérez V, Garrido JM & Juste RA (2015) Detection of mycobacteria, Mycobacterium avium subspecies, and Mycobacterium tuberculosis complex by a novel tetraplex real-time PCR assay. *Journal of clinical microbiology* **53**: 930-940.

Sharma P, Jha AB, Dubey RS & Pessarakli M (2012) Reactive oxygen species, oxidative damage, and antioxidative defense mechanism in plants under stressful conditions. *Journal of botany* **2012**:

Sidorenko V, Rot M, Filipenko M, Nevinsky G & Zharkov D (2008) Novel DNA glycosylases from Mycobacterium tuberculosis. *Biochemistry (moscow)* **73**: 442-450.

Soboleski MR, Oaks J & Halford WP (2005) Green fluorescent protein is a quantitative reporter of gene expression in individual eukaryotic cells. *The FASEB journal* **19**: 1-20.

Springer B, Sander P, Sedlacek L, Hardt WD, Mizrahi V, Schär P & Böttger EC (2004) Lack of mismatch correction facilitates genome evolution in mycobacteria. *Molecular microbiology* **53**: 1601-1609.

Sykes JE & Gunn-Moore DA (2013) Mycobacterial infections. *Canine and Feline Infectious Diseases-E-BOOK* 418.

Tang J, Yam W-C & Chen Z (2016) Mycobacterium tuberculosis infection and vaccine development. *Tuberculosis* **98**: 30-41.

Torrelles JB & Schlesinger LS (2017) Integrating Lung Physiology, Immunology, and Tuberculosis. *Trends in Microbiology* **25**: 688-697.

Valerie K & Povirk LF (2003) Regulation and mechanisms of mammalian double-strand break repair. *Oncogene* **22**: 5792.

Van Der Meeren O, Hatherill M, Nduba V, Wilkinson RJ, Muyoyeta M, Van Brakel E, Ayles HM, Henostroza G, Thienemann F & Scriba TJ (2018) Phase 2b controlled trial of M72/AS01E vaccine to prevent tuberculosis. *New England Journal of Medicine* **379**: 1621-1634.

Wallace SS (2002) Biological consequences of free radical-damaged DNA bases. *Free Radical Biology and Medicine* **33**: 1-14.

Wallace SS, Bandaru V, Kathe SD & Bond JP (2003) The enigma of endonuclease VIII. *DNA repair* **2**: 441-453.

Weiss G & Schaible UE (2015) Macrophage defense mechanisms against intracellular bacteria. *Immunological reviews* **264**: 182-203.

Who (2017) *TUBERCULOSIS REPORT* 147.

Who (2020) Global tuberculosis report 2020: executive summary.

Wiederholt CJ, Patro JN, Jiang YL, Haraguchi K & Greenberg MM (2005) Excision of formamidopyrimidine lesions by endonucleases III and VIII is not a major DNA repair pathway in Escherichia coli. *Nucleic acids research* **33**: 3331-3338.

Yanagawa H, Ogawa Y & Ueno M (1992) Redox ribonucleosides. Isolation and characterization of 5-hydroxyuridine, 8-hydroxyguanosine, and 8-hydroxyadenosine from Torula yeast RNA. *Journal of Biological Chemistry* **267**: 13320-13326.

Zhang J, Wang S, Abee T & Van Der Veen S (2020) Role of base excision repair in Listeria monocytogenes DNA stress survival during infections. *The Journal of Infectious Diseases*

## Appendix A: Materials

### 1. MEDIA preparations and solutions for *M. smegmatis*

Difco 7H9 media

Weigh 4.23 g of 7H9 difco powder in a 1 litre autoclaved bottle. Add 890 ml of distilled water and 5 ml of glycerol. Mix the solution until dissolved then autoclave as per conditions (Mode 2 at 121°C for 15 minutes). After autoclaving is done, cool media then add 10 ml of glucose salts solution also 25% 1 ml tween solution. Additionally, the media can also be supplemented with antibiotics of choice.

Non-difco 7H10 media

Weigh 17.1 g of 7H9 non-difco powder in a 1 litre autoclaved bottle. Add 890 ml of distilled water and 5 ml of glycerol. Mix the solution until dissolved then autoclave as per conditions (Mode 1 at 121°C for 25 minutes). After autoclaving is done, cool media then add 10 ml of glucose salts solution. Additionally, the media can also be supplemented with antibiotics of choice.

Luria-Bertani Agar (LA)

Weigh (5 g yeast extract, 10 g tryptone, 10 g NaCl and 1.5 g) in a 1 litre autoclaved bottle. Add 890 ml of distilled water. Mix the solution until dissolved then autoclave as per condition (Mode 1 at 121°C for 15 minutes). However, the media can also be supplemented with antibiotics of choice.

Luria- Bertani Broth (LB)

Weigh (5 g yeast extract, 10 g tryptone and 10 g NaCl) dissolved in 1L sd$H_2O$ in a 1 litre autoclaved bottle. Add 890 ml of distilled water. Mix the solution until dissolved then autoclave as per condition (Mode 2 at 121°C for 15 minutes). However, the media can also be supplemented with antibiotics of choice.

2 TY

10 g yeast extract, 16 g tryptone and 10 g NaCl dissolved in 1L sdH2O.

**Table A1 Supplements for media**

| Media supplements | components |
|---|---|
| Glucose salts (100X) | 20 g glucose and 8.5 g NaCl dissolved in 100 ml sdH2O. |
| Tween (20%) | 10 ml Tween80 dissolved in 40 ml sd$H_2O$. |
| X-gal (25%) | 1 g X- gal dissolved in 50 ml deionized DMF |
| Sucrose (25%) | 75 g sucrose dissolved in 100 ml sdH2O |
| NaCl | 5 M NaCl in sdH2O (autoclaved) |
| | |

**Table A2 Solutions for DNA extraction**

| Solutions | components |
|---|---|
| CTAB/NaCl | 4.1% NaCl and 10% N – acetyl- N, N, N – trimethyl ammonium bromide dissolved in sdH2O. Filter sterilize. |
| TE buffer | 10 mM Tris- HCl (pH 8) and 10 mM EDTA dissolved in sdH2O. Autoclave. |
| Chloroform: Isoamyl alcohol | 24 ml chloroform and 1ml isoamyl alcohol. |
| Sodium Acetate | 3 M sodium acetate dissolved in sdH2O (pH5.2). Autoclave. |
| Solution I | 50 mM Glucose, 25mM Tris-HCl, 10mM EDTA dissolved in sdH2O.Autoclave. |
| Solution II | 1% SDS, 0.2M NaOH dissolved in sdH2O. |
| Solution III | 3M Potassium acetate, 11.5% acetic acid dissolved in sdH2O. |

**Table A3 Solutions to make Agarose gels.**

| TAE | 50 X stock solution: 242 g Tris base 57.1 ml glacial acetic and 100 ml EDTA (pH 8) made up to 1L with sdH2O. |
|---|---|
| Ethidium bromide | 10 mg/ml dissolved in sdH2O. |

**Table A4 Agarose powder**

| Gel % | Amount of agarose (g) to use in 50 ml of buffer |
|---|---|
| 0.8 | 0.4 |
| 1 | 0.5 |
| 2 | 1 |

**Table A5 Southern blot solutions**

| Reagents | Components |
|---|---|
| Denaturation solution | 1.5 M NaCl and 0.5 M NaOH dissolved in sdH2O. |
| Depurination solution | 0.25 M HCl dissolved in sdH2O. |
| TBE (1X) | 100 ml 10 X Tris-Borate-EDTA (Sigma) dissolved in 900 ml sdH2O. |
| SSC (20X) | 0.3 M Sodium citrate and 3 M NaCl dissolved in sdH2O. |
| SDS (10%) | 10 g SDS powder dissolved in 100 ml sdH2O. |
| Solution 1 | 0.1% SDS and 2 X SSC dissolved in sdH2O. |
| Solution 2 | 0.1% SDS and 0.5 X SSC dissolved in sdH2O. |
| Maleic Acid Buffer | 1.5 M NaCl and 1 M Maleic acid dissolved in sdH2O. Adjusted to pH 7.5 with NaOH pellets. |
| Wash buffer | 0.1 M Maleic Acid Buffer and 0.3% Tween20. |
| Blocking solution (Roche) | 1 X blocking solutions dissolved in Maleic Acid Butter. |
| Detection buffer | 0.1 M NaCl and 0.1 M Tris-HCl dissolved in sdH2O (pH 9.5) |
| Antibody solution (Roche) | Dilute 1: 10000 in blocking solution. |
| Stripping solution | 0.2 M NaOH and 0.1% SDS dissolved in sdH2O. |

**Molecular markers used.**

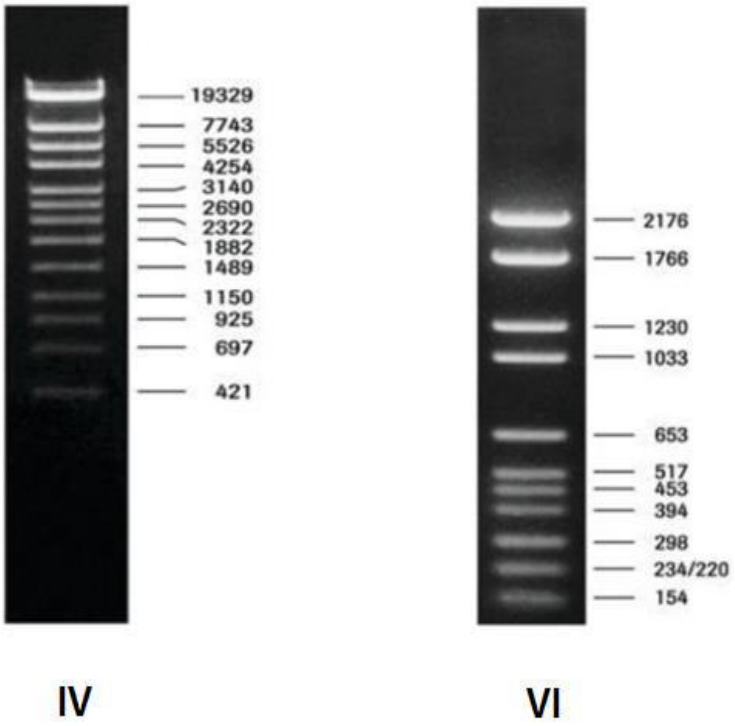


Figure A1: DNA molecular weight markers used in this study.

## Appendix B: Supplementary figures

## Fluctuation assay databased on the Luria-Delbruck method

### B1: Fluctuation assay 1

$mc^2$

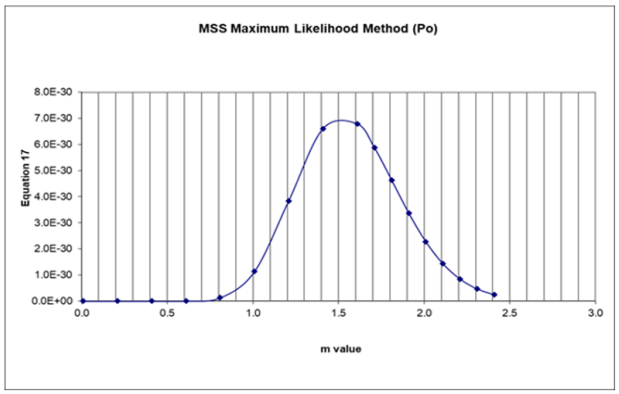


*Δnth*

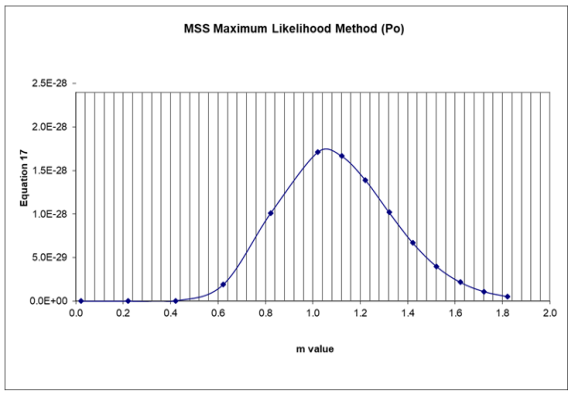


*Δnei*

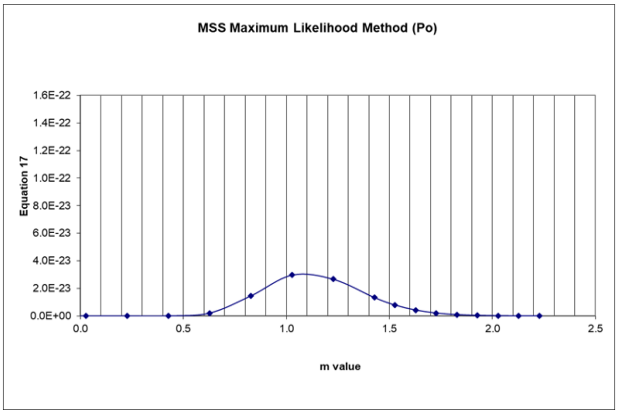


*ΔnthΔnei*

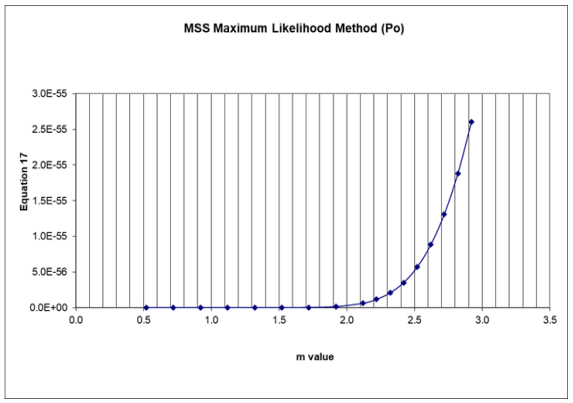

*ΔcydA*

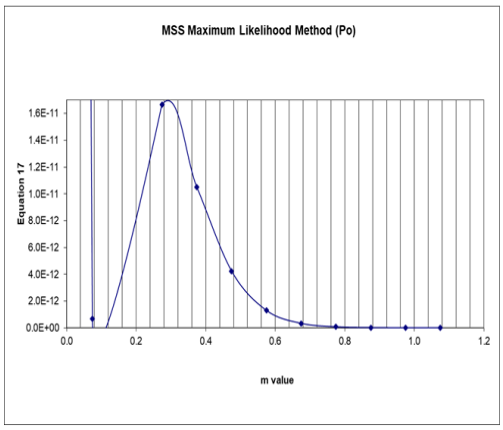


*ΔnthΔcydA*

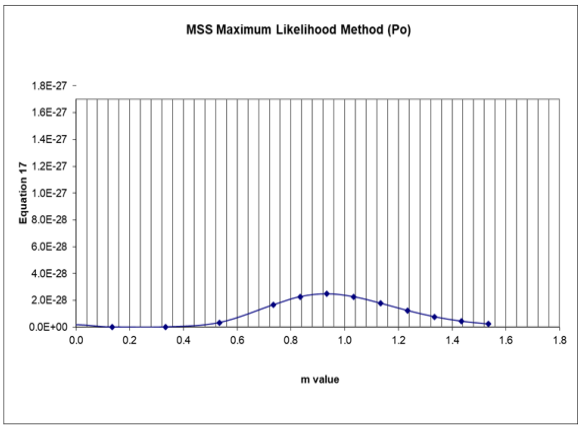


*ΔthΔneiΔcydA*

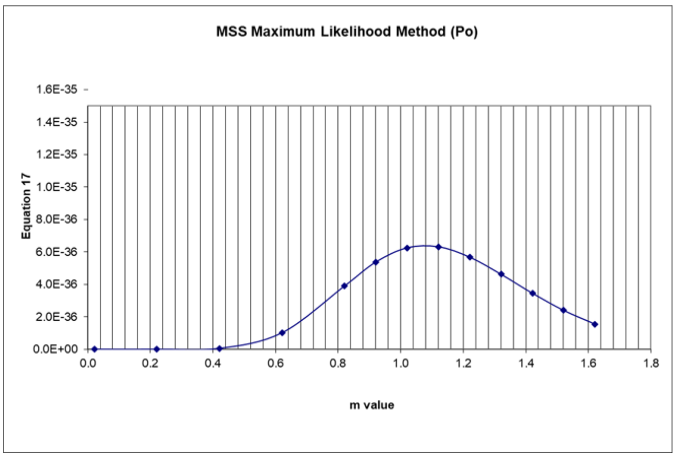


**Figure 33 MSS distribution LC curves used to estimate the mutation rate for the parental and mutant strains for experiment 1 of the fluctuation assay**. These graphs show the peak at which the strains m-value is determined. The m value represents the distribution of the mutations and it was used to calculate the mutation rate for the parental strain by the use the excel spreadsheet created at the CBTBR lab (Machowski *et al*., 2007). In this spreadsheet, the possible values of m were plotted on the x-axis and equation 17 data was plotted on the y-axis.

Table B1 shows the m values for the wild type and mutant strains for fluctuation assay experiment 1, 2 and 3. These values were calculated with the excel spreadsheet that was created by (Machowski *et al*., 2007). To calculate the mutation rates, the m value was incorporated in equation 17 in the spreadsheet.

**Table B1. The value of m (number of mutations per culture) for 3 experiments**

| Strain | Experiment 1 | Experiment 2 | Experiment 3 |
|---|---|---|---|
| | Mutations per culture (m) | | |
| $mc^2$ | 1.61 | 0.92 | 0.58 |
| ***Δnth*** | 1.02 | 0.82 | 0.73 |
| ***Δnei*** | 1.43 | 0.27 | 0.39 |
| ***ΔnthΔnei*** | 2.21 | 1.61 | 0.82 |
| ***ΔcydA*** | 0.27 | 0.82 | 0.22 |
| ***ΔnthΔcydA*** | 0.73 | 1.43 | 0,27 |
| ***ΔnthΔneiΔcydA*** | 0.82 | 1.43 | 0.17 |

## B2: Fluctuation assay 2

mc²

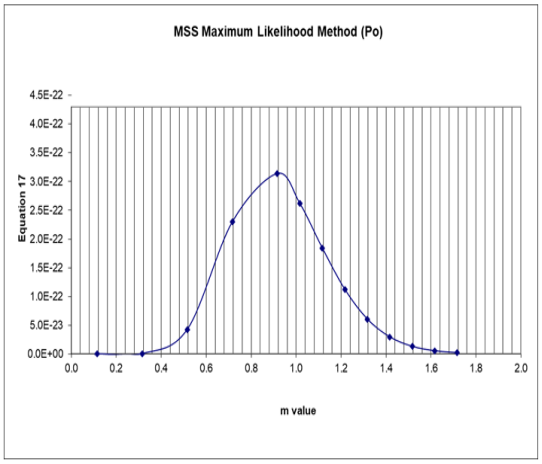


*Δnth*

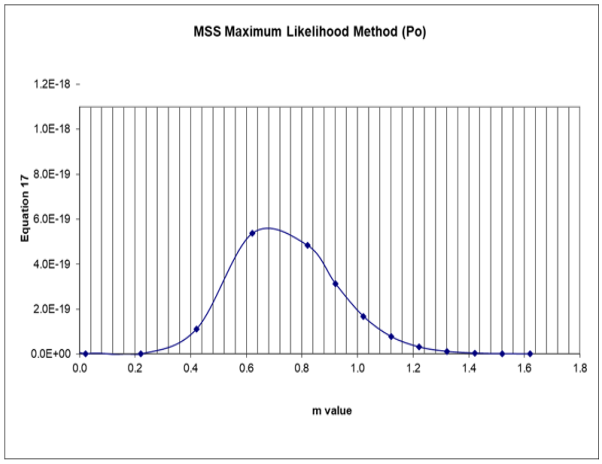


*Δnei*

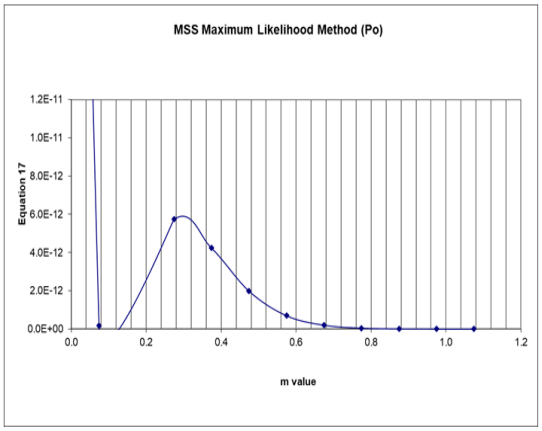


*Δnth*Δnei

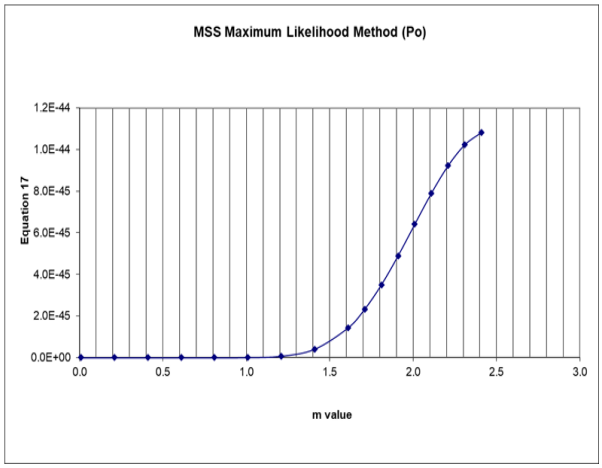

*ΔcydA*

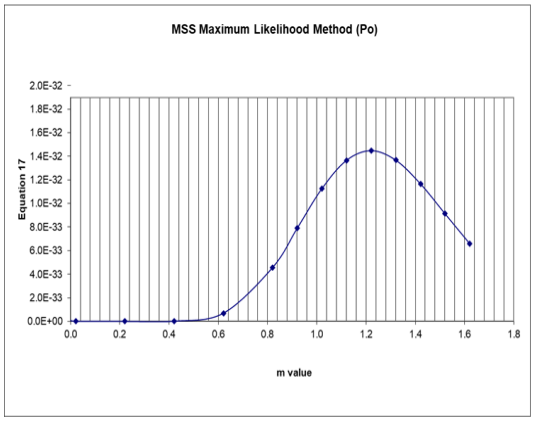


*ΔnthΔcydA*

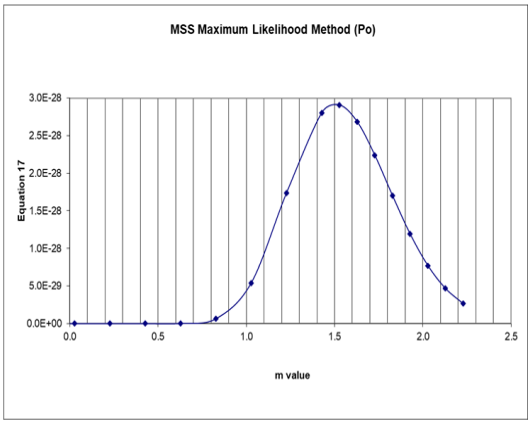


*ΔnthΔneiΔcydA*

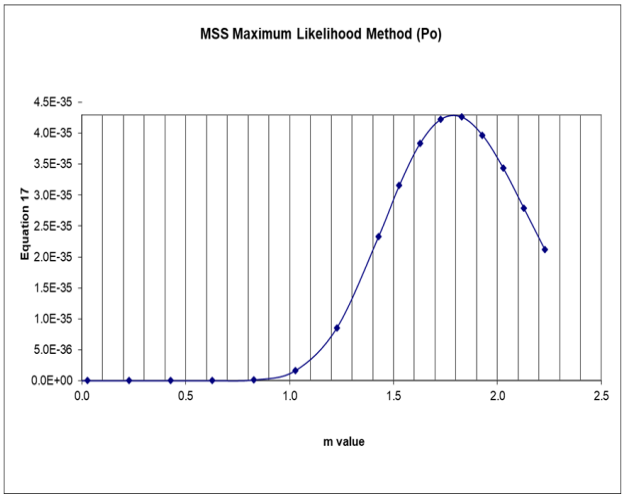


**Figure 34 MSS distribution LC curves used to estimate the mutation rate for the parental and mutant strains for experiment 2 of the fluctuation assay**. These graphs show the peak at which the strains m-value is determined. The m value represents the distribution of the mutations and it was used to calculate the mutation rate for the parental strain by the use the excel spreadsheet created at the CBTBR lab (Machowski *et al*., 2007).In this spreadsheet, the possible values of m were plotted on the x-axis and equation 17 data was plotted on the y-axis.

## B3: Fluctuation assay 3

$mc^2$

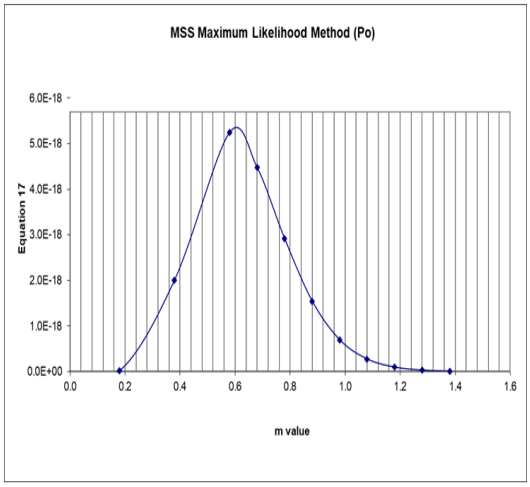


*Δnth*

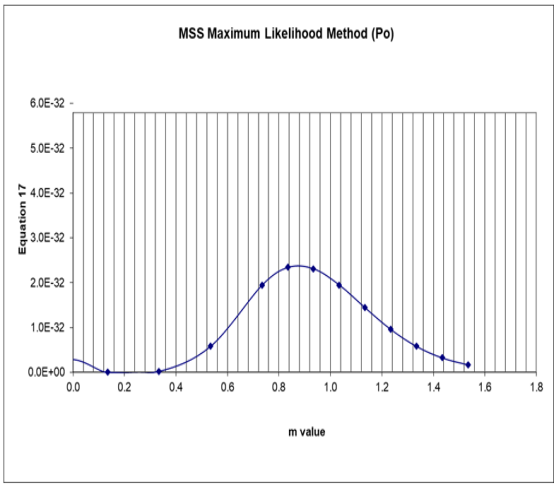


*Δnei*

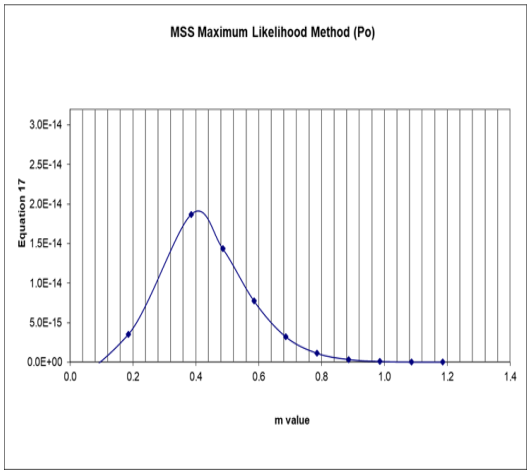


*ΔnthΔnei*

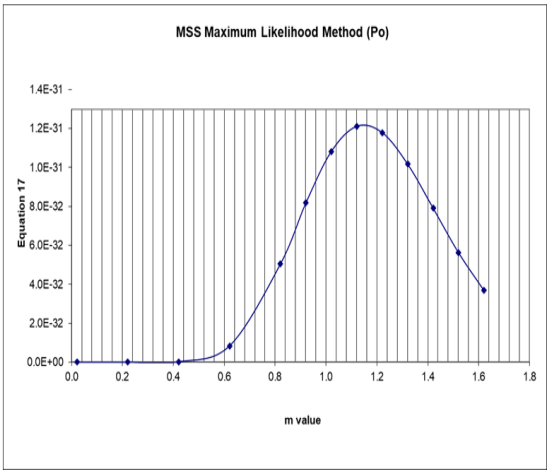

ΔcydA

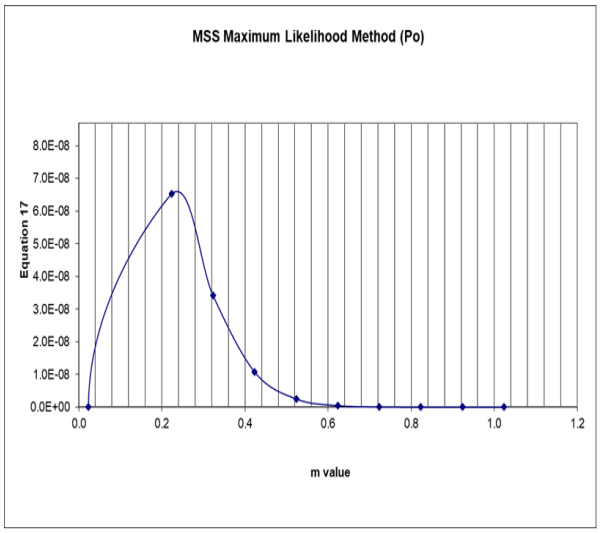


ΔnthΔcydA

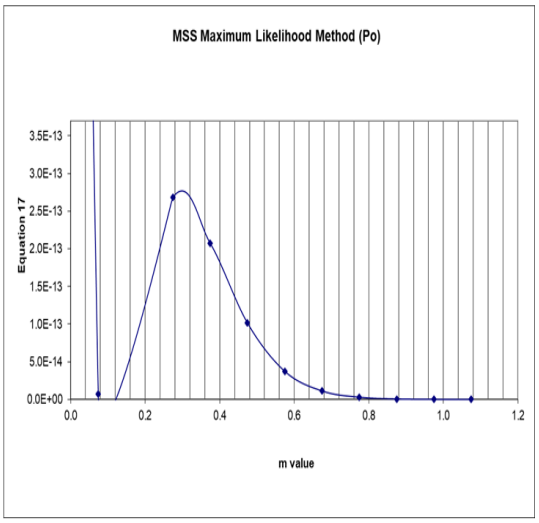


ΔnthΔneiΔcydA

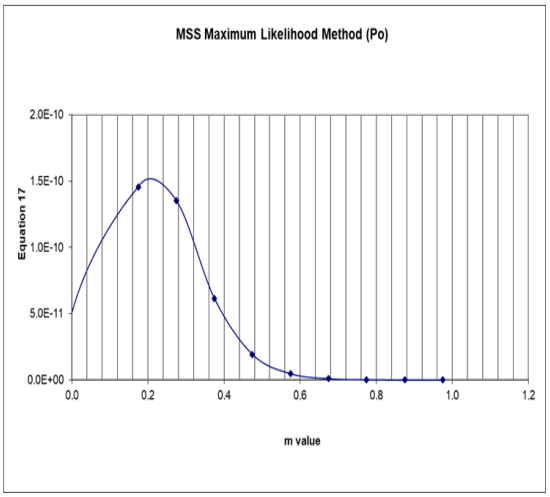


**Figure 35. MSS distribution LC curves used to estimate the mutation rate for the parental and mutant strains for experiment 3 of the fluctuation assay**. These graphs show the peak at which the strains m-value is determined. The m value represents the distribution of the mutations and it was used to calculate the mutation rate for the parental strain by the use the excel spreadsheet created at the CBTBR lab (Machowski et al., 2007). In this spreadsheet, the possible values of m were plotted on the x-axis and equation 17 data was plotted on the y-axis.

## Appendix C

Flow cytometry dot plots for assessment of the redox heterogeneity of the parental and mutant GFP-marked strains with CHP, DTT and menadione.

1. $mc^2$-GFP

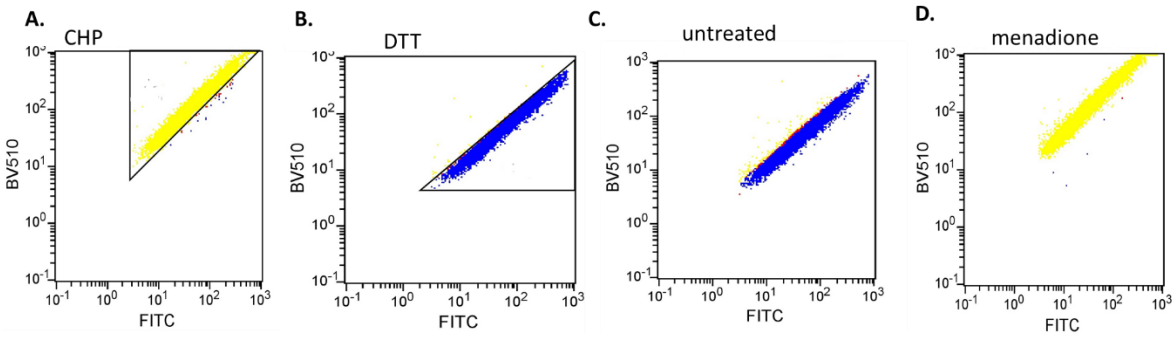


2. *Δnth-GFP*

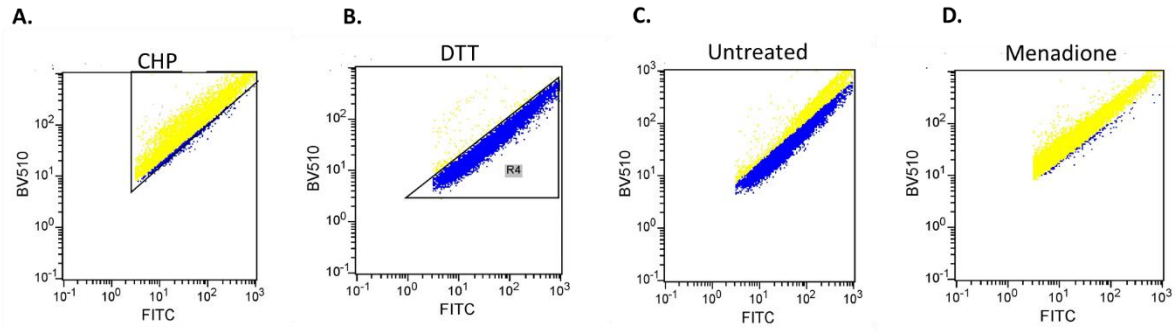


3. *ΔneiI-GFP*

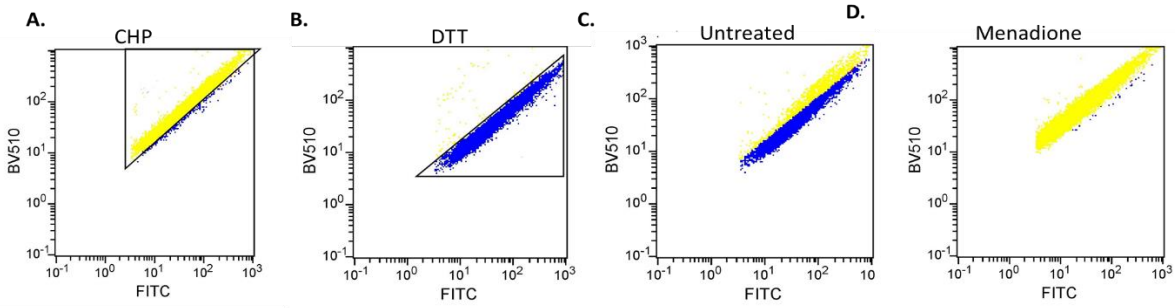


4. *ΔnthΔneiI-GFP*

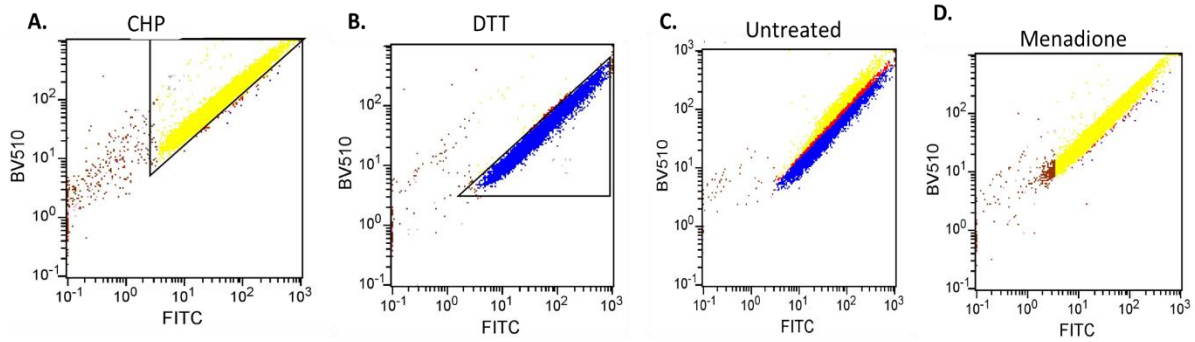

5. *ΔcydA-GFP*

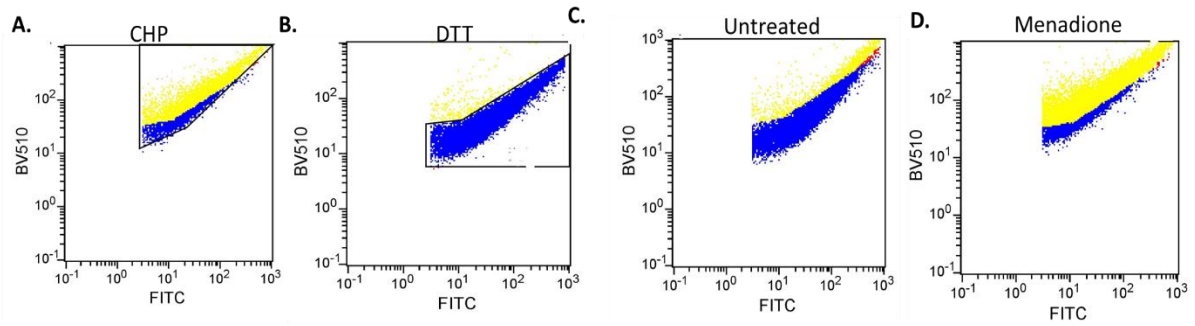


6. *ΔnthΔcydA-GFP*

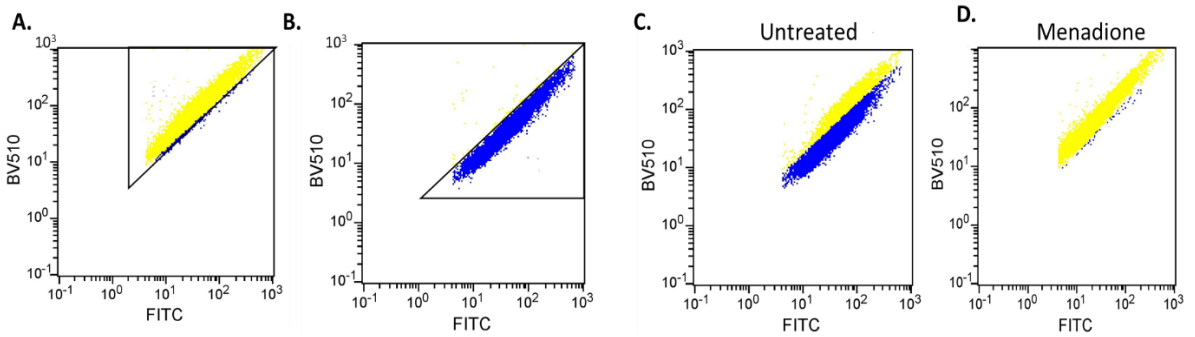


7. *ΔnthΔneiIΔcydA-GFP*

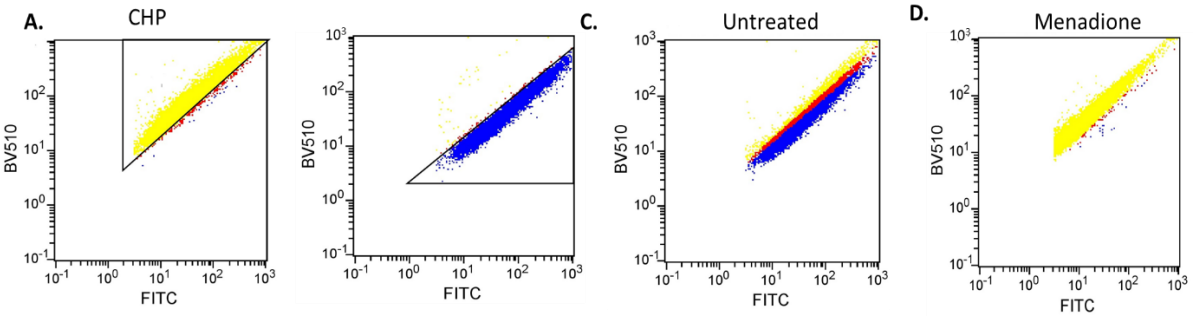


**Figure 36. Flow cytometry graphs illustrating the redox heterogeneity of seven GFP marked strains.** Strains (mc$^2$-GFP, Δ*nth-GFP*, Δ*nei1-GFP*, Δ*nth*Δ*nei1-GFP*, Δ*cydA-GFP*, Δ*nth*Δ*cydA-GFP* and Δ*nth*Δ*neiI*Δ*cydA-GFP*) were grown to exponential phase ($OD_{600nm}$=0.5-0.8). These were treated with different concentrations of CHP (10mM), DTT (40mM) and menadione (1mg/ml)**.** The program FCSalyzer was used to analyse and categorise each population (basal, oxidized and reduced). The dot plots for each mutant show emission of the fluorescence of the redox state shift when treated with the 3 compounds. The brilliant violet (BV510) is an auto fluorescence channel representing a dye that can be measured using an optical filter that measures signals between 500 and 520nm. The fluorescein isothiocyanate (FITC) represents a fluorescent dye which detects increased sensitivity and environmentally insensitive fluorescence. The dot plot display the shift towards oxidizing or reduction state respectively. Yellow represent oxidised, blue is for reduced and red dot for basal state.

## Appendix C2

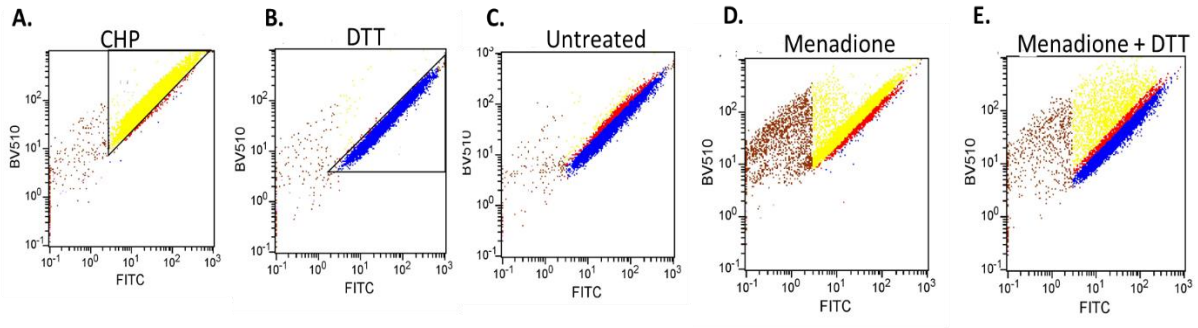


**Figure 37. Flow cytometry dot plot displaying the heterogeneity of wild type GFP marked strain.** The strain was grown to log phase ($OD_{600nm}$ = 0.5) thereafter it was treated with CHP (10mM), DTT (40mM), menadione (1mg/ml) and menadione (1mg/ml) followed by DTT (40mM) to assess if treatment of cells with more of the oxidizing and reducing compounds will enhance their redox state or not. BV510 is an auto fluorescence channel used to detect the fluorescence signal between 500-520 nm. FITC detects fluorescence sensitivity. The dot plot display the shift towards oxidizing or reduction state respectively. Yellow represent oxidised state, blue is for reduced state and red for basal state. The brown is excess sample that the fluorescence signal could detect.